[2014]

International Journal of Computational Engineering Research

Volume 04 Issue 11 November 2014

International Journal of Computational Engineering Research (IJCER) is dedicated to protecting personal information and will make every reasonable effort to handle collected information appropriately. All information collected, as well as related requests, will be handled as carefully and efficiently as possible in accordance with IJCER standards for integrity and objectivity.

IJCER

Open access Journal

Editorial Board

Editor-In-Chief

Prof. Chetan Sharma
Specialization: Electronics Engineering, India
Qualification: Ph.d, Nanotechnology, IIT Delhi, India

Editorial Committees

DR.Qais Faryadi
Qualification: PhD Computer Science
Affiliation: USIM(Islamic Science University of Malaysia)

Dr. Lingyan Cao
Qualification: Ph.D. Applied Mathematics in Finance
Affiliation: University of Maryland College Park,MD, US

Dr. A.V.L.N.S.H. HARIHARAN
Qualification: Phd Chemistry
Affiliation: GITAM UNIVERSITY, VISAKHAPATNAM, India

DR. MD. MUSTAFIZUR RAHMAN
Qualification: Phd Mechanical and Materials Engineering
Affiliation: University Kebangsaan Malaysia (UKM)

Dr. S. Morteza Bayareh
Qualificatio: Phd Mechanical Engineering, IUT
Affiliation: Islamic Azad University, Lamerd Branch
Daneshjoo Square, Lamerd, Fars, Iran

Dr. Zahéra Mekkioui
Qualification: Phd Electronics
Affiliation: University of Tlemcen, Algeria

Dr. Yilun Shang
Qualification: Postdoctoral Fellow Computer Science
Affiliation: University of Texas at San Antonio, TX 78249

Lugen M.Zake Sheet
Qualification: Phd, Department of Mathematics
Affiliation: University of Mosul, Iraq

Mohamed Abdellatif
Qualification: PhD Intelligence Technology
Affiliation: Graduate School of Natural Science and Technology

Meisam Mahdavi
Qualification: Phd Electrical and Computer Engineering
Affiliation: University of Tehran, North Kargar st. (across the ninth lane), Tehran, Iran

Dr. Ahmed Nabih Zaki Rashed
Qualification: Ph. D Electronic Engineering
Affiliation: Menoufia University, Egypt

Dr. José M. Merigó Lindahl
Qualification: Phd Business Administration
Affiliation: Department of Business Administration, University of Barcelona, Spain

Dr. Mohamed Shokry Nayle
Qualification: Phd, Engineering
Affiliation: faculty of engineering Tanta University Egypt

CONTENTS:

ISSN (e): 2250 – 3005 || Vol, 04 || Issue, 11 || November– 2014 ||
International Journal of Computational Engineering Research (IJCER)

Optimization of Corridor Observation Method to Solve Environmental and Economic Dispatch Problem

Stève Perabi Ngoffe[1], Salomé Ndjakomo Essiane[2], Adolphe Moukengue Imano[3], Grégoire Abessolo Ondoa[4]

[1]*Doctorate Student, Electronic, Electrotechnic, Automatic and Telecommunications Laboratory, ERSEE, University of Douala - Cameroon*

[2]*Lecturer, Electronic, Electrotechnic, Automatic and Telecommunications Laboratory, ERSEE, University of Douala - Cameroon*

[3]*Associate Professor, Electronic, Electrotechnic, Automatic and Telecommunications Laboratory, ERSEE, University of Douala, BP. 8698 Douala – Cameroon*

[4]*Master of Sciences with thesis student, Electronic, Electrotechnic, Automatic and Telecommunications Laboratory, ERSEE , University of Douala - Cameroon*

ABSTRACT:

This paper presents an optimization of corridor observation method (COM) which is an applicable optimization algorithm based on the evolutionary algorithm to solve an environmental and economic Dispatch (EED) problem. This problem is seen like a bi-objective optimization problem where fuel cost and gas emission are objectives. In this method, the optimal Pareto front is found using the concept of corridor observation and the best compromised solution is obtained by fuzzy logic. The optimization of this method consists to find best parameters (number of corridor, number of initial population and number of generation) which improve solution and reduce a computational time. The simulated results using power system with different numbers of generation units showed that the new parameters ameliorate the solution keep her stability and reduce considerably the CPU time (time is minimum divide by 4) comparatively at parameterization with originals parameters.

Keywords: *bi-objective, corridors observation, fuel cost, gas emission, new parameters, optimal Pareto front, optimization, original settings*

I. INTRODUCTION

The economic dispatching (ED) is one of the key problems in power system operation and planning. The basic objective of economic dispatch is to schedule the committed generating unit outputs so as to meet the load demand at minimum operating cost, while satisfying all equality and inequality constraints. This makes the ED problem a large – scale highly constrained non-linear optimization problem. In addition, the increasing public awareness of the environmental protection and the passage of the Clean Air Act Amendments of 1990 have forced the utilities to modify their design or operational strategies to reduce pollution and atmospheric emissions of the thermal power plant.

Several strategies to reduce the atmospheric emissions have been proposed and discussed. These include: installation of pollutant cleaning equipment, switching to low emission fuels, replacement of the aged fuel-burners with cleaner ones, and emission dispatching. The first three options require installation of new equipment and/or modification of the existing ones that involve considerable capital outlay and, hence, they can be considered as long-term options. The emission dispatching option is an attractive short-term alternative in which the emission in addition to the fuel cost objective is to be minimized. Thus, the ED problem can be handled as a multi-objective optimization problem with non-commensurable and contradictory objectives. In recent years, this option has received much attention [1–5] since it requires only small modification of the basic ED to include emissions.

In the literature concerning environmental/economic dispatch (EED) problem, different technics have been applied to solve EED problem. In [1, 2] the problem was reduced to a single objective problem by treating the emission as a constraint. This formulation, however, has a severe difficulty in getting the trade-off relations between cost and emission. Alternatively, minimizing the emission has been handled as another objective in addition to the cost [5]. However, many mathematical assumptions have to be given to simplify the problem.

Furthermore, this approach does not give any information regarding the trade-offs involved. In other research direction, the multi-objective EED problem was converted to a single objective problem by linear combination of different objectives as a weighted sum [3], [6]. The important aspect of this weighted sum method is that a set of non-inferior (or Pareto-optimal) solutions can be obtained by varying the weights. Unfortunately, this requires multiple runs as many times as the number of desired Pareto-optimal solutions. Furthermore, this method cannot be used in problems having a non-convex Pareto optimal front. To overcome it, certain method optimizes the most preferred objective and considers the other objectives as constraints bounded by some allowable levels [5]. The most obvious weaknesses of this approach are that, they are time-consuming and tend to observe weakly non-dominated solutions [5].

The other direction is to consider both objectives simultaneously as competing objectives. The recent review to the Unit Commitment and Methods for Solving [7] showed that evolutionary algorithms are the most used in this case; certainly because they can efficiently eliminate most of the difficulties of classical methods [5]**.** The major problems of these algorithms, is to find the Pareto optimal front, to conserve the non- dominated solutions during the search and relatively long time to find the solution.

In [8] we have proposed one method, based on the evolutionary method where the optimal Pareto front is obtained by the concept of corridor observation and the loses of non-dominated solution is reduce by the dynamism of archives during the different generations. The quality of solution and CPU time depend to the number of corridors, the initial population and the number of generations. In this paper, we propose some parameters which keep stable the solution and reduce considerably CPU time of COM. In the second part of this paper, we present materials and methods to solve the EED problem and in the third part, simulation and results are presented to enable us to find the new parameters and demonstrate their effectiveness by comparing it with the original settings.

II. MATERIALS AND METHODS [8]

In this part, we formulate the EED problem and present our approach to solve it.

2.1. Problem formulation

The EED problem is to minimize two competing objective functions, fuel cost and emission, while satisfying several equality and inequality constraints. Generally the problem is formulated as follows:

2.1.1. Problem objectives

- Minimization of fuel cost

The generator cost curves are represented generally by quadratic functions. The total fuel cost ($/h) in terms of period T, can be expressed as:

$$F\left(p_{i,t}\right) = \sum_{t=1}^{T} \sum_{i=1}^{Ng} c_{fi}(p_{i,t}) I_{i,t} + ST_{i,t}(1 - I_{i,t-1}) I_{i,t} \quad (1)$$

where

$$c_{fi}(p_{i,t}) = a_i + b_i p_{i,t} + c_i p_{i,t}^2 \quad (2)$$

and $c_{fi}(p_{i,t})$ is the generator fuel cost function; a_i, b_i and c_i are the cost coefficients of i^{th} generator; $P_{i,t}$, is the electrical output of i^{th} generator; Ng is the number of generators committed to the operating system ; $I_{i,t}$ the statut of different generators; ST_i the start-up cost .

- Minimization of gas emission

The atmospheric pollutants such as sulphur dioxides (SO_2) and nitrogen oxides (NO_X) caused by fossil-fuelled thermal units can be modelled separately. However, for comparison purposes, the total emission (ton/h) in one period T of these pollutants can be expressed as:

$$E\left(p_{i,t}\right) = \sum_{t=1}^{T} \sum_{i=1}^{Ng} e_{fi}(p_{i,t}) I_{i,t} \quad (3)$$

where

$$e_{fi}(P_{i,t}) = (\alpha_i + \beta_i p_{i,t} + \delta_i p_{i,t}^2) \quad (4)$$

and α_i, β_i, δ_i are the emission coefficients of the i^{th} generator.

2.1.2. Objective constraints

- Power balance constraint

$$p_{load,t} - \sum_{i=1}^{Ng} p_{i,t} I_{i,t} = 0 \tag{5}$$

- Spinning reserve constraint :

$$p_{load,t} + R_t - \sum_{i=1}^{Ng} p_{max,i} I_{i,t} \leq 0 \tag{6}$$

- Generation limit constraints :

$$p_{min,i} I_{i,t} \leq p_{i,t} \leq p_{max,i} I_{i,t} \quad , i = 1 ..... Ng \tag{7}$$

- Minimum up and down time constraint :

$$I_{i,t} = \begin{cases} 1 \text{ if } T_i^{on} \prec T_i^{up} \\ 0 \text{ if } T_i^{off} \prec T_i^{down} \\ 0 \text{ or } 1 \text{ otherwise} \end{cases} \tag{8}$$

Where T_i^{up} represent the minimum up time of unit- i ; T_i^{down} the minimum down time of unit i T_i^{off} is the continuously off time of unit i and T_i^{on} the continuously on time of unit- i .

- Start-up cost

$$ST_i = \begin{cases} HST_i \text{ if } T_i^{down} \leq T_i^{off} \leq T_i^{down} + T_i^{cold} \\ CST_i \text{ if } T_i^{off} \succ T_i^{cold} + T_i^{down} \end{cases}$$

2.2. The corridors observation method [8]

The different steps of the COM are presented in the following figure

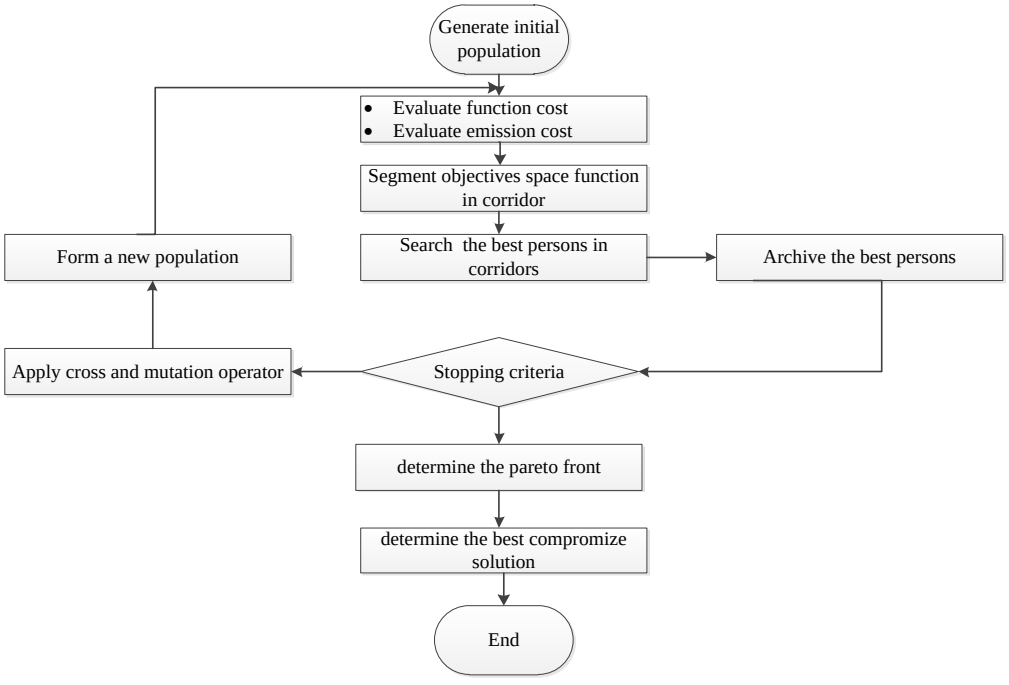

Figure 1: Different steps of the algorithms [8]

- **Step 1**

In the first step, we start with to the status of different units generation, where we create randomly the initial population. Each individual is a combination of each power generation unit

- **Step 2**

In the second, using equations (1) and (3) we evaluate the objective functions of this population

- **Step 3**

Using the minimum of the different objective functions of individuals who respect the constraints (5) to (8), we define the space solution and segment it to the corridors observations following the different axes which are specify by each function.

- **Step 4**

In each corridor, we search the best individuals who have the minimum objectives functions, and the non feasible solutions are classified using the number and the rate of violation constraints. Those solutions will be used to increase the number of feasible solutions.

- Step 5

We keep in the archives those best individuals

- **Step 6**

We verify the stopping criteria define as [10]:

$$\xi = \ln(d) \tag{9}$$

where

$$d = \sum_{j=1}^{N_F} \left[\frac{1}{Cl} \sqrt{\sum_{i=1}^{cl} \left(\frac{F_{j,i}^{t} - F_{j,i}^{t-1}}{F_{\max} - F_{\min}} \right)} \right] \tag{10}$$

Explain the metric progression of the best individuals in each corridor. N_F is the number of objectives functions ; Cl the number of corridor ; $F^{t}_{j,i}$, $F^{t-1}_{j,i}$ the j^{th} objective function of the best individual in i^{th} corridor ; F_{min} and F_{max} the minimum and maximum of the j function ; t is the present generation, t-1 the anterior generation. At times the maximum number of generation can be the alternative stopping criteria

- **step 7**

If the stopping criteria is not verified, we construct the new population using the selection, cross and mutation operators apply to the archive population and we return to step 2.

- **Step 8**

If the stopping criteria is verified we find the best compromise solution among the individuals of the Pareto front. Due to imprecise nature of the decision maker's judgment, each objective function of the i-th solution is represented by a membership μ_i function defined as

$$\mu_i = \begin{cases} 1 & if \quad F_i \le F_i^{\min} \\ \dfrac{F_i^{\max} - F_i}{F_i^{\max} - F_i^{\min}} & if \quad F_i^{\min} \le F_i \le F_i^{\max} \\ 0 & if \quad F_i \ge F_i^{\max} \end{cases} \tag{11}$$

For each non-dominated solution, the normalized membership function is μ^k calculated as :

$$\mu^k = \frac{\sum_{i=1}^{N_F} \mu_i^k}{\sum_{k=1}^{M} \sum_{i=1}^{N_F} \mu_i^k} \tag{12}$$

where M is the number of non-dominated solutions. The best compromise solution is the one having the maximum of μ^k .

III. SIMULATION AND RESULTS

In order to find the new parameters of COM and solve the EED, a 3-units generation system is tested [11]. And extent at 6, 10 and 15 units generation. These parameters are applied in COM with the same software and computer used in [8]. The results are compared with the originals settings of COM. The data concerning the units generation are given in tables 1 and 2 [11].

Table 1. The 3-units system data

Unit	P_i^{max} (MW)	P_i^{min} (MW)	a ($ /h)	b ($ /MWh)	c ($ /MW^2h)	R_i^{up} ($ /MW)	R_i^{down} ($ /MWh)
1	600	150	561	7.29	0.00156	100	100
2	400	100	310	7.85	0.00194	80	80
3	200	50	78	7.97	0.00482	50	50

Table 2. SO_2 and NOx coefficients emission gas data of 3-units

Units	$\alpha_{so\,2}$ (ton/h)	α_{Nox} (ton/h)	$\beta_{so\,2}$ (ton/MWh)	β_{Nox} (ton/MWh)	$\delta_{so\,2}$ (ton/MW^2h)	δ_{Nox} (ton/MW^2h)
1	0,5783298	0,04373254	0,00816466	-9,4868099 e^{-6}	1,6103e^{-6}	1,4721848 e^{-7}
2	0,3515338	0,055821713	0,00891174	-9,7252878 e^{-5}	5,4658 e^{-6}	3,0207577 e^{-7}
3	0,0884504	0,027731524	0,00903782	-3,5373734 e^{-4}	5,4658 e^{-6}	1,9338531 e^{-6}

In the implementation, we add the different coefficients of each gas per groups to have the coefficient of the whole gas

3.1. Study of objectives according to the number of generation

The study of convergence with the same parameters of [8] i.e., 50 corridors, 300 number of initial population is presented in figure 2

.

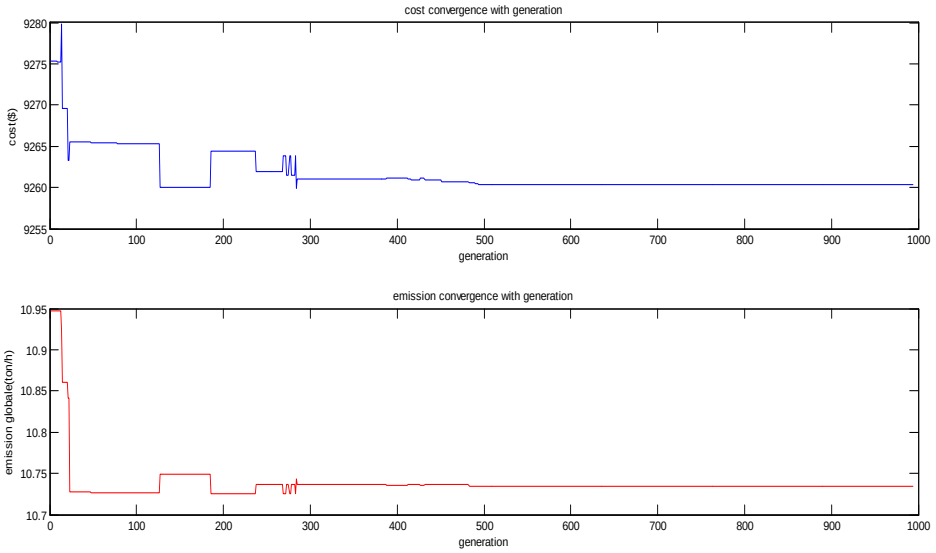

Figure 2: Convergence of fuel cost ($) and gas emissions (ton/h) objective functions (1000MW).

These curves convergence show that since the 500 generations fuel cost and gas emission is uniform so, if we choose the number of generations at the value greater or equal than 500 generations the solution will be the same. So we can take 500 like the new number of generations.

3.2. Study of objectives according to the number of corridors

The representation of objectives, according to the number of corridor, with initial population number and number of generations set respectively at 300 and 1000 is shown in figure 3.

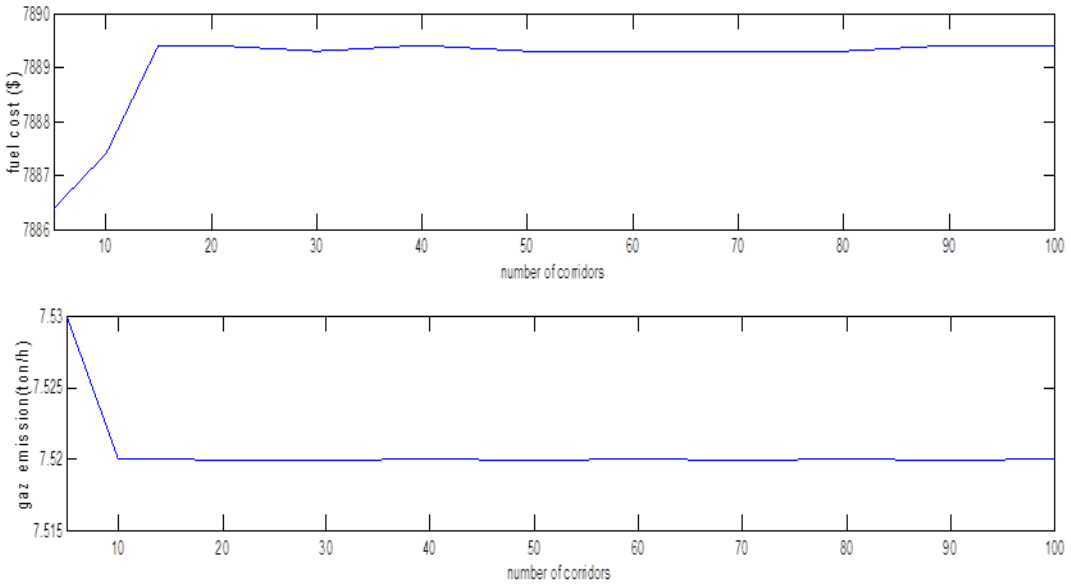

Figure 3: Evolution of fuel cost ($) and gas emissions (ton/h) according to the number of corridors (850 MW). These curves shows that from 20 corridors fuel cost and gas emission are almost uniform. The Pareto front at this value of number of corridors is represented in figure 4.

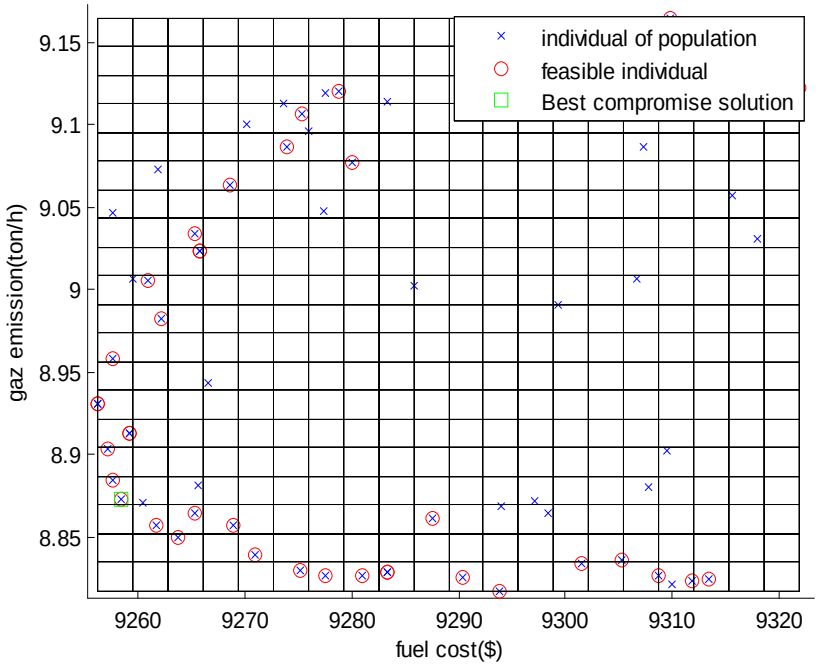

Figure 4: Pareto front with the new parameters.

Comparing with the Pareto front obtained with the original parameters [8] in figure 5

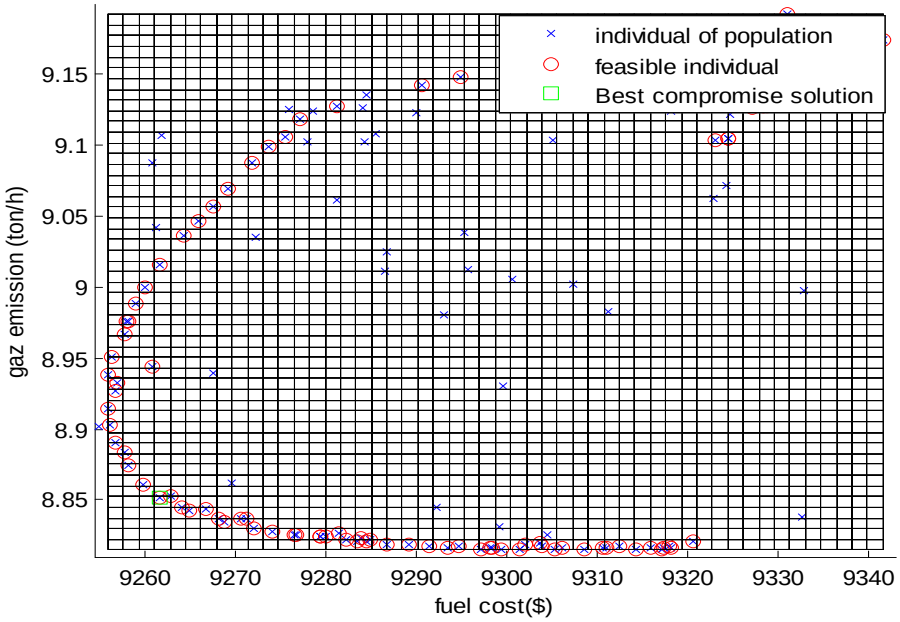

Figure 5: Pareto front with the original parameters.

We can conclude that the increase of corridors number improves the Pareto front but from 20 corridors, the optimal solution is almost uniform. So we can consider 20 like new number of corridor.

3.3. Study of objectives according to the number of initial population

The representation of objectives, according to initial population, with number of corridor and number of generations set respectively at 50 and 1000 is shown in figure

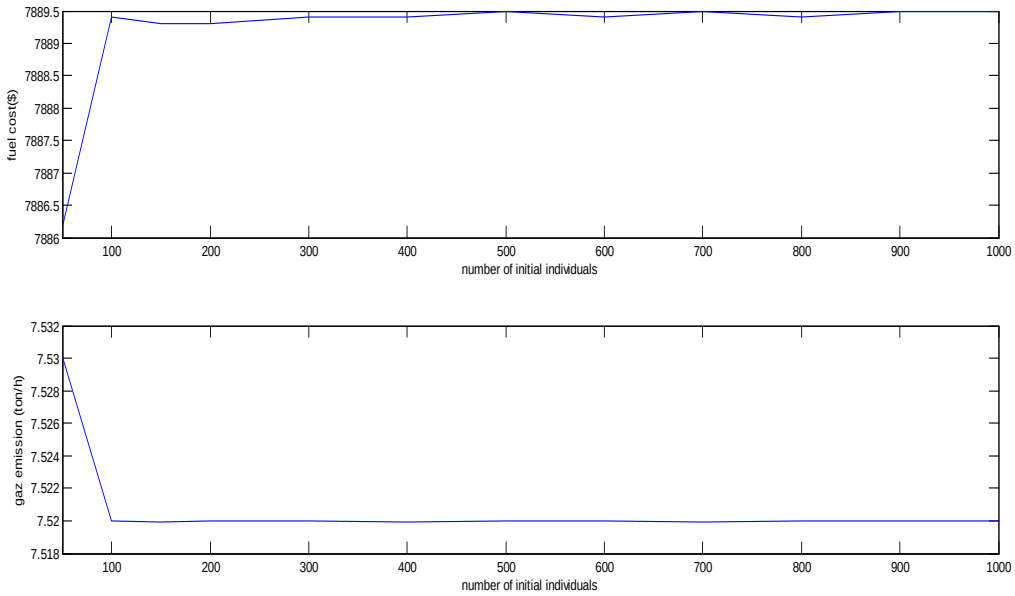

Figure 6: Evolution of fuel cost ($) and gas emissions (ton/h) according to the number of initial individuals (850MW)

These representations show that from an initial population of 200, fuel cost and gas emission are almost uniform. So we can set this parameter at 200.

3.4. Comparative study between the original parameters and new

To present the effectiveness of the new parameters in COM to unit commitment and EED, we applied it to a production plan of 3-units during 5 hours and made the comparison study with the original setting.

Table 3. Unit commitment and EED during 5 hours with the two groups of parameters

Hours (H)	Demands (MW)	P1 (MW)	P2 (MW)	P3 (MW)	Fuel cost X10^3($)	Emission gaz (ton/h)	Average CPU time (s)
With original parameters							
1	550	0	0	549.9	5.0415	5.6380	
2	600	0	0	599.9	5.4957	6.1468	
3	650	108.0382	0	541.8742	5.9646	6.6979	**23.29**
4	700	114.5484	0	585.351	6.4169	7.2059	
5	750	150.228	0	599.67	6.8777	7.7323	
With new parameters							
1	550	0	0	549.9	5.0417	5.6383	
2	600	0	0	599.9	5.4957	6.1468	
3	650	100.5037	0	549.39	5.9647	6.6967	**5.1**
4	700	106.2763	0	593.6432	6.4179	7.2054	
5	750	152.6171	0	597.32	6.8787	7.7343	

The findings of this table are as follows: in terms of unit commitment, the results are identical; sensibly the same in terms of EED but the CPU average times is considerably reduced. This study have extended with 6, 10, and 15 unit in table 4 findings was the same but the convergence speed according to the number of units is reduce with news parameters

Table 4. Comparative study with 3, 6, 10 and 15 units generation

Number of units	3	6	10	15
With original parameters				
Fuel cost x 10^3($)	9.2606	9.1911	9.176	9.177
Gas emission(ton/h)	10.7347	10.2771	10.3679	10.3683
Average times (s)	23.29	31.92	49.40	104.61
With new parameters				
Fuel cost x10^3($)	9.2583	9.1922	9.1844	9.1806
Gas emission (ton/h)	10.7617	10.1988	10.2854	10.3898
Average time (s)	5.14	5.74	7.03	34.30

IV. CONCLUSION

In this paper, news parameters are proposed to optimize COM. COM have been proposed in [8] to solve environmental/economic power dispatch optimization problem and unit commitment. The study of objectives according to the number of generation, of corridors and initial population have allowed us to propose new parameters that are 20 corridors, 200 individuals for initial population and 500 generations. The parameterization of COM with these settings conserves the quality of solution in terms of unit commitment and EED. The principal advantages of this parameterization are the reduction of CPU time (the time is minimum divided by 4) and the convergence speed according to the number of generation units comparatively at the parameterization with originals settings (50 corridors, 200 individuals and 1000 generation).

REFERENCES

[1]. Brodesky SF, Hahn RW. Assessing the influence of power pools on emission constrained economic dispatch. IEEE Trans Power Syst 1986; 1 (1). PP: 57–62.

[2]. Granelli GP, Montagna M, Pasini GL, Marannino P. Emission constrained dynamic dispatch. Electr Power Syst Res 1992; 24. pp: 56–64.

[3]. Chang CS, Wong KP, Fan B. Security-constrained multiobjective generation dispatch using bicriterion global optimization. IEE Proc—Gener Transm Distrib 1995;142 (4) : 406–14.

[4]. R Manoj Kumar. Bavisetti, T.Kranthi Kiran. Optimization Of Combined Economic and Emission Dispatch Problem – A Comparative Study for 30 Bus Systems. IOSR Journal of Electrical and Electronics Engineering (IOSR-JEEE) 2012 ; Vol 2. PP 37-43

[5]. M. A. Abido. Environmental/Economic Power Dispatch Using Multiobjective Evolutionary Algorithms. IEEE transactions on power systems; 2003 Vol. 18, N^O. 4. PP : 1529-1537

[6]. Alkhalil Firas. «Supervision, économie et impact sur l'environnement d'un système d'énergie électrique associé à une centrale photovoltaïque »thèse de Doctorat Paris tech. 2011

[7]. Samani.h, Razmezani.M and Naseh.M.R.. Unit Commitment and Methods for Solving; a Review . J. Basic. Appl. Sci. Res; 2013, 3(2s) 358-364

[8]. S. Ndjakomo Essiane, S. Perabi Ngoffe, A. Moukengue Imano, G. Abessolo Ondoa. Bi-objective Optimization Apply to Environmental and Economic Dispatch Problem Using the Method of Corridor Observations. International Journal of Computational Engineering Research (IJCER); 2014; Vol 4. PP: 16-23

[9]. Lubing Xie, Songling Wang & Zhiquan Wu. Study on Economic, Rapid and Environmental Power Dispatch. Modern applied science vol.3 N^{0}6. 2009. Pp : 38-44

[10]. Jean Dipama. « Optimisation multi-objectif des systèmes énergétiques ».thèse soutenue à l'université de MONTREAL. 2010

[11]. Farid Benhamida, Rachid Belhachem. Dynamic Constrained Economic/Emission Dispatch Scheduling Using Neural Network . Power Engineering and Electrical Engineering. Vol: 11 N^{0}1 .2013.pp :1-9

ISSN (e): 2250 – 3005 || Vol, 04 || Issue, 11 || November– 2014 ||
International Journal of Computational Engineering Research (IJCER)

Face Detection for identification of people in Images of Internet

Rodolfo Romero Herrera[1], Francisco Gallegos Funes[2]
[1]Escuela Superior de Computo (ESCOM) IPN,
[2]Escuela Superior de Ingeniería Mecánica y Eléctrica (ESIME) IPN

Abstract:
One method for searching the internet faces in images is proposed by using digital processing topological with descriptors. Location in real time with the development of a database that stores addresses of internet downloaded images, in which the search is done by text, but by finding facial image, is achieved.

Face recognition in images of Internet has proved to be a difficult task, because the images vary considerably depending on viewpoint, illumination, expression, pose, accessories, etc. The descriptors for general information: containing low-level descriptors.

Developments on face recognition systems have improved significantly since the first system; image analysis is a topic on which much emphasis is being given in order to identify parameters, visual features in the image that provide environment data that it is represented in the image, but without the intervention of a person.

In this project raises its realization using the method of viola and jones as face descriptor. We can distinguish even different parts of the face such as eyes, eyebrows, nose and mouth.One method for searching faces in image taken from internet intends to use digital processing using topological descriptors. It is located the face in real time.

Keywords: *Face Recognition, viola and jones, identifying people, Internet, descriptor for points.*

I. INTRODUCTION

The system has a key content manager, who also supplies the database so that the main features or image patterns are stored. The system has a key content manager, who also supplies the database so that the main features or image patterns are stored. The query module applies the same algorithms as the administrator to generate the object description and comparing them with those stored in the database using the Mahalanobis distance [1]. The query module sends the results to the block "Result Set". See figure 1.

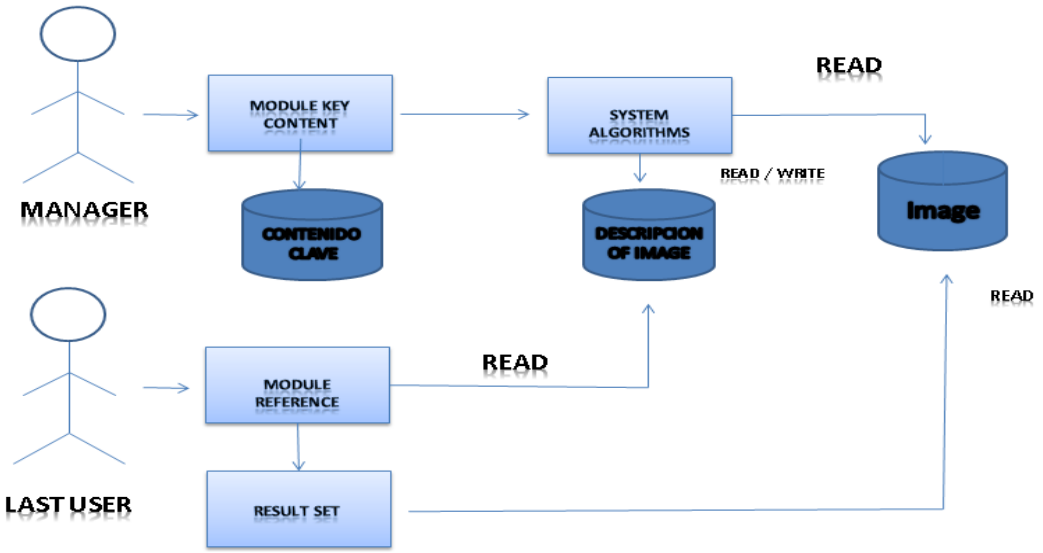

Figure 1. Block diagram system

The shape of an object in an image may consist of a single region or set of regions as shown in the Figure 2:

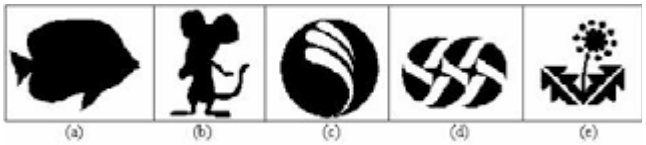

Figure.2 . Examples of images with which they work.

A descriptor can classify them according to the features to be identified, so that we can compare different forms of such images and see if it is the same object or similar objects. The great advantages of this descriptor are its small size and speed [2].

The face recognition is a task that humans perform routinely and effortlessly. So much so that the run almost every day without realizing.The low cost of computers and technological advancement has enabled has a huge interest in automating processes and video image processing. The research worldwide recognition has been motivated by the number of applications that require the identification of the individual.

The problem is based on:

Given an image, the goal of face detection is to identify all image regions which contain a face.

It is difficult to detect faces due to the following parameters [3]:

• Pose

• Image orientation

• Tone of individuals and the background image

II. FACE DETECTOR

The system performs a scan the entire image at different scales for detecting faces in different sizes. See figure 3.The implementation of the detector system consists of two stages:

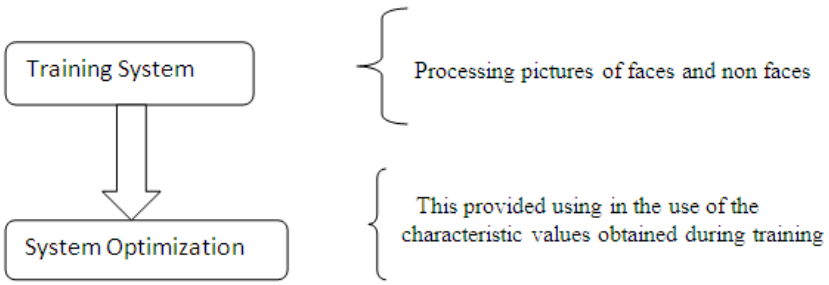

Figure 2 Detector system

The images for training are preprocessed by changing the color image to a grayscale image and then resizing is performed. See Figure 4.

Figure 4 Scaling to gray.

The flow chart of Figure 5 shows the procedure for face detection.

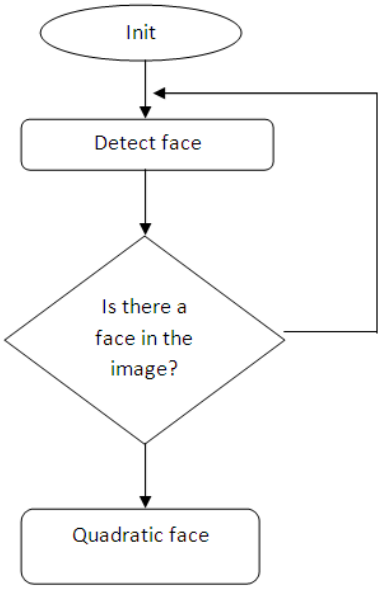

Figure 5 Workflow of face recognition

III. FACE DETECTION AND LOCATION

A technique proposed by Paul Viola and Michael J. Jones was analyzed. [4]. This method is basically the face location by using a group of rectangular features, which operates faster than a pixel based on system [4]. The two, three and four boxes: three kinds of features are used. Said rectangular features (CRs) are 10 different types shown in Figure 6.

How you use these CRsr, is put in a certain position within the image and calculate the difference between the sum of the pixels within the clear part and the dark part of the CR, obtaining an integer value that must exceed a threshold for a finding that is on facial feature is desired. The training phase is to find the CRs in a certain scale and position within a window of a certain size located a characteristic feature of a face, this CR is called classifier. In Figure 7 can be seen a set of classifiers in the classifier where only figure 4d locate a feature of the face.

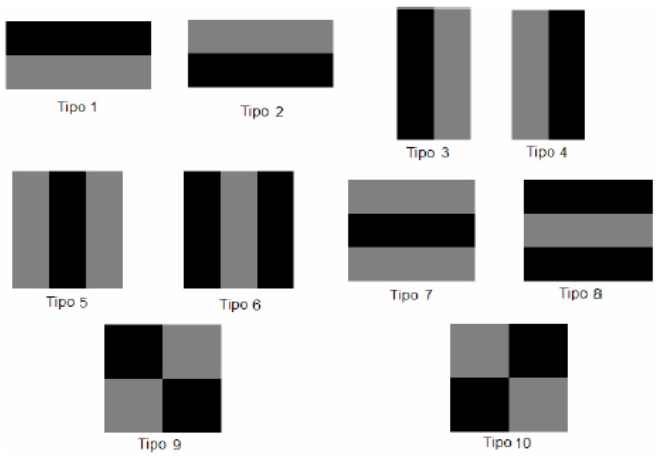

Figure 6 Set of ten CRs used in the process of locating faces.

Figure 7. Four rectangular features from a) to d) which only d) is a useful feature that can be considered how classifier.

The method of Viola & Jones is to train or find a set of classifiers, and thresholds, testing each of the classifiers in each position and scale of a set of test images used for this, the learning algorithm AdaBoost [5].This set consists of a group of images in which faces and a standard set of pictures in which there are faces; classifiers with the highest number of correct classification of the faces and the lowest number of false positives obtained are selected.

To calculate the CRs rapidly at various scales an intermediate image representation (integral image) is used. Once obtained the CR is calculated at any scale and location in constant time. The integral image at a position x, y contains the sum of the pixels above and to the left of x, y. Equation 1.

$$ii(x,y) = \sum_{x' \le x, y \le y} i(x', y') \tag{1}$$

Where ii (x, y) is the integral image and i (x, y) is the original image (Figure 8). Using the following pair of recurrences:

$$S(x,y) = S(x,y-1) + i(x,y) \tag{2}$$
$$ii(x,y) = ii(x-1,y) + s(x,y)$$

Where s (x, y) is the cumulative sum of the values of the pixels in the row, s (x, -1) = 0, and ii (-1, y) = 0), the integral image is calculated in a single pass over the original image.

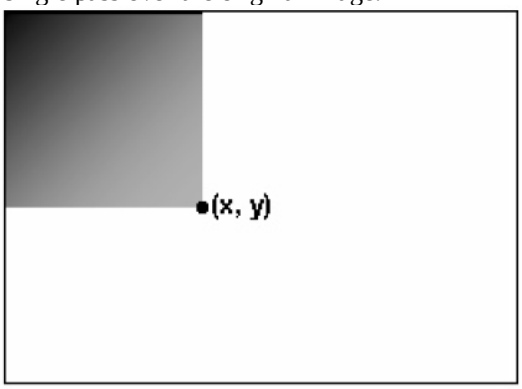

Figure 8 The value of an integral image at a point (x, y) is the sum of all pixels above and to the left.

Using the integral image any amount of a rectangle is calculated using an array of four references (see Figure 9). Also the difference between two sums of rectangles is computed eight references. As the characteristics of two rectangles (types 1, 2, 3 and 4) defined above have adjacent rectangular sums calculated with an arrangement of six references, eight for the characteristics of three rectangles and nine for four rectangles.

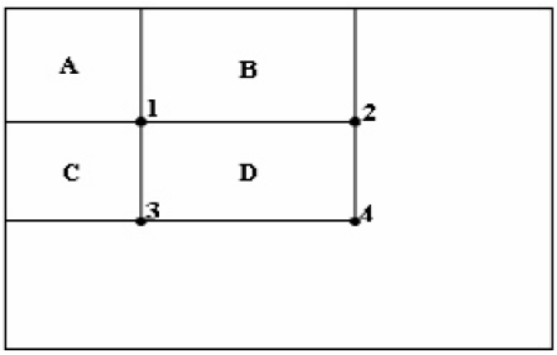

Figure .9 Sum of pixels.

The sum of the pixels within the rectangle D can be calculated with an arrangement of four references. The value of the integral image at the position 1 is the sum of the pixels in the rectangle A. The value at position 2 is A + B, in the 3 position is A + C, in position 4 is A + B + C + D. The sum within D can be calculated as 4 + 1 - (2 + 3).

IV. MAHALANOBIS DISTANCE

In statistics, Mahalanobis distance is a distance measure introduced by Mahalanobis in 1936 Its utility is that it is a way to determine the similarity between two multi-dimensional random variables. It differs from Euclidean distance in that takes into account the correlation between random variables [6].

Distance is called the length of the shortest path between two entities. From a formal point of view, for a set of elements X, distance is defined as any binary function d (a, b) of X xX in $\mathbb{R}$ verifying the following conditions:

No negativity:

$$d(a,b) \geq 0 \; \forall \; a,b \; \in X \tag{3}$$

Symmetry:

$$d(a.b) = d(b,a) \forall \; a,b \; \in X \tag{4}$$

Triangle inequality:

$$d(a,b) \leq d(a,c) + d(c.b) \forall \; a,b \; \in X \tag{5}$$

It called Euclidean distance between two points A (x, y) 11 and B (x, y) 22 to the length of the line segment whose endpoints A and B. It is expressed mathematically as [7]:

$$d = \sqrt{(X_2 - X_1)^2 + (y_2 - y_1)^2} \tag{6}$$

The distance between a point P and a line R is the length of the shortest path connecting point P (x, y) 11 with the line R: Ax + By + C = 0 is expressed mathematically as:

$$d = \frac{AX_1 + B\,y_1 + C}{\sqrt{A^2 + B^2}} \tag{7}$$

The distance between two parallel lines is the length of the shortest path between them and any point of the other. The distance between a point P and L plane is the length of the shortest path between P (x1, y1, z1) point and the plane L=Ax + By + Cz + D. Mathematically it is expressed as:

$$d = \frac{AX_1 + BY_1 + CZ_1 + D}{\sqrt{A^2 + B^2 + C^2}} \tag{8}$$

Formally, the Mahalanobis distance between two random variables with the same probability distribution $\vec{x}$ and $\vec{y}$ with covariance matrix Σ is defined as:

$$d_m(\vec{X},\vec{Y}) = \sqrt{(\vec{X} - \vec{Y})^T \sum^{-1} (\vec{X} - \vec{y})} \tag{9}$$

V. REGIONS

For detection; once having the position of the face within the imageis done an estimate of where the eyebrows are located, nose and mouth. This position can be estimated, due to the method of locating faces, wherein the facial parts near the same position will be obtained. (See Figure 10). Subsequently, processes each of these areas with special image processing for each region [8].

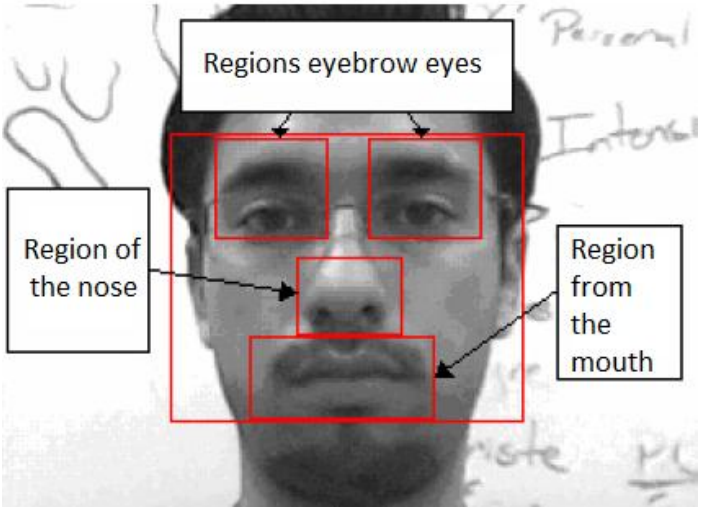

Figure .10 Location eyebrows eyes, nose, and mouth.

VI. Eyebrows Detection

For detection of eyebrows, once estimated position within the facial area in an area of 45 x 40 and the grayscale image as that of Figure 11a proceed to make the following image processing:

1. Equalization image eyebrow area is performed; Figure 11b.
2. The procedure to perform a sum of equalized image to itself; figure 11c
3. Applies an adaptive enhanced with a 3x3 window with values of k1 = 1 and k2 = 1; Figure 11d.
4. Then proceed to perform binarization with a threshold of 40; Figure 11e.
5. Proceeds to convex components labeling; Figure 11f.
6. The largest component of the top of the area is selected and the rest is eliminated, thereby generating the image of the eyebrow; Figure 11g.

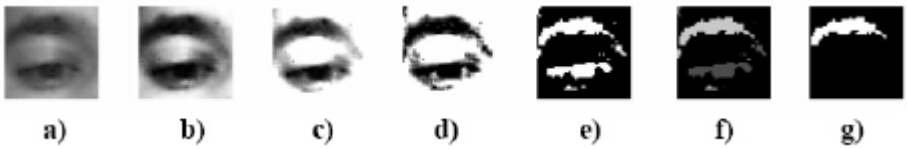

Figure 11 Processing eye.

The next step is to locate the points with the Xs highest and lowest brow, obtaining the UA A and B to the right eyebrow (Figure 12) and C and D for the left eyebrow.

Figure 12 Action Units A and B located on the right eyebrow.

VII. DETECTION OF MOUTH.

For detection of the mouth, as eyebrows, once it has been estimated position in an area of 74x33, and the image in grayscale (Figure 13a) is determined, the image processing that described below:

1. Subtraction is performed between the image and its causes enhanced adaptive; Figure 13b.
2. Subtraction is performed between the image obtained in step 1 and the image of the mouth and is binarized equalized to a threshold of 40 (Figure 13c).
3. Convex component labeling is performed; Figure 13d.
4. The largest component is chosen; Figure 13e.

Figure 13 Getting mouth.

The next step is to locate the points with theXs highest and lowest of the mouth, obtaining action units F and G (Figure 14).

Figure 14 Action Units F and G obtained with the digital image processing of the mouth.

After obtaining the red spots on the images to the mouth, nose, eyebrows and eyes, Mahalanobist distance is applied to determine how closely a face over another, suggesting a threshold. The distance between red dots is calculated and also determines how far (in terms similar) is an image of another.

VIII. ANALYSIS OF RESULTS

Finally in the center point of the nose (UA E) is positioned in the center of the window in the region of the nose. This is because it is only used as a benchmark to measure the distances shown; which are the basis for analysis of the expression of the user.

Figure 15A low Light and without glasses

With the same light that the previous experiment with new lenses were found manner that does not affect the use of the lens system Figure 16.

Figure 16- A low Light and with glasses

By using brightness of incandescent without a focus lenses or eyeglasses in figure 16. Figure 17 can be seen giving more points that do not belong to the characteristics of the face.

Figure 17 Incandescent light without glasses

Having that was found Cloudy with a face, an appropriate threshold equal to 2, with or without glasses and with a white fund plain background. Now the question was how the system would affect the brightness which makes testing varying brightness. In conducting the experiment in low light without glasses and the system could find features of the face but showing items that are not part of the features of the face, figure 18.

The faces of the individuals are located and red squares are drawn on their faces. For Figure 14 shows the detection of 5 faces in a picture of Internet.

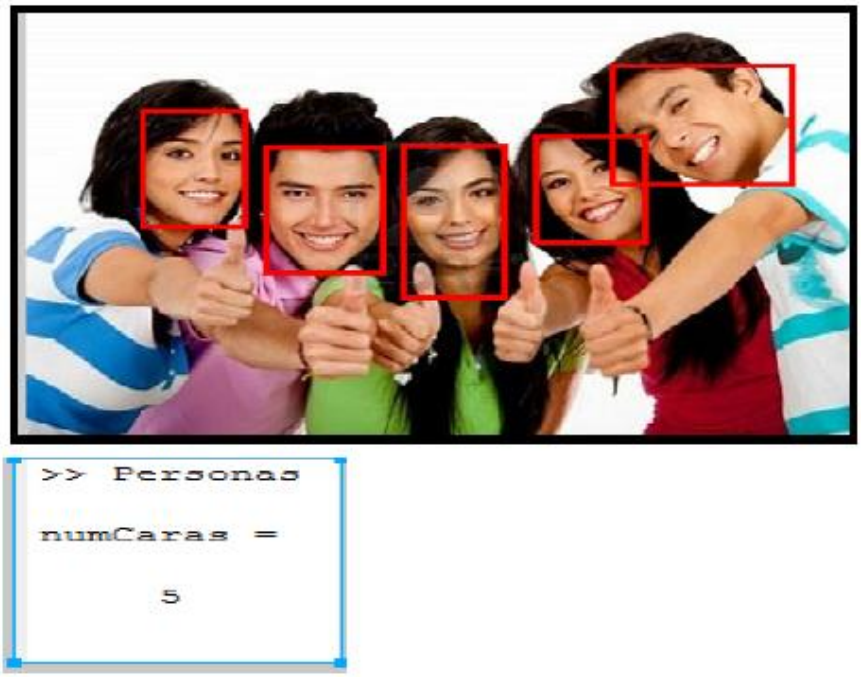

Figure 16 Location of five faces.

The method works for the location of one or more face as seen in Figures 19.

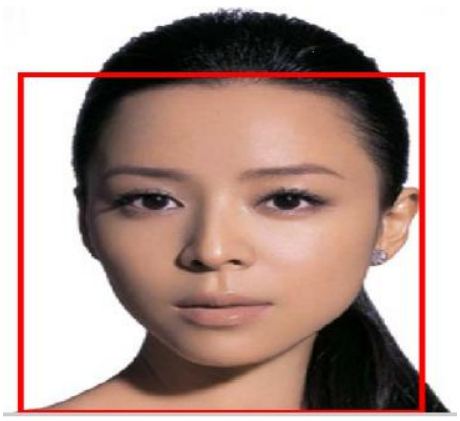

Figure 19 Location of a face.

IX. CONCLUSIONS

Face Detection efficiency depends on the lighting that you have when this image was taken. But there was no trouble locating the face even if the person has glasses, moustache, etc.

As for the location of faces in images from the Internet, there is also no problem, even if the image has more than one face.

The location of faces in internet pages without using text, we believe it is important because most search engines do not perform that search this manner; and is especial as well that you have a new option especially for those who cannot accomplish this using a keyboard or text.

The proposed method can be added more easily descriptors and thus enhance the search. Use for example those that are invariant objects, count the number of holes or the Euler number.

ACKNOWLEDGEMENTS

The authors acknowledge the support received from the Instituto Politécnico Nacional and the Escuela Superior de Computo.

REFERENCES

[1]. María Teresa Escobedo Portillo, Jorge A. Salas Plata MendozaP. CH. Mahalanobis y las aplicaciones de su distancia estadística; CULCyT, 2008.

[2]. Lira Chávez, J.. Introducción al tratamiento digital de imágenes. Ciencia de la Computación, InstitutoPolitécnico Nacional, Universidad Nacional Autónoma de México.2002.

[3]. Guevara, M. L., Echeverry Correa, J. D., & Ardila Urueña, W. (2008). Detección de rostros en imágenes digitales usando clasificadores en cascada. Scientia.

[4]. VIOLA, Paul y JONES, Michael "Robust Real-Time Object Detection" En International Conference on Statistical and Computational Theories of Vision – Modeling, Learning, Computing and Sampling (2001, Vancouver, Canada). Memorias. Canada.

[5]. FREUND Yoav, y Robert E., SCHAPIRE. "A decision-theoretic generalization of on-line learning and an application to boosting". En Computational Learning Theory: Eurocolt '95, pp. 23–37. Springer- Verlag, 1995

[6]. Mahalanobis, P. C. .On the generalized distance in statistics.Proceedings of the National Institute of Sciences (Calcutta), 2, 49-55, 1936.

[7]. Danielsson, P. E..Euclidean distance mapping. Computer Graphics and image processing, 14(3), 227-248.1980

[8]. PANTIC, Maja y ROTHKRANTZ, León M. "An Expert System for Recognition of Facial Actions and their Intensity". En Seventeenth National Conference on Artificial Intelligence and Twelfth Conference on Innovative Applications of Artificial Intelligence (2000, Austin, Texas).Memorias.EUA.ed. AAAI Press / The MIT Press. 2000. pp. 1026 – 1033.A. Blake and M. Isard. Active Contours.Springer, 1998.

ISSN (e): 2250 – 3005 || Vol, 04 || Issue, 11 || November– 2014 ||
International Journal of Computational Engineering Research (IJCER)

Design, Analysis and Manufacturing of Hydro-pneumatic Press Machine

Gaurav Pradip Sonawane[1], Gaurav Shashikant Udgirkar[1], Shailesh Vijay Shirsath[1], Manish Sudhir Deshpande[1]

(B.E. Students, Department of Mechanical Engineering, K. K. Wagh Institute of Engineering Education and Research)

ABSTRACT

A Hydro-pneumatic press is a press machine utilizing both air and oil in its operation and gives higher outlet hydraulic pressure with lower inlet pneumatic pressure. In this project the press is design and manufacture for pressing sleeve bearing into the circular casting part. Casting part is thick cylinder and sleeve bearing is kind of cylindrical bearing. Two actuators are used in the press one is for vertical pressing and other is for horizontal pressing. This paper includes the concept development, design, analysis and manufacturing of press machine. Various parts of the press are modelled by using Pro-E modelling software. Structural analysis has been applied on the parts of press machine by using analyzing software ANSYS.

KEYWORDS: *Hydro-pneumatic, High outlet pressure, Low inlet pressure, Circular casting part, Sleeve bearing, Pro-E, ANSYS.*

I. INTRODUCTION

A system utilizing both air and oil in its operation and gives higher outlet hydraulic pressure with lower inlet pressure is called as hydro-pneumatic system. Hydro-pneumatic systems can give maximum pressure up to 700 bar. No worry of handling oil pumps or tanks and it comes in compact unit. The frame is designed for pressing of four sleeve bearing two are horizontally and two are vertically into circular casting part hence following points are take into considerations[1]. Figure 1.1 shows model hydro-pneumatic press.

- Arrangement for two actuators, one is horizontal and other is vertical
- Use of arrangement on which hitch yoke is placed for assembly and worker can access it in straight comfortable position
- For achieving positional accuracy some sliding arrangement should provided so that yoke can easily placed or lift with the help of hoists and then slide at proper position for pressing
- Yoke should place on the machining surface to achieve dimensional accuracy

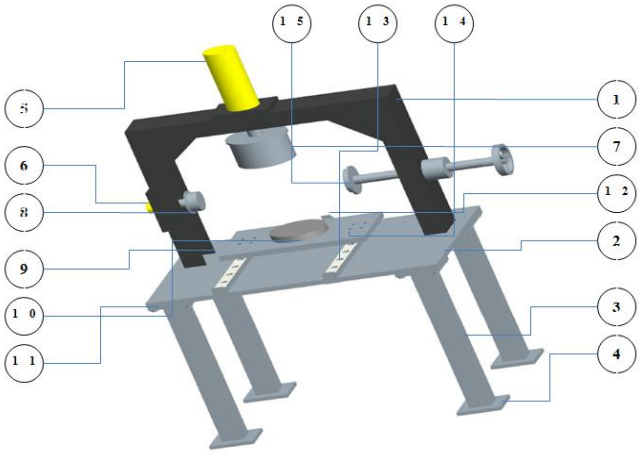

Figure 1.1: Pro-E model of press machine

Table 1.1 includes details of all components required for building the actual model of hydro-pneumatic press.

Table 1.1 List of component.

Component number	Description	Quantity
1	C - Frame	1
2	Base Plate	1
3	Support Column	4
4	Support Plate	8
5	Central Cylinder	1
6	Side Cylinder	1
7	Central Ram	1
8	Side Ram	1
9	Sliding Plate	1
10	Circular Plate	1
11	Bolts	38
12	Stopper	1
13	Rail	2
14	Block Bearing	2
15	Side Support	1

II. WORKING

Hydro-pneumatic system is divided into two main components i.e. hydro-pneumatic pump and cylinder. Main components of hydro-pneumatic pump are air motor, gearbox, eccentric, pump and oil reservoir. Spring operated check valve is provided at inlet port of pump. Connect the pump to the pneumatic connection of compressor. Air motor rotates by air and rotates the shaft of gear box. Reduction gear reduces the speed of outlet shaft on which eccentric cams are mounted. Cams move the pistons of two piston pumps and hydraulic oil enter into cylinders at continuous flow rate and hence smooth stroke is obtained.

Now connect the pump to central cylinder by quick acting coupling and operate the control valve which gives the forward stroke to press first two bearings. The oil enters in the cylinder from pump at controlled rate hence slow forward stroke is achieved. After pressing first bearing, again operate the control valve which releases the pressure on cylinder and return stroke is achieved with help of spring. Similarly connect the pump to the side cylinder and press side bearings. Figure 2.1 shows the circuit diagram of press machine.

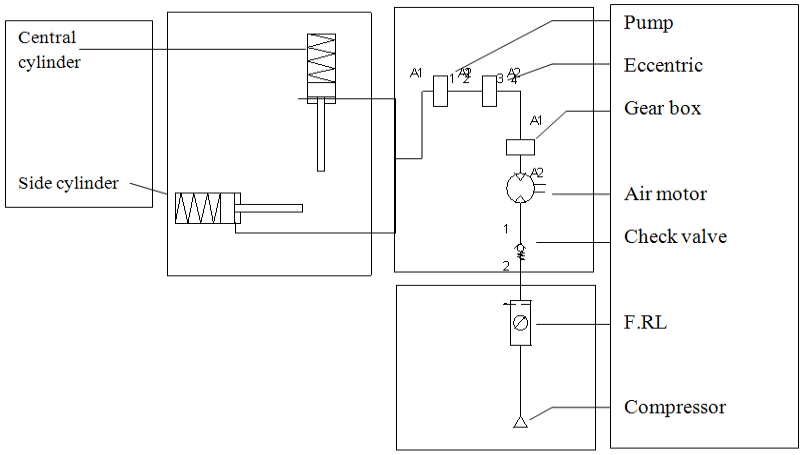

Figure 2.1: Circuit diagram of press machine

III. MATERIAL SELECTION

Material is selected based on properties such as high bending & tensile strength, ease of availability, ease of machining, welding, finishing, cutting etc. and cost factor. Component number 1, 2, 3, 4, 8, 9, 10, 12 and 15 will use the Mild steel/ plain carbon steel (25C8/ AISI 1025). Material Properties of 25C8 are given in Table 3.1 below:

Table 3.1 Material property

Parameter	Details
Material	25C8
Tensile strength, (σ_t)	390 N/mm^2
BHN	170 HB
Elastic modulus, (E)	210 GPa

http://www.btss.in/technical.php

IV. DESIGN CALCULATION

Following are the main components required for design of press and they are designed considering the specification given in the Table 4.1.

a) C – Frame.
b) Base plate
c) Sliding plate.
d) Support column.
e) Side support.

Table 4.1 shows required cylinder specifications of machine.

Parameter	Central Cylinder	Side Cylinder
Press load	23 *KN*	8 *KN*
Stroke length	304 *mm*	54 *mm*

4.1 Design of C-frame

Functional requirement: Length of upper beam = 900 mm and length of side column = 700 mm are taken considering the job size, horizontal stroke and vertical stroke length required for pressing operation.

C-frame design is divided into two main parts as;
a. Design of upper beam b. Design of left and right side column

a. Design of upper beam

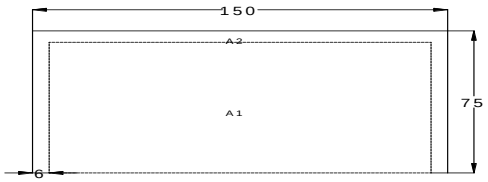

Figure 4.1: Cross section of upper beam & side column

Position of neutral axis, $Y = \frac{A_1 Y_1 - A_2 Y_2}{A_1 - A_2}$ [2]

A_1 = 75 x 150 = 11250 mm^2 A_2 = (150-12) x (75-6) = 9522 mm^2
y_1 = 75/2 = 37.5 mm y_2 = (75-6)/2 = 34.5 mm

$Y = \frac{(11250 \times 37.5) - (9522 \times 34.5)}{11250 - 9522}$ = 54.03 mm

Moment of Inertia, $I = I_{xx1} - I_{xx2} = (I_{G1} + A_1 h_1^2) - (I_{G2} + A_2 h_2^2)$ [2]

$$I = \frac{150 \times 75^3}{12} + [11250 \times (54.03 - 37.5)^2] - \frac{138 \times 69^3}{12} + [9522 \times (54.03 - 34.5)^2]$$

$I = 940 \times 10^3$ mm^4 ----------(1)

Since the beam is subjected to hogging bending moment, compression neutral axis
$y = y_c = 54.0$ mm, $y_t = 75 - 54.03 = 20.97$ mm
Bending moment M from loading diagram
$M_A = R_B \times 900 - 23 \times 400 = 0$
$R_B = 10.22$ KN $R_A + R_B = 23$ $R_A = 12.77$ KN

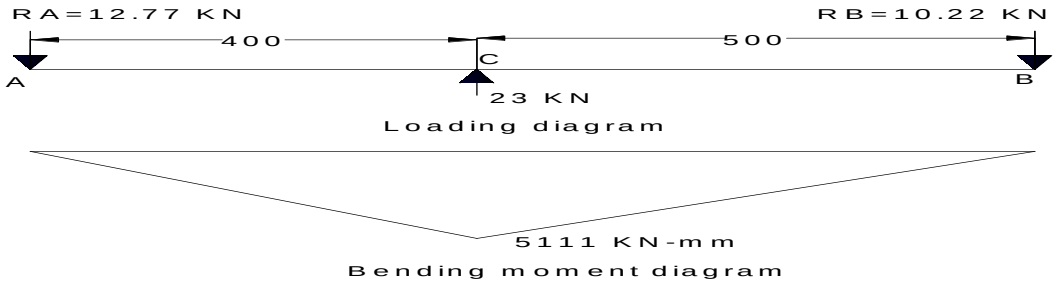

Figure 4.2: Loading & Bending moment diagram of upper beam

Moment at C= M_C = 10.22 x 500 = 5111 KN-m

Compressive stress at C= Max stress $= \frac{M_C Y_C}{I} = \frac{(5111 \times 103 \times 54.03)}{940 \times 10^3}$ = 114.01 N/ mm^2

Material of beam is 25C8, S_{yt}= 390$\frac{N}{mm^2}$ [5]

Max allowable stress = 390 / 1.5 = 260 N /mm^2------ (Assume F.O.S. = 1.5)

Max. allowable stress > Max. compressive stress in beam, Hence design is safe

b. Design of left and right side column

Figure 4.1 shows the dimensions of selected column cross-section.

Consider column AB of length L is fixed at one end and other end is hinged

Effective length, $L_e = L/\sqrt{2}$ = 700 /1.4142 = 494.97 mm [3]

Least moment of inertia I = 940 x 10 ^{3} mm^4 ---------- from (1)

Modulus of elasticity for 25C8, E= 200 x 10 ^{3} N/ mm^2 [5]

Crippling load by Euler's formula[3],$P_c = (\pi^2 EI)/L_e^{\,2} = \frac{(\pi^2 \times 200 \times 10^3 \times 940 \times 10^3)}{494.97^2} = 7.573 \times 10^6$ N

Safe load $P_s = P_c/F.O.S. = {}^{(7.573 \times 10^6)}/_{3}$---------- (Assume F.O.S. = 3)

= 2.52 x 10^6 N > 23318.825 N Hence design is safe

4.2 Design of base plate

Functional requirement: Length = 1000 mm and width = 700 mm of base plate is required for easy mounting of all components and easy pressing operation.

Total load acting on base plate = {(7Kg (Upper cylinder) + 2 Kg (Side cylinder) + 23.5 Kg (Sliding plate) + 11.775 Kg (Mounting plates) + 16.120 Kg (Upper ram) + 8.9 Kg (Side ram) + 22.75 Kg (Rails) + 20.22 Kg (Support) + 6.81 Kg (Circular plate) + 93.9 Kg (Hitch yoke) } x 9.81 + 23000 N (Force by cylinder)
= 25089.28 N

From loading diagram shown in Figure 4.3

Moment at C = Max. Moment [4]= $WL^2/8 = [(25.08 \times 10^{-3}) \times 1000^2]/8$ = 3135 KN-mm

Moment of Inertia (I)= $bt^3/12 = 700 \times d^3/12 = 58.33 \times t^3 mm^4$

Using bending formula, $\frac{M}{I} = \frac{\text{bending stress}}{y}$; $\frac{(3135 \times 10^3)}{(58.33 \times t^3)} = \frac{\text{bending stress}}{y}$ [4]

For 25C8, Syt = 390 N / mm^3 [5]

Allowable bending stress = $\frac{S_{yt}}{F.O.S.} = \frac{390}{1.5}$---- (Assume F.O.S =1.5)

= 260 N / mm2

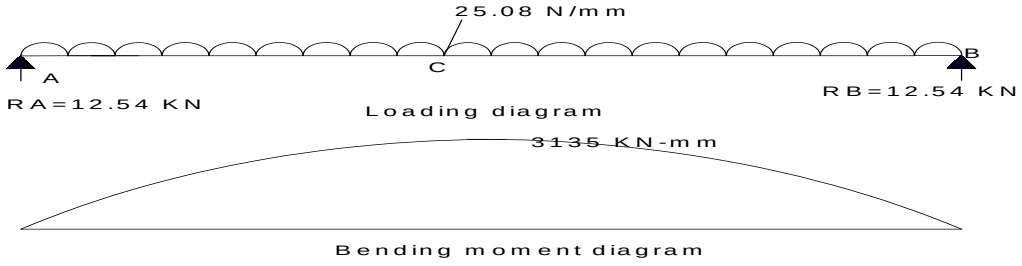

Figure 4.3: Loading & Bending moment diagram of base plate

Therefore $\frac{(53745.92)}{(t^3)} = \frac{130}{t}$

Thickness of plate, t = 20.33 mm

Hence plate with thickness 22 mm is selected for safe design

4.3 Design of sliding plate

Functional requirement: Length = 500 mm and width = 300 mm of sliding plate is restricted for easy rail mounting and considering the yoke size.

Total load acting on base plate = {(6.81 Kg (Circular plate) +93.9 Kg (Hitch yoke)} x 9.81 + 23000 N (Force by cylinder)
= 23927.969 N

From loading diagram shown in Figure 4.4
Moment at C = Max. Moment =11.96 × 200 – (0.124 × 96 ×96/2) =1820.60 KN-mm
Moment of Inertia, (I) =$bt^3/12$= 300 d^3/12 = 25t^3 mm^4

Using bending formula, $\frac{M}{I} = \frac{\text{bending stress}}{y}$; $\frac{1820.60\times10^3}{25t^3} = \frac{\text{bending stress}}{y}$ [4]
for 25C8,Syt = 390 N / mm^3 [5]
Allowable bending stress, $\frac{S_{yt}}{F.O.S.} = \frac{390}{1.5}$-------- (Assume F.O.S =1.5)
= 260 N / mm^2

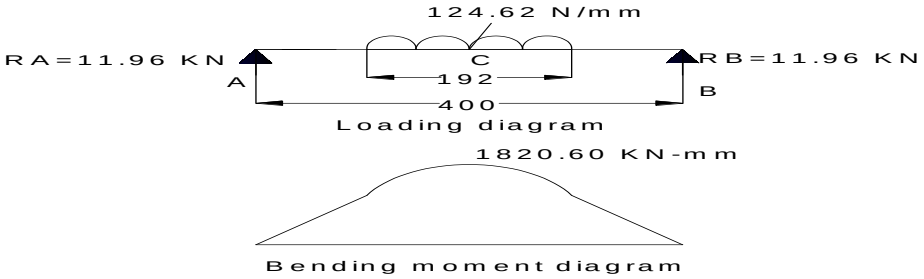

Figure 4.4: Loading & Bending moment diagram of sliding plate

Therefore $\frac{72824}{t^3} = \frac{130}{t}$
Thickness of plate, t = 23.66 mm
Hence plate with thickness 25 mm is selected for safe design

4.4 Design of support column
Functional requirement: Length = 700 mm of support column is required for easy operating and comfort of worker.

Consider column AB of length L is fixed at both ends

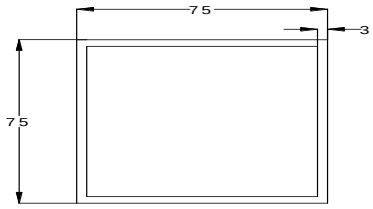

Figure 4.5: Cross section of support column

Effective length [2], $L_e = L/\sqrt{2}$= 700 /1.4142 = 494.97 mm
Least moment of inertia $I = BD^3/12 - bd^3/12 = 75 \times 75^3/12 - 69 \times 69^3/12$
$=747.792 \times 10^3$ mm^4

Modulus of elasticity for 25C8, E= 200 x 10^3 N/ mm^2 [5]
Crippling load by Euler's formula,$P_c = (\pi^2 EI)/L_e^2 = \frac{(\pi^2\times200\times10^3\times747.792\times10^3)}{494.97^2}$ [2]
$= 6.024 \times 10^6$ N
Safe load $P_s = P_c/F.O.S. = {(6.024 \times 10^6)}/{3}$ ---------- (Assume F.O.S. = 3)
= 2008.31KN> 6.25 KN Hence design is safe

4.5 Design of side support

Functional requirement: Length of rod = 450 mm is required easy access and safe operation.

Max. Pressure = $p_{max=}$ 150 bar = 15 $\frac{N}{mm^2}$

$$\text{pressure } (p) = \frac{\text{force}}{\text{area}}$$

Force = $15\times (\frac{\pi}{4} d^2) = 117.809\times 10^3$ N

Max. Force = f_{max} = $(117.809\times 10^3) \times (0.6\times 9.81\times 100) = 118.397\times 10^3$ N

Allowable stress = $\sigma_{allowable} = \frac{s_{ut}}{Nf} = \frac{390}{3} \frac{N}{mm^2} = 130 \frac{N}{mm^2}$ for 25C8 [5]

Maximum stress = $\sigma_{max} = \frac{F_{max}}{area} = 130 \times 10^3 = \frac{118.397\times 10^3}{\frac{\pi}{4} d^2}$

Diameter of rod = d =$38.07 \approx 40$mm [4]

V. ANALYSIS

This section shows the details of Finite Element Analysis of this developed model. The Finite Element Method is the easy technique to the theoretical method to find out the stress developed in various components of press. In this paper Finite Element Analysis is carried out in ANSYS Workbench 11 to determine the maximum stress developed in press. Also the deformation is found out for various component of press.

5.1 Steps in analysis:

a. Step 1: Import geometry

Figure 5.1 shows Pro-E model imported in Ansys.

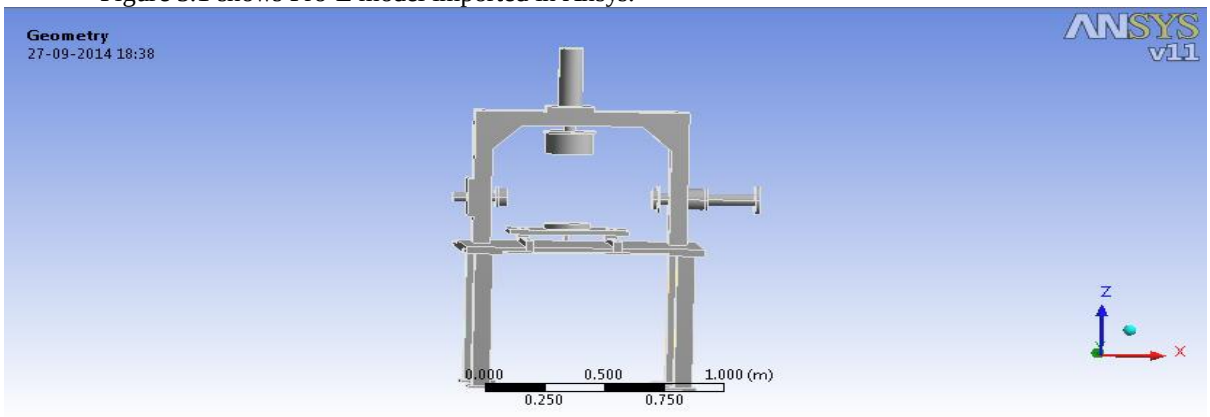

Figure 5.1: 3-D geometry of hydro-pneumatic press machine

b. Step 2: Meshing

Figure 5.2 shows the component meshing. Cores meshing of geometry are performed.

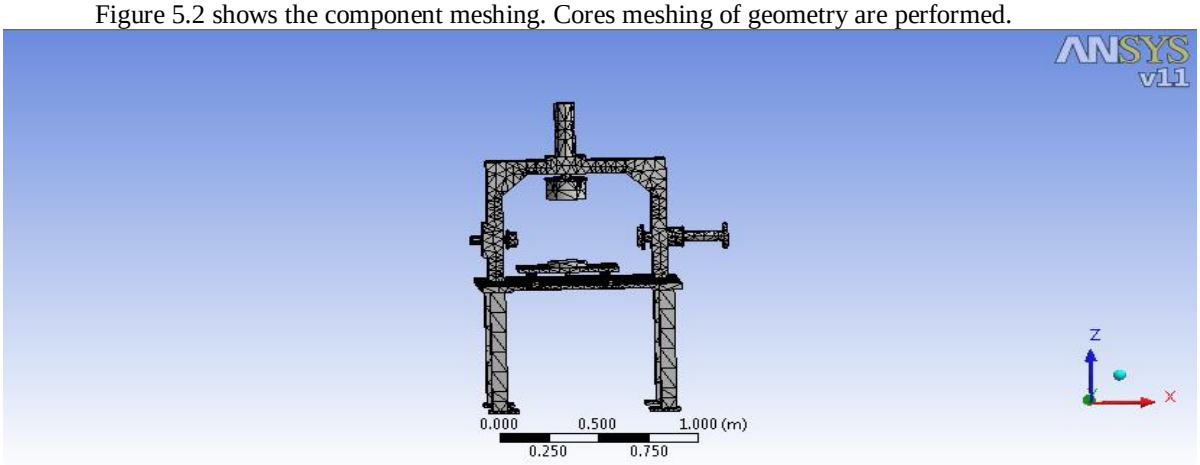

Figure 5.2: Coarse mesh of hydro-pneumatic press machine

c. Step 3: Boundary conditions:

Base columns are fixed as per required initial condition. The load of 23000 N is applied on the central ram and the sliding plate and 8000 N is applied on the side ram and side support which replicate actual working condition in simulation. Figure 5.3 shows the boundary conditions.

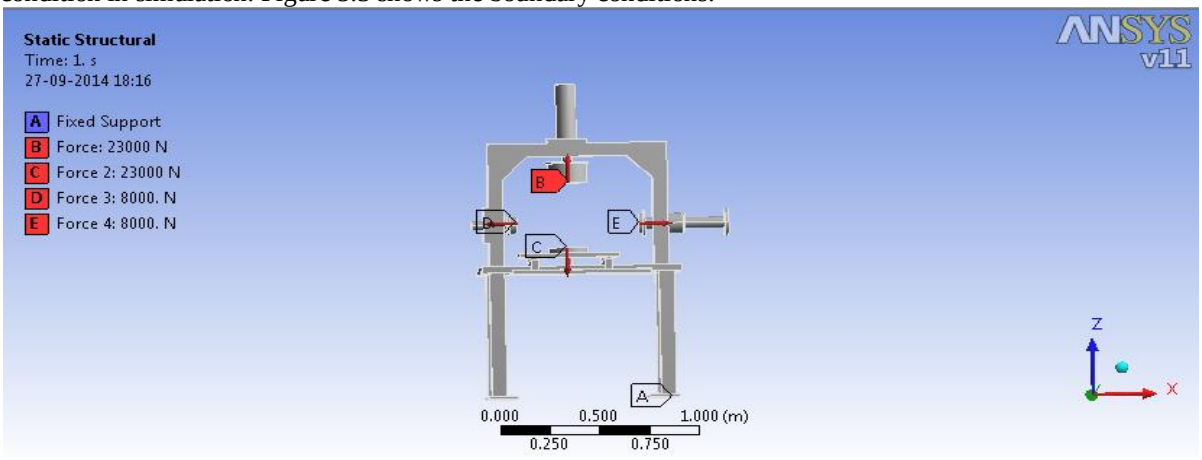

Figure 5.3: Boundary conditions.

VI. RESULTS AND DISCUSSION

The design had main focus on reducing operator fatigue and increase safety, improving the flexibility and makes operation more convenient, and to achieve dimensional and positional accuracy. Components of press are designed to avoid bending failure due to applied load. Mild steel is selected as material based on its properties such as high bending & tensile strength, it compatibility with operation like machining, welding, finishing, cutting etc. and cost as economic factor.

Result of the Finite Element Analysis, it shows that the maximum nodal displacement magnitude on the hydro pneumatic press is 0.00034255 mm as shown in Figure 6.1 when maximum load 23000 N is applied on base plate due to action of actuator. Following result shows that maximum Von Misses stress, maximum principle stress, maximum shear stress values in safe point because analyzed stress < calculated stress. Compression between analyzed and allowable material value of stress are in Table 6.1 below:

Table 6.1 Stress comparison table

Parameter	Analytical	Allowable	Safety
Von-miss stress	108.54 N/mm^2	*130 N/mm^2*	Safe
Max. Principle stress.	123.09 N/mm^2	*130 N/mm^2*	Safe
Max shear stress	58.06 N/mm^2	65 N/mm^2	Safe

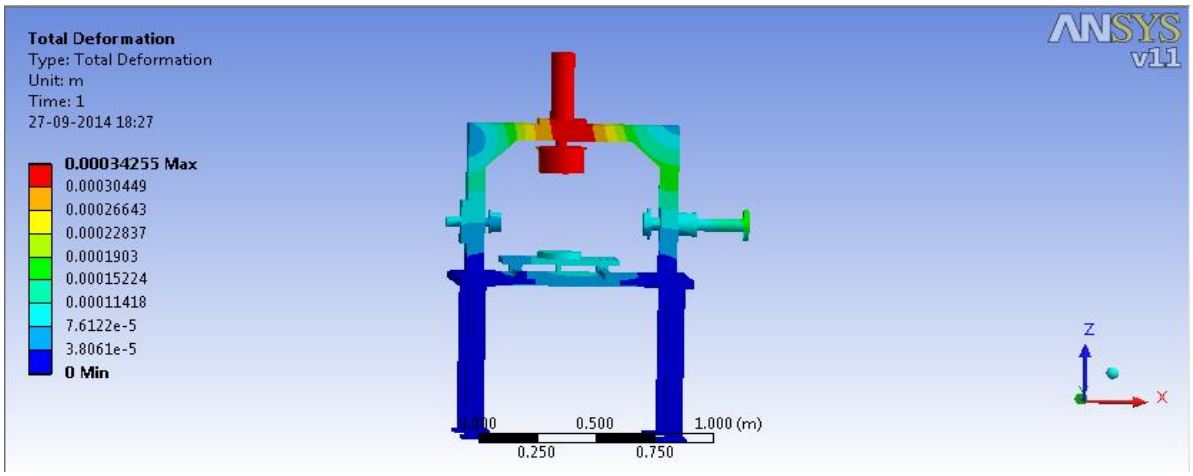

Figure 6.1: Deformation pattern for hydro-pneumatic press machine

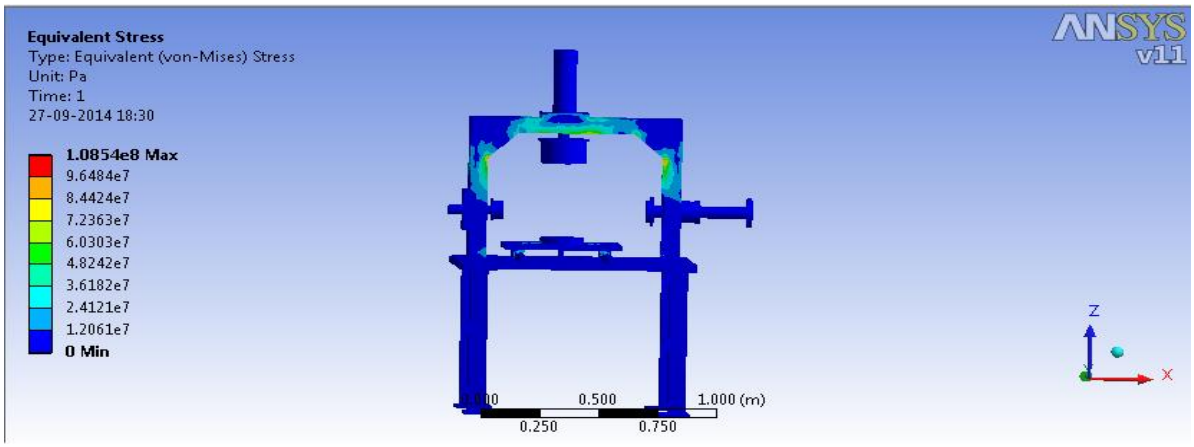

Figure 6.2: Von Miss Stress distribution.

VII. MANUFACTURING PROCEDURE

Plates of size 1000x700x22 mm, 500x300x25 mm, 150x150x16 mm; Hollow columns of size 75x75x700 mm; C-channel of size 150x75x6 mm and Rods of size ϕ192x30 mm, ϕ40x490 mm obtained from the structural steel vendor. All of the above are slightly finished by the hand grinder.

Base plate is manufactured from 1000x700x22 mm plate by drilling 16 holes of ϕ14 at each corner using vertical drilling machine and tapped to ϕ16 mm, same holes are obtained on four plates of size 150x150x16 mm. 18 holes of ϕ12mm are drilled and tapped to ϕ14mm on base plate by keeping 100mm offset from centre on which rails are fitted by bolts. Four plates of size 150x150x16 with holes and four more such a plate without holes are welded on both ends of four hollow columns of size 75x75x700 mm. These columns are then bolted to the base plate by std. bolts of ϕ16 mm dia. as shown in Figure 7.1

Fig 7.1: Stage 1.

Fig 7.2: Stage 2.

The sliding plate i.e. 500x300x25 mm plate is drilled on both sides with four holes of ϕ8mm and tapped to ϕ12mm. Central hole of ϕ8mm is also drilled on this plate on which the rod of ϕ192x30mm is joined by inserting a pin. The whole assembly is then mounted on the block bearing of rails as shown in Figure 7.2

C-channel is cut using the power hacksaw for the length of 500mm, 700mm and 700mm. 45 degree cuts are obtained on C-channel which is then end mill on HMC machine and weld together using arc welding to obtain C-frame. Holes are drilled on C-channel for mounting of hydrodynamic cylinder on which support plate are welded for rigidity. Support of hitch yoke is made from ϕ40x490mm rod which is turn on lathe machine and handle is weld at one end, this is inserted in the bush which mounted on C-frame. Finally the C-frame is welded on base plate using arc welding and cylinders are mounted on the C-frame as shown in Figure 7.3.

Fig 7.1: Actual Hydro – Pneumatic Press machine.

VIII. CONCLUSION

The press was developed after studying the pneumatic system, hydraulic system and hydro – pneumatic system, were it was found that hydro – pneumatic system is more effective the pneumatic and cost efficient than hydraulic system. The system has shown noticeable improvements in various sectors like operation time and cost of operation. It is observed that operation time is reduced from 3 hours to 30 min per assembly and cost of operation is reduced approximately by 90 %. The further advantages of the system has covered the safety of operator and made operation more convenient (reducing fatigue), improved dimensional and positional accuracy of assembly.

REFERENCES

[1]. MalachySumaila and AkiiOkonigbonAkaehomenIbhadode , (Jan. 2011), "Design and Manufacture of 30 ton hydraulic press", Mechanical Engineering Department, Federal University of TechnologyYola, Admawa State Nigeria; A.U.J.T. 14(3): 196-200.
[2]. Bhandari, V.B. (2009), "Design of Machine element", Tata McGraw-Hill Education.
[3]. Khurmi, R.S. and Gupta, J.K. (2005), "A Teaxtbook of Machine Design", Eurasia Publication House (P.V.T.) Ltd. 14th Edition, 1230pp. ISBN: 81-219-2537-1.
[4]. "Fundamentals of Machine Elements", Bernand J. Hamrock, Bo Jacobson, Steven R. Schmid; WCB/McGraw-Hill International Edition; 1999.
[5]. S.G. College of Technology. (2000), "Design Data Book", Coimbatore Publication, 4_{th} Edition.

ISSN (e): 2250 – 3005 || Vol, 04 || Issue, 11 || November– 2014 ||
International Journal of Computational Engineering Research (IJCER)

Performance Characteristics of various Corrugated Roofing Sheets in Nigeria

A. J. Ujam[1]*, S. O. Egbuna[2] and S. Idogwu[1]
[1]*Department of Mechanical & Production Engineering, Enugu State university of Science And Technology,(ESUT), Enugu.*
[2]*Department of Chemical Engineering, Enugu State university of Science And Technology,(ESUT), Enugu.*

ABSTRACT:
This Paper is based on an experiment carried out on different roofing sheets namely aluminum, galvanized steel, plastic and asbestos of various grades. The aluminum samples were obtained from two different companies in Nigeria namely First Aluminum and Tower Aluminum; the Asbestos was obtained from Emenite while the Steel and Plastic samples were bought from the market. The samples were cut into a particular size (8cm by 5cm) and immersed in various media namely acidic ***(H_2SO_4)****, alkaline* ***(NaOH)****,* ***Sea water*** *and* ***Rain water*** *in 2litres plastic beakers. The Rain water was used as the control medium for the experiment. The experiment was carried out for 70days and each grade was cut into 14 pieces of the same dimension. The samples were washed, weighed and tagged before immersion in the media. Each sample was removed every 5 days, washed thoroughly, dried and re-weighed. Some of the samples corroded while some resisted corrosion. The differences in the weights of the samples, and hence their respective rates of corrosion were obtained depending on the reacting media. The values that were obtained, the weight loss and weight gain were used to determine the corrosion rates per unit area per unit time. Graphs of specific weight loss/gain against time were plotted for each medium and each sample. Based on our graphs and observations, we can say that the coated samples are more resistant to corrosion, and therefore more durable.*

KEYWORDS: *Roofing Sheets, Aluminum, Galvanized Steel, Corrosion, Asbestos.*

I. INTRODUCTION

It is an indisputable fact that the roofing of one house turns reddish or brownish after awhile while another doesn't change or react at the same rate under the same environmental condition though they may be roofed with the same or different corrugated roofing sheets.

This aroused our interest to investigate the effect of different media on the corrosion kinetics of different types of corrugated roofing sheets in Nigeria.

Corrosion is defined in different ways, but the usual interpretation of the term is "an attack on a metallic material by reaction with its environment". **[1]** The material is progressively destroyed by the chemical action of the environment on it.

The concept of corrosion can also be used in a broader sense, where this includes attack on nonmetallic materials. Corrosion does occur in polymers and ceramics, but the mechanisms are quite different from those of metals, and are more often known as degradation. **[2]**Metallic systems are the predominant materials of construction, and as a class, are generally susceptible to corrosion. Consequently the bulk of corrosion science focuses on metals and alloys.

With a few exceptions, metals are unstable in ordinary aqueous environments. Certain environments offer opportunities for these metals to combine chemically with elements to form compounds and return to their lower energy levels, which is more stable and non-reactive. **[3]**

Generally, this destruction takes place on its surface in the form of material dissolution or re-deposition in some other form. Corrosion may occur over an entire exposed surface, more or less uniformly corroding the surface or may be localized at micro or macroscopic discontinuities in the metal to form pits or cracks. **[4]**

The most familiar example of corrosion is the rusting of iron, a complex chemical reaction in which the iron combines with both oxygen and water to form hydrated iron oxide. The oxide is a solid that retains the same general form as the metal from which it is formed but, porous and somewhat bulkier, and it is relatively weak and brittle, and still allows the corrosion effect of the environment to get to through to the uncorroded underlying metal. **[5]**

Because corrosion is a diffusion controlled process, it occurs on exposed surfaces. As a result, methods to reduce the activity of the exposed surface, such as passivation, galvanizing, chromate-conversion, etc can increase a material's corrosion resistance. However, some corrosion mechanisms are less visible and less predictable. **[6]**

Corrosion affects our Nation's force effectiveness and readiness levels through the diminished safety and reliability of structures, mechanisms and electronics.

In many cases, corrosion is the life-limiting factor of a component. Corrosive failures can occur unexpectedly and at the worst possible moment.

Metallurgical factors that affect corrosion are chemical composition, material structure, grain boundaries, alloying elements, mechanical properties, heat treatment, surface coating, welding and manufacturing conditions. Understanding these factors are of great importance to decrease and control corrosion problem in many industrial applications. **[7]**

Corrosion testing can consume enormous blocks of time, particularly in the case of outdoor atmospheric tests. Unfortunately, the timescales involved in such tests preclude the opportunity for proper materials selection. In typical circumstances, new systems may be halfway through their lifecycle before real data on the fielded system would indicate any corrosion problems. **[8]**

The serious consequences of the corrosion process have become a problem of worldwide significance. Managing corrosion in structural components and critical systems to extend service life and ensure reliability is paramount. **[9]**

Corrosion resistance and control is a process by which humans employ the application of sound principles and try to regulate the rate of corrosion in different materials and for different environments, keeping it acceptable or at least predictable limits for the life of the structure. **[10]**

Effective corrosion control requires meaningful test data in a reasonable time frame such that it may be employed to influence materials selection and protection efforts.**[11]**

Corrosion control is achieved by recognizing and understanding corrosion mechanisms, by using corrosion- resistant materials and designs, and by using protective systems, devices, and treatments**.[12]**

The control of corrosion through the use of coatings, metallurgy, and nonmetallic materials for constructions, cathodic protection and other methods has evolved into a science in its own right and has created industries devoted solely to corrosion control.

Major corporations, industries, and government agencies have established groups and committees to look after corrosion-related issues, but in many cases the responsibilities are spread between the manufacturers or producers of systems and their users.

II. MATERIALS AND METHOD

This study consists of series of tests and experiment carried out over a period of seventy (70) days on the samples:

- First Aluminum brand
- Tower Aluminum brand
- Double Hand Steel brand
- Swan Milligram Steel brand
- Plastic sheets
- Asbestos sheets

The samples were tested in different environments, to find out and observe the effect of the media on the sample, the rate of corrosion by weight loss or weight gain, weight loss or gain per unit area.

The media which the tests were carried out in are:

Acid Medium: Tetraoxo Sulphate VI acid, H_2SO_4

- Alkali Medium: Sodium Hydroxide, NaOH
- Sea water Medium
- Rain water Medium

2.1 Sample Sourcing

The materials used for this study are: aluminum roofing sheets, obtained from First Aluminum and Tower Aluminum, asbestos roofing sheets obtained from Emenite, galvanized steel roofing sheets, swan milligram and double hand brand and plastics roofing sheets were all obtained from Eke Awka Market, Awka in Anambra state of Nigeria.

2.2 Sample Preparation

The samples were arranged and named as follows:
Aluminum sample 1: First Aluminum (Al 1, coated)
Aluminum sample 2: Tower Aluminum (Al 2, uncoated)
Aluminum sample 3: Tower Aluminum (Al 3, coated)
Steel sample 1: Swan Milligram (St 1, uncoated)
Steel sample 2: Double hand (St 2, uncoated)
Steel sample 3: Coated brand (St 3, coated)
Plastic sample 1: colored (Pl 1)
Asbestos sample 1: plain (Ab 1)
Asbestos sample 2: colored (Ab 2)

2.2.1 Cutting

The samples were cut to the same dimension of 8cm by 5cm. The cutting was done with a pair of scissors and was marked out with the aid of a meter rule.

2.2.2 Washing

The cut samples were washed thoroughly, to remove all traces of dirt, oil or grime, and were then dried thoroughly before weighing. This was to make sure the weight gotten was accurate, and to prevent reactions with impurities.

2.2.3 Tagging

All the samples were individually tagged and labeled using masking tape, for easy identification and recognition, to avoid mistakes of mixing the samples up. The beakers we used were perforated in preparation for hanging in the samples for immersion in the medium; these were also properly tagged and named.

2.2.4 Weighing

The samples were all weighed using an electronic digital meter. These weights make up the initial weights of the samples.
The thickness of each sample was equally obtained with the aid of a micro meter screw gauge.

2.3 Media/Solution Preparation

The solution used was 0.01M (mole) of tetraoxosulphate VI acid H_2SO_4, 0.01M sodium hydroxide NaOH, Sea water obtained from Atlantic Ocean and Rain water.

2.3.1 Acid Concentration Preparation

Amount to produce 0.01 molar concentration of H_2SO_4
=molecular weight/ (specific gravity x percentage purity)
=98.08/ (1.84 x 0.98) = 54.4ml
= 0.01 X 54.4 = 0.544ML
0.544ml of H_2SO_4 was needed to make up 1dm³of deionized water to obtain 0.01 molar concentration of acid.

2.3.2 Alkali Concentration Preparation

Amount to produce 0.01 molar concentration of NaOH
= 40g of NaOH in 1dm³ of deionized water make up I molar NaOH
i.e. 40g/L = 1M
Therefore, 0.01M = 0.4g of NaOH
0.4g of NaOH was weighed and 1dm³ of water was poured in to make 0.01 molar concentration of sodium hydroxide.
The various PHs of the environments were taken before the samples were immersed. They are:
Acidic medium: pH of 2.0
Alkaline medium: pH of 11.0
Sea water medium: pH of 6.0
Rain water medium: pH of 6.0

2.4 The Trial Test

This trial test was carried out on the samples in the acidic and alkaline media. The molar concentration used was 2.5 M, for both the acid and base solutions. This was done to determine the time it would take for each of the samples to completely deteriorate. This helped us choose the molar concentration we eventually used, and the interval for the withdrawal of the samples from the solutions.

The rate of reaction of the samples in the 2mole solution of both the acid and base was very spontaneous, and within 24 hours, all the samples had deteriorated.

This led us to use a molar concentration (0.01) that was not so far from the ambient condition (0.001), but still capable of yielding results in the given duration of our experiment.

2.5 Sample Immersion

The prepared samples were then immersed in 1.5dm³ of each of the solutions listed above. The different samples, 14 pieces each for each sample were immersed in each of the environments for seventy (70) days.

After every 5-day interval, one sample from each environment is removed from solution, washed thoroughly in deionized water, to remove all residual traces of the solution it was removed from, and to stop further reactions. The washed samples were hung to effect quick drying, and then reweighed to get their final weights.

Fig. 1 The Experimental Set-Up

III. RESULT AND DISCUSSIONS

3.1 Presentation of Results

The results we obtained from this experiment carried out for seventy days are presented in tables and graphs, for ease of presentation and analysis.

3.2 Tables

Table 1: Aluminum sample 1: First aluminum (coated). Thickness – 0.58mm in 0.01 mole H_2SO_4

Time (days)	Initial weight (grams)	Final weight (grams)	Weight loss (Iw-Fw) (grams)	Specific weight loss (g/(cm)²)
5	4.15	4.15	0.00	0.00000
10	4.17	4.17	0.00	0.00000
15	4.20	4.20	0.00	0.00000
20	4.20	4.19	0.01	0.00025
25	4.21	4.20	0.01	0.00025
30	4.24	4.23	0.01	0.00025
35	4.24	4.23	0.01	0.00025
40	4.27	4.26	0.01	0.00025
45	4.28	4.26	0.02	0.00050
50	4.28	4.26	0.02	0.00050
55	4.30	4.28	0.02	0.00050
60	4.31	4.29	0.02	0.00050
65	4.34	4.31	0.03	0.00075
70	4.36	4.33	0.03	0.00075

Table 2:Aluminum sample 1: First aluminum (coated) Thickness – 0.58mm in 0.01 mole NaOH

Time (days)	Initial weight (grams)	Final weight (grams)	Weight loss (Iw-Fw) (grams)	Specific weight loss (g/(cm)²)
5	4.20	4.20	0.00	0.00000
10	4.20	4.20	0.00	0.00000
15	4.21	4.20	0.01	0.00025
20	4.22	4.21	0.01	0.00025
25	4.23	4.22	0.01	0.00025
30	4.23	4.22	0.01	0.00025
35	4.23	4.22	0.01	0.00025
40	4.25	4.24	0.01	0.00025
45	4.26	4.25	0.01	0.00025
50	4.26	4.24	0.02	0.00050
55	4.27	4.24	0.03	0.00075
60	4.28	4.25	0.03	0.00075
65	4.28	4.24	0.04	0.00100
70	4.30	4.25	0.05	0.00125

Table 3: Aluminum sample 1: First aluminum (coated) Thickness – 0.58mm in Sea water

Time (days)	Initial weight (grams)	Final weight (grams)	Weight loss (Iw-Fw) (grams)	Specific weight loss (g/(cm)²)
5	4.14	4.14	0.00	0.00000
10	4.14	4.14	0.00	0.00000
15	4.15	4.14	0.01	0.00025
20	4.16	4.15	0.01	0.00025
25	4.18	4.17	0.01	0.00025
30	4.19	4.18	0.01	0.00025
35	4.20	4.19	0.01	0.00025
40	4.20	4.19	0.01	0.00025
45	4.22	4.20	0.02	0.00050
50	4.23	4.21	0.02	0.00050
55	4.24	4.21	0.03	0.00075
60	4.24	4.21	0.03	0.00075
65	4.29	4.26	0.03	0.00075
70	4.31	4.28	0.03	0.00075

Table 4:Aluminum sample 1: First aluminum (coated) Thickness – 0.58mm in Rain water

Time (days)	Initial weight (grams)	Final weight (grams)	Weight loss (Iw-Fw) (grams)	Specific weight loss (g/(cm)²)
5	4.18	4.18	0.00	0.00000
10	4.18	4.18	0.00	0.00000
15	4.19	4.19	0.00	0.00000
20	4.21	4.20	0.01	0.00025
25	4.21	4.20	0.01	0.00025
30	4.24	4.23	0.01	0.00025
35	4.25	4.24	0.01	0.00025
40	4.25	4.24	0.01	0.00025
45	4.26	4.25	0.01	0.00025
50	4.29	4.27	0.02	0.00050
55	4.31	4.29	0.02	0.00050
60	4.31	4.29	0.02	0.00050
65	4.32	4.30	0.02	0.00050
70	4.32	4.30	0.02	0.00050

Table 5:Aluminum sample 2:Tower aluminum (uncoated) Thickness: 0.57mm in 0.01 mole H_2SO_4

Time (days)	Initial weight (grams)	Final weight (grams)	Weight loss (Iw-Fw) (grams)	Specific weight loss (g/(cm)²)
5	3.12	3.11	0.01	0.00025
10	3.12	3.11	0.01	0.00025
15	3.14	3.13	0.01	0.00025
20	3.15	3.14	0.01	0.00025
25	3.17	3.15	0.02	0.00050
30	3.18	3.16	0.02	0.00050
35	3.19	3.16	0.03	0.00075
40	3.20	3.17	0.03	0.00075
45	3.20	3.17	0.03	0.00075
50	3.22	3.18	0.04	0.00100
55	3.23	3.19	0.04	0.00100
60	3.23	3.19	0.04	0.00100
65	3.24	3.19	0.05	0.00125
70	3.25	3.20	0.05	0.00125

Table 6:Aluminum sample 2:Tower aluminum (uncoated) Thickness: 0.57mm in 0.01 mole NaOH

Time (days)	Initial weight (grams)	Final weight (grams)	Weight loss (Iw-Fw) (grams)	Specific weight loss (g/(cm)²)
5	3.16	3.26	-0.10	-0.00250
10	3.16	3.28	-0.12	-0.00300
15	3.17	3.30	-0.13	-0.00325
20	3.18	3.32	-0.14	-0.00350
25	3.18	3.32	-0.14	-0.00350
30	3.19	3.31	-0.14	-0.00350
35	3.21	3.35	-0.14	-0.00350
40	3.21	3.35	-0.14	-0.00350
45	3.22	3.37	-0.15	-0.00375
50	3.22	3.39	-0.17	-0.00425
55	3.24	3.46	-0.22	-0.00550
60	3.25	3.48	-0.23	-0.00575
65	3.25	3.48	-0.23	-0.00575
70	3.26	3.51	-0.25	-0.00625

Table 7:Aluminum sample 2:Tower aluminum (uncoated) Thickness: 0.57mm in Sea Water

Time (days)	Initial weight (grams)	Final weight (grams)	Weight loss (Iw-Fw) (grams)	Specific weight loss (g/(cm)²)
5	3.11	3.11	0.00	0.00000
10	3.13	3.13	0.00	0.00000
15	3.14	3.13	0.01	0.00025
20	3.15	3.14	0.01	0.00025
25	3.15	3.14	0.01	0.00025
30	3.17	3.16	0.01	0.00025
35	3.18	3.16	0.02	0.00050
40	3.19	3.17	0.02	0.00050
45	3.21	3.18	0.03	0.00075
50	3.22	3.19	0.03	0.00075
55	3.22	3.18	0.04	0.00100
60	3.23	3.18	0.05	0.00125
65	3.24	3.18	0.06	0.00150
70	3.24	3.18	0.06	0.00150

Table 8:Aluminum sample 2:Tower aluminum (uncoated) Thickness: 0.57mm in Rain Water

Time (days)	Initial weight (grams)	Final weight (grams)	Weight loss (Iw-Fw) (grams)	Specific weight loss (g/(cm)²)
5	3.12	3.11	0.01	0.00025
10	3.12	3.11	0.01	0.00025
15	3.14	3.13	0.01	0.00025
20	3.15	3.13	0.02	0.00050
25	3.18	3.16	0.02	0.00050
30	3.19	3.17	0.02	0.00050
35	3.19	3.16	0.03	0.00075
40	3.18	3.15	0.03	0.00075
45	3.20	3.17	0.03	0.00075
50	3.21	3.17	0.04	0.00100
55	3.21	3.17	0.04	0.00100
60	3.23	3.18	0.05	0.00125
65	3.23	3.17	0.06	0.00150
70	3.25	3.19	0.06	0.00150

Table 9: Steel sample 1: Swan Milligram (uncoated) Thickness: 0.19mm in 0.01 mole H_2SO_4

Time (days)	Initial weight (grams)	Final weight (grams)	Weight loss (Iw-Fw) (grams)	Specific weight loss (g/(cm)²)
5	5.80	5.80	0.00	0.00000
10	5.82	5.81	0.01	0.00025
15	5.83	5.82	0.01	0.00025
20	5.83	5.81	0.02	0.00050
25	5.85	5.83	0.02	0.00050
30	5.86	5.83	0.03	0.00075
35	5.89	5.86	0.03	0.00075
40	5.90	5.86	0.04	0.00100
45	5.92	5.86	0.06	0.00150
50	5.94	5.86	0.08	0.00200
55	5.94	5.85	0.09	0.00225
60	5.95	5.85	0.10	0.00250
65	5.97	5.87	0.10	0.00250
70	5.99	5.87	0.12	0.00300

Table 10: Steel sample 1: Swan Milligram (uncoated) Thickness: 0.19mm in 0.01 mole NaOH

Time (days)	Initial weight (grams)	Final weight (grams)	Weight loss (Iw-Fw) (grams)	Specific weight loss (g/(cm)²)
5	5.78	5.78	0.00	0.00000
10	5.81	5.80	0.00	0.00000
15	5.83	5.80	0.01	0.00075
20	5.83	5.80	0.01	0.00075
25	5.85	5.81	0.01	0.00100
30	5.86	5.81	0.02	0.00125
35	5.87	5.80	0.02	0.00175
40	5.88	5.80	0.03	0.00200
45	5.92	5.84	0.03	0.00200
50	5.94	5.85	0.03	0.00225
55	5.95	5.85	0.06	0.00250
60	5.98	5.87	0.06	0.00275
65	6.00	5.87	0.07	0.00325
70	6.01	5.87	0.08	0.00350

Table 11: Steel sample 1: Swan Milligram (uncoated) Thickness: 0.19mm in Sea Water

Time (days)	Initial weight (grams)	Final weight (grams)	Weight loss (Iw-Fw) (grams)	Specific weight loss (g/(cm)²)
5	5.79	5.78	0.01	0.00025
10	5.82	5.81	0.01	0.00025
15	5.83	5.81	0.02	0.00050
20	5.84	5.82	0.02	0.00050
25	5.85	5.83	0.02	0.00050
30	5.86	5.83	0.03	0.00075
35	5.89	5.86	0.03	0.00075
40	5.90	5.86	0.04	0.00100
45	5.92	5.88	0.04	0.00100
50	5.94	5.89	0.05	0.00125
55	5.94	5.89	0.05	0.00125
60	5.95	5.90	0.05	0.00125
65	5.96	5.90	0.06	0.00150
70	5.98	5.91	0.07	0.00175

Table 12:Steel sample 1: Swan Milligram (uncoated) Thickness: 0.19mm in Rain water

Time (days)	Initial weight (grams)	Final weight (grams)	Weight loss (Iw-Fw) (grams)	Specific weight loss (g/(cm)²)
5	5.82	5.82	0.01	0.00000
10	5.82	5.82	0.01	0.00000
15	5.83	5.82	0.04	0.00025
20	5.84	5.83	0.05	0.00025
25	5.85	5.83	0.06	0.00050
30	5.87	5.83	0.07	0.00100
35	5.89	5.85	0.07	0.00100
40	5.90	5.86	0.07	0.00100
45	5.92	5.88	0.07	0.00100
50	5.94	5.89	0.08	0.00125
55	5.94	5.89	0.08	0.00125
60	5.95	5.90	0.09	0.00125
65	5.97	5.91	0.10	0.00150
70	5.98	5.92	0.10	0.00150

Table 13: Steel sample 2: Double hand (uncoated). Thickness: 0.22mm in 0.01 mole H_2SO_4

Time (days)	Initial weight (grams)	Final weight (grams)	Weight loss (Iw-Fw) (grams)	Specific weight loss (g/(cm)²)
5	5.98	5.97	0.05	0.00125
10	5.99	5.97	0.03	0.00075
15	6.01	5.98	0.02	0.00050
20	6.03	5.99	-0.01	-0.00025
25	6.04	5.98	-0.01	-0.00025
30	6.06	5.99	-0.03	-0.00075
35	6.06	5.95	-0.04	-0.00100
40	6.08	5.94	-0.05	-0.00125
45	6.09	5.92	-0.06	-0.00150
50	6.11	5.92	-0.07	-0.00175
55	6.12	5.92	-0.09	-0.00225
60	6.14	5.91	-0.11	-0.00275
65	6.14	5.90	-0.14	-0.00350
70	6.16	5.89	-0.15	-0.00375

Table 114: Steel sample 2: Double hand (uncoated). Thickness: 0.22mm in 0.01 mole NaOH

Time (days)	Initial weight (grams)	Final weight (grams)	Weight loss (Iw-Fw) (grams)	Specific weight loss (g/(cm)²)
5	6.00	6.00	0.00	0.00000
10	6.00	6.00	0.00	0.00000
15	6.01	6.00	0.01	0.00025
20	6.03	6.02	0.01	0.00025
25	6.04	6.03	0.01	0.00025
30	6.05	6.03	0.02	0.00050
35	6.06	6.04	0.02	0.00050
40	6.07	6.05	0.02	0.00050
45	6.09	6.07	0.02	0.00050
50	6.10	6.07	0.03	0.00075
55	6.12	6.09	0.03	0.00075
60	6.14	6.11	0.03	0.00075
65	6.16	6.12	0.04	0.00100
70	6.17	6.12	0.05	0.00125

Table 15: Steel sample 2: Double hand (uncoated). Thickness: 0.22mm in Sea Water

Time (days)	Initial weight (grams)	Final weight (grams)	Weight loss (Iw-Fw) (grams)	Specific weight loss (g/(cm)²)
5	5.97	5.97	0.00	0.00000
10	5.99	5.98	0.01	0.00025
15	6.01	5.98	0.03	0.00075
20	6.03	6.00	0.03	0.00075
25	6.04	6.00	0.04	0.00100
30	6.05	6.00	0.05	0.00125
35	6.06	6.01	0.05	0.00125
40	6.08	6.02	0.06	0.00150
45	6.09	6.03	0.06	0.00150
50	6.11	6.05	0.06	0.00150
55	6.13	6.07	0.06	0.00150
60	6.14	6.07	0.07	0.00175
65	6.14	6.06	0.08	0.00200
70	6.15	6.07	0.08	0.00200

Table 16: Steel sample 2: Double hand (uncoated). Thickness: 0.22mm in Rain Water

Time (days)	Initial weight (grams)	Final weight (grams)	Weight loss (Iw-Fw) (grams)	Specific weight loss (g/(cm)²)
5	5.99	5.99	0.00	0.00000
10	5.99	5.98	0.01	0.00025
15	6.01	5.99	0.02	0.00050
20	6.03	5.99	0.04	0.00100
25	6.04	5.99	0.05	0.00125
30	6.06	5.99	0.07	0.00175
35	6.06	5.98	0.08	0.00200
40	6.08	6.00	0.08	0.00200
45	6.09	6.00	0.09	0.00225
50	6.11	6.02	0.09	0.00225
55	6.12	6.03	0.09	0.00225
60	6.13	6.03	0.10	0.00250
65	6.14	6.04	0.10	0.00250
70	6.18	6.07	0.11	0.00275

Table 17: Plastic Sample 1 in 0.01 mole H_2SO_4

Time (days)	Initial weight (grams)	Final weight (grams)	Weight loss (Iw-Fw) (grams)	Specific weight loss (g/(cm)²)
5	3.40	3.40	0.00	0.00000
10	3.45	3.44	0.01	0.00025
15	3.45	3.44	0.01	0.00025
20	3.46	3.45	0.01	0.00025
25	3.52	3.51	0.01	0.00025
30	3.52	3.51	0.01	0.00025
35	3.57	3.56	0.01	0.00025
40	3.57	3.55	0.02	0.00050
45	3.61	3.59	0.02	0.00050
50	3.63	3.61	0.02	0.00050
55	3.68	3.65	0.03	0.00075
60	3.71	3.68	0.03	0.00075
65	3.72	3.68	0.04	0.00100
70	3.76	3.72	0.04	0.00100

Table 18: Plastic Sample 1 in 0.01 mole NaOH

Time (days)	Initial weight (grams)	Final weight (grams)	Weight loss (Iw-Fw) (grams)	Specific weight loss (g/(cm)²)
5	3.41	3.41	0.00	0.00000
10	3.43	3.42	0.01	0.00025
15	3.44	3.43	0.01	0.00025
20	3.44	3.43	0.01	0.00025
25	3.46	3.45	0.01	0.00025
30	3.47	3.46	0.01	0.00025
35	3.49	3.48	0.01	0.00025
40	3.51	3.49	0.02	0.00050
45	3.51	3.49	0.02	0.00050
50	3.52	3.50	0.02	0.00050
55	3.53	3.50	0.03	0.00075
60	3.54	3.51	0.03	0.00075
65	3.55	3.52	0.03	0.00075
70	3.55	3.51	0.04	0.00100

Table 19: Plastic Sample 1 in Sea Water

Time (days)	Initial weight (grams)	Final weight (grams)	Weight loss (Iw-Fw) (grams)	Specific weight loss (g/(cm)²)
5	3.36	3.36	0.00	0.00000
10	3.38	3.38	0.00	0.00000
15	3.40	3.40	0.00	0.00000
20	3.41	3.41	0.00	0.00000
25	3.42	3.41	0.01	0.00025
30	3.45	3.44	0.01	0.00025
35	3.47	3.46	0.01	0.00025
40	3.49	3.48	0.01	0.00025
45	3.50	3.48	0.02	0.00050
50	3.51	3.49	0.02	0.00050
55	3.51	3.49	0.02	0.00050
60	3.53	3.50	0.03	0.00075
65	3.55	3.52	0.03	0.00075
70	3.58	3.55	0.03	0.00075

Table20: Asbestos sample 1: (colorless) in atmospheric environment

Time (days)	Initial weight (grams)	Final weight(Fw) (grams)	Weight gain (Fw-Iw) (g)
5	12.00	12.57	0.57
10	12.85	13.57	0.72
15	12.95	13.70	0.85
20	13.20	14.25	1.05
25	13.40	14.57	1.17
30	13.65	14.96	1.31
35	13.80	15.30	1.50
40	14.05	15.77	1.72
45	14.25	16.11	1.86
50	14.50	16.51	2.01
55	14.70	17.02	2.32
60	14.78	17.33	2.55
65	14.90	17.50	2.60
70	14.98	17.69	2.71

Table 21: Asbestos sample 2:(colored) in atmospheric environment

Time (days)	Initial weight (grams)	Final weight (grams)	Weight gain (Fw-Iw) (grams)
5	12.35	12.79	0.44
10	12.48	12.99	0.51
15	12.63	13.27	0.64
20	12.77	13.47	0.70
25	12.86	13.81	0.95
30	13.09	14.16	1.07
35	13.21	14.37	1.16
40	13.35	14.58	1.23
45	13.48	14.90	1.42
50	13.65	15.14	1.49
55	13.72	15.25	1.53
60	13.95	15.57	1.62
65	14.20	15.91	1.71
70	14.58	16.61	2.03

3.3 Graphs

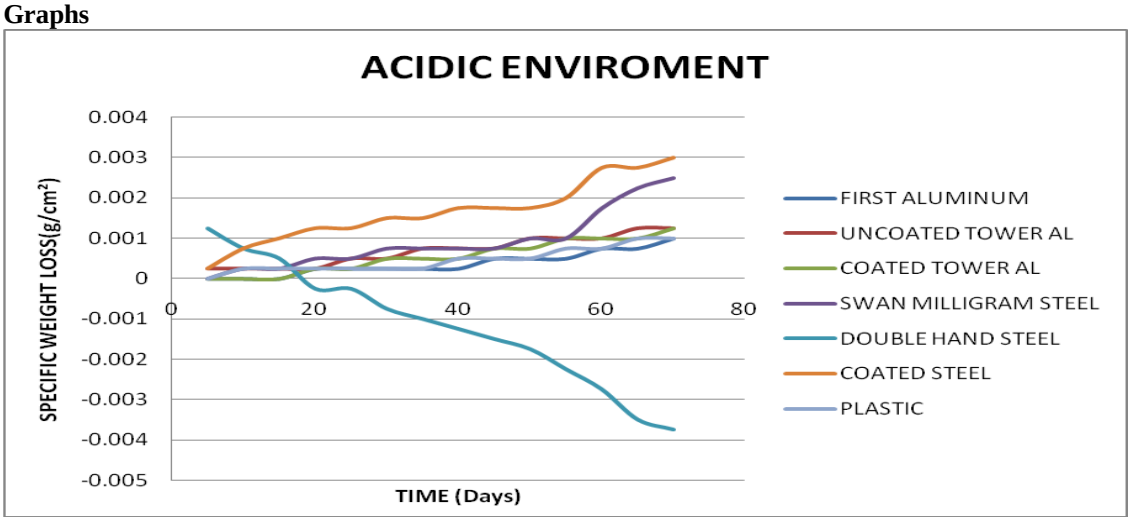

Fig.2: Rates of corrosion of the different samples in the acidic environment, 0.01 mole H_2SO_4.

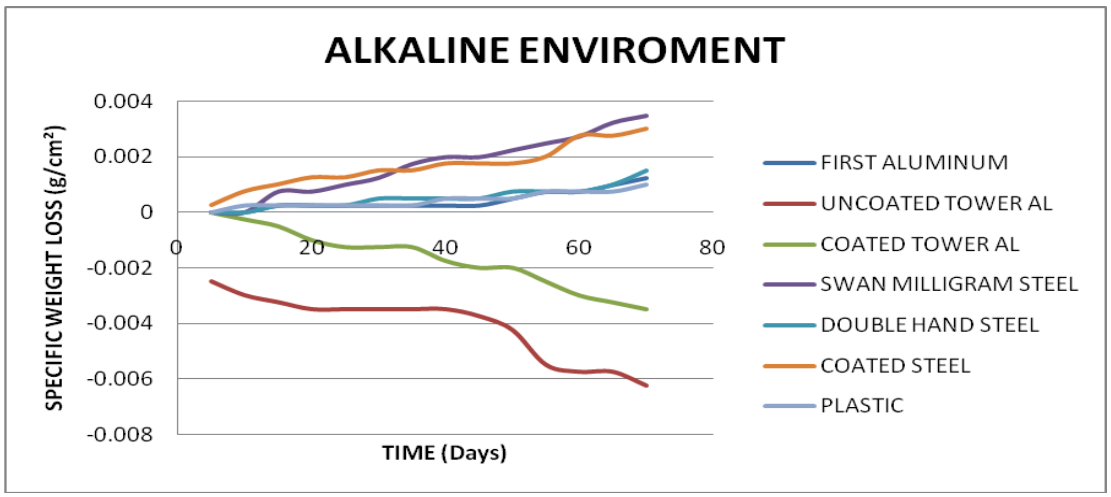

Fig.3: Rate of corrosion of the different samples in alkaline environment, 0.01 mole NaOH.

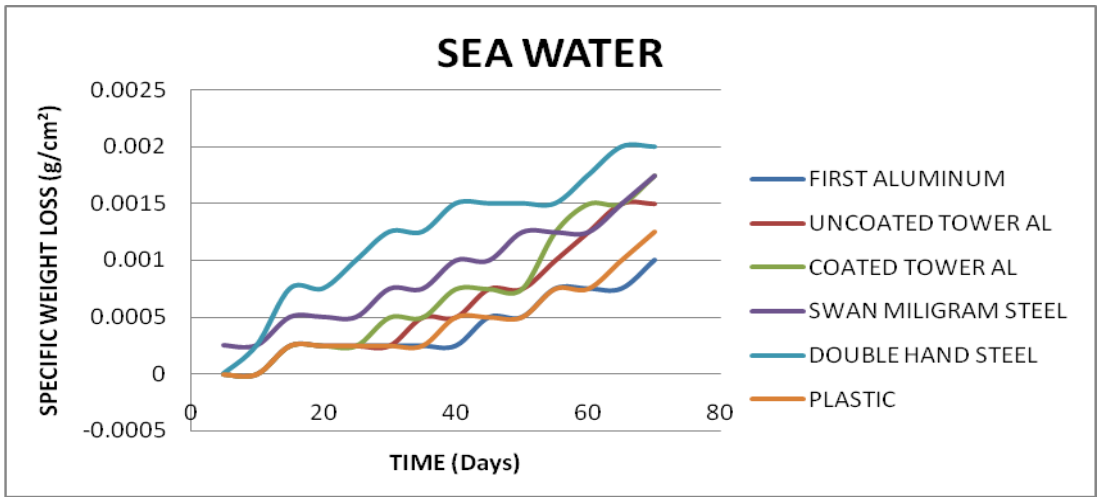

Fig.4: Rate of corrosion of the different samples in sea water environment.

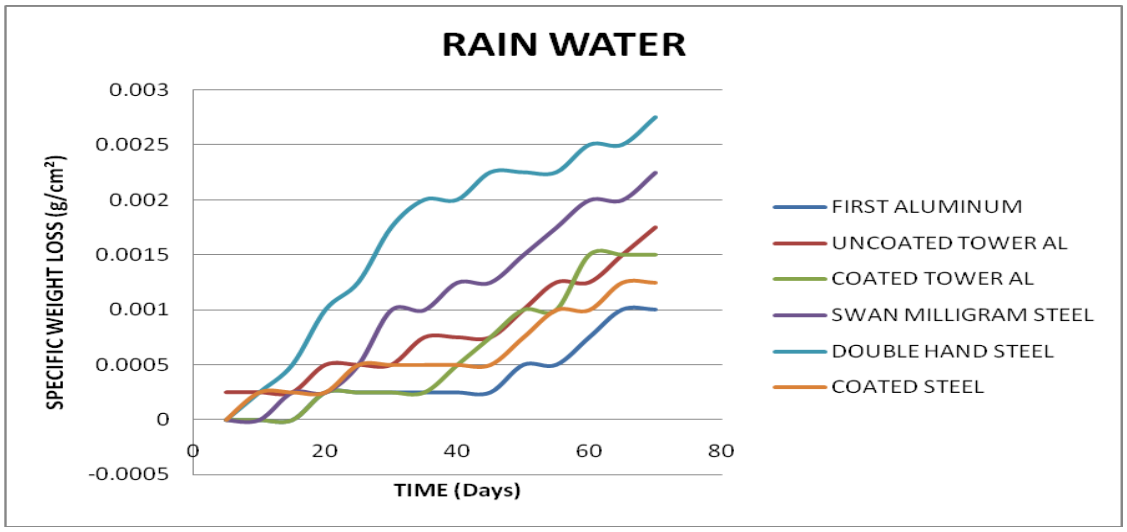

Fig.5: Rate of corrosion of the different samples in rain water environment.

IV. DISCUSSIONS AND OBSERVATIONS

4.1 Acidic Environment

At the beginning of the experiment, the pH of the acidic medium was 2, but it increased gradually to 4 as the experiment progressed. This was due to the formation of corrosion films in the medium.

4.1.1 First Aluminum Sample: It was observed that there was minimal weight loss which may be as a result of the presence of a high amount of aluminum in the sample. The elements the sample was alloyed with increased its strength and caused it to resist corrosion to a reasonable extent.

4.1.2 Tower Aluminum (Uncoated) Sample: There was a visible change in appearance. However the alloying materials may have induced corrosion and given rise to the formation of intermediate products.

4.1.3 Tower Aluminum (Coated) Sample: It progressively deteriorated in the course of the experiment. There was no weight gain rather we observed insignificant weight loss. It is possible that this sample maybe purely aluminum and hence is known to resist rusting. Though rusting did occur but the level was insignificant.

4.1.4 Swan Milligram Sample: Weight loss was observed, it is possible that the thickness of the galvanizing material (zinc) was very small. The chemical content of the medium (sulphur oxide) has been known to increase in galvanized steel. [35]

4.1.5 Double hand Sample: Initially this sample experienced weight loss and then weight gain. It may be an alloy containing some other elements which induce electrolysis which brought about deposition and formation of heavier or intermediate compounds deposited on the sample.

4.1.6 Green coated Sample: There was irregularity in weight loss and this can be attributed to changes in weather and atmospheric condition of our environment.

We observed that the acid attacked the paint used in coating the sheet, therefore, we suspect that the paint used for the coating is inferior, and could not properly protect the metal from corrosion.

Steel is a heavy metal and as acid reacts with it, it forms oxides and chlorides of the metal which pull out of the metal and go into the solution. Hence giving rise to weight loss.

4.1.7 Plastics: There was little or no significant weight loss. Plastics do not encourage microbial degradation that promotes rusting or degradation. They equally react with environmental acid but the level of the reaction is low, perhaps due to the unsaturated nature of the polymer.

4.2 Alkaline Environment

The pH of this medium reduced from 11 to 8 as the experiment progressed. This is due to the formation of oxide films that dissolved in the medium, thereby making the pH of the solution tend towards neutral.

4.2.1 First Aluminum Sample: There was insignificant loss in weight but as of the 60th day of the experiment, it was observed that sheet has lost its shiny appearance and there was very little powdery substance on the surface of the metal. This didn't give rise to weight loss because it was in minute quantities.

4.2.2 Tower Aluminum Uncoated Sample: There was significant weight gain as a result of the reaction of aluminum with NaOH.

$2Al_3 + 9NaOH \rightarrow 3Al_20_3 + {}^{9}/_{2}H_2 + 9Na$

Aluminum oxide is an intermediate that is formed and it is heavier than the base metal. This can be due to electrolytic reaction as sodium metal is more reactive than aluminum which turns deposit on the aluminum samples.

4.2.3 Tower Aluminum Coated Sample: There was significant weight gain as a result of the reaction of aluminum with NaOH.

$2Al_3 + 9NaOH \rightarrow 3Al_20_3 + {}^{9}/_{2}H_2 + 9Na$

Aluminum oxide is an intermediate that is formed and it is heavier than the base metal.

4.2.4 Swan Milligram Steel Sample: There was a progressive weight loss observed in this sample with deposits in the alkaline solution. This may have been as a result of intermediates formed but maybe they weren't heavier than the base metal.

4.2.5 Double Hand Steel Sample: Weight loss was observed but wasn't significant. This could be as a result the trace elements present in the sample, which helped to reduce the rate of corrosion.

4.2.6 Green Coated Steel Sample: There was a progressive weight loss observed in this sample with brownish deposits in the alkaline solution but not as much as that in the swan milligram. This may have been as a result of intermediates formed but maybe they weren't heavier than the base metal.

4.2.7 Plastic: There was little or no significant weight loss. Plastics don't encourage microbial degradation that promotes rusting or degradation. They equally react with environmental acid but the level of the reaction is low, perhaps due to the unsaturated nature of the polymer.

4.3 Sea Water Environment

The pH of this medium was 6, which was constant throughout the period of the experiment.

4.3.1 First Aluminum Sample: The rate of corrosion of this sample was insignificant. The salt in the medium was deposited on the metal surface.

4.3.2Tower Aluminum (Uncoated) Sample: The weight loss observed in this medium was not significant. The sample deteriorated visibly with time.

4.3.3Tower Aluminum (Coated) Sample: The uncoated side of the sample was experienced more attached than the coated side. Thus the rate of attach was insignificant when compare with uncoated tower aluminum.

$Al + 3NaCl \rightarrow AlCl_3 + 3Na$

The sodium metal formed from the reaction above attaches the surface of the aluminum sample.

4.3.4 Swan Milligram Steel: During the period of this experiment this sample experienced more attack than the aluminum sample this is due to the fact that oxidation of iron is more rapid than aluminum.

4.3.5 Double Hand Steel Sample: Weight loss was observed but wasn't significant. This could be as a result the trace elements present in the sample, which helped to reduce the rate of corrosion.

Some metals have naturally slow reaction kinetics, even though their corrosion is thermodynamically favorable. These include such metals as zinc, magnesium, and cadmium. While corrosion of these metals is continuous and ongoing, it happens at an acceptably slow rate. This is the why these metals are used as alloying element.

V. CONCLUSION

Generally, coated or painted samples are preferred to uncoated samples in most of the media. This is the reason why most coated samples did not corrode in their respective media. Based on the results of our experiment, First Aluminum (Al sample 1) was recommended as the best roofing sheet in Nigeria. This is due to fact that, the sample retained its shiny appearance in control medium (rain water) throughout the 70days of the experiment. The rate of weight loss in acidic and alkaline media was highly insignificant. Although plastic sample did not corrode during the period of our experiment, its low temperature resistance makes it not suitable for roofing because it becomes brittle on continuous expansion and contraction and it is not fireproof. In conclusion, aluminum samples are highly reactive in alkaline medium and thus it is not advisable to use them in alkaline-prone environments. The steel samples are highly reactive in acidic environments, care should be taken to ensure that they are always coated and crack free at all times, to avoid exposure of the surface to the acids.

Though galvanizing with zinc protects it from corrosion, in the presence of sulphur compounds, which are present in highly industrial urban areas, the presence of the zinc aids corrosion. Therefore, galvanized products have a shorter life span in urban industrial areas than in rural unindustrialized areas.

REFERENCES

[1]. Fathy M. Bayoumi, and Wafaa A. Ghanem, "**Materials letters**",Vol. 59, pp. 3806- 3809, 2005.
[2]. Liu Chenglong, Yang Dazhi, Lin Guoqiang and Qi Min, "**Materials Letters**",Vol.59, pp. 3813, 2005.
[3]. J. Hu, W. Y. Chu, W. C. Ren, C. K. Yao and L.J. Qiao, **"Corrosion"**, The Journal of Science and Engineering, Vol.60, No.2, pp. 181-182, 2004.
[4]. S.U. Koh, B.Y. Yang, and K.Y. Kim, **"Corrosion"**, Journal of Science and Engineering,
[5]. Vol.60, No.3, pp. 262, 2004.
[6]. S.U. Koh, J.S. Kim, B.Y. Yang, and K.Y. Kim, **"Corrosion"**, Journal of Science and Engineering, Vol.60, No.3, pp. 244-245, 2004.
[7]. R.Chu, W. Chen, S.H. Wang, T.R. Jack, and R.R. Fesser, **"Corrosion"**, Journal of Science and Engineering, Vol.60, No.3, pp. 275-276, 2004.
[8]. Q. meng, G.S. Frankel, H.O. Colijn, and S.H. Goss, **"Corrosion"**, Journal of Science and

[9]. Engineering, Vol.60, No.4, pp. 346, 2004.
[10]. F. Zucchi, G. Trabanelli, V. Grassi, and A. Frignani, **"Corrosion"**, Journal of Science and
[11]. Engineering, Vol.60, No.3, pp.363-364, 2004.
[12]. S. Wang and R.C. Newman, **"Corrosion"**, Journal of Science and Engineering, Vol.60, No.5, pp. 448-449, 2004.
[13]. J.R. Kish, M.B. Lves, and J.R. Rodds, **"Corrosion"**, Journal of Science and Engineering,
[14]. Vol.60, No.6, pp. 523, 2004.
[15]. D.A. Moreno, B. Molina, C. Ranninger, F. Montero, and J. Izquierdo, **"Corrosion"**, Journal of Science and Engineering, Vol.60, No.6, pp. 573-583, 2004.
[16]. Z. Zeng, K. Natesan, and M. Grimsditch, **"Corrosion"**, Journal of Science and Engineering, Vol.60, No.7, pp. 632-633, 2004.

ISSN (e): 2250 – 3005 || Vol, 04 || Issue, 11 || November – 2014 ||
International Journal of Computational Engineering Research (IJCER)

A Particle Swarm Optimization for Reactive Power Optimization

Suresh Kumar[1], Sunil Kumar Goyal[2]
PG Student [Power System], Dept. of EE, AIET, Jaipur (Rajasthan), India[1]
Associate Professor, Dept. of EE, AIET, Jaipur (Rajasthan), India[2]

ABSTRACT:
This paper presents implementation of new algorithm Particle Swarm Optimization (PSO) for Energy Saving through minimizing power losses. The PSO Algorithm Solution is tested in standard IEEE 30 Bus system. The objective is to optimize the reactive power dispatch with optimal setting of control variables without violating inequality constraints and satisfying equality constraint. Control Variables are of both types: Continuous and Discrete. The continuous control variables are generator bus voltage magnitudes;whereas the discrete variables are transformer tap settings and reactive power of shunt compensators (Capacitor banks) .

KEYWORDS: *Energy Saving by Particle Swarm Optimization, Optimal Reactive Power Dispatch.*

I. INTRODUCTION

Power system economics procedure includes of two aspects: active power regulation and reactive power dispatch. This forms a global optimization problem of a large-scale industrial system.The reactive power problem is less manageable to solve than the active power problem due to its more complicated relationship between variables. The reactive power problem is largelyassociated to voltage stability.Reactive power and voltage control is incredibly essential for the right operation and control of power system. Reactive power dispatch is one of the necessary tasks in the operation and control of power system.Voltage stability is a drawback in power systems that are heavily loaded, faulted or have a deficiency of reactive power. The character of voltage stability may be analysed by examining the generation, transmission and consumption of reactive power. Transfer of reactive Power is toughbecause of extremely high reactive power losses; that's why the reactive power needed for voltage control is generated and consumed at the control area.Optimization is a mathematical procedurewhich discusses the finding of maxima or minima of functions in some realistic region. There's no industry or businessthat is not involved in solving optimization problems.By Optimizing reactive power Dispatch in Power systems, the maximum active power transfer capability to the distribution systems can be improved. Stand-by reactive power sources (capacitor banks generally) are needed for loss minimization, in order to maintain the voltage stability in the Power systems [11-12].

For solving all optimization problems, there is no known single optimization method available. For solving the differentkinds of optimization problems, plenty of optimization techniques have been established in recent years. Linear programming (LP), non-linear programming and gradient based techniques were traditional optimization techniques [1], [4] for solving Reactive Power optimization problems. Since, Approximations are used in linearized models, thus LP results don't signify optimal result for objective function utilized in reactive power optimization problem. Traditional solution strategies have tendency to converge to a local optimal solution instead of the global one. Expert System methodologies [5] have been recommended for the reactive power based calculations. Expert System methodology is based mostly on 'if-then' based rules.Evolutionary computational techniques like Genetic algorithm (GA), Evolutionary programming (EP) and Evolutionary strategy have additionally been projected to solve the optimizations problems relating to the reactive power dispatch [6-8].The contemporary (non-traditional) optimization approaches are very powerful and popular approaches for solving complex engineering problems. These approaches are neural networks, genetic algorithm, ant colony optimization, fuzzy optimization and particle swarm optimization algorithm Particle Swarm Optimization (PSO) stands as acomparatively new, modern, and powerful technique of optimization that has been virtually shown to perform well on several of these optimization problems [13-14]. PSO exists as a population based stochastic optimization technique. PSO algorithm is applied while not violating inequality constraints and satisfying equality constraint.The aim of minimising reactive power losses is achieved by appropriate adjustment of reactive power variables like generator voltage magnitudes (V_{gi}), reactive power generation of capacitor banks (Q_{ci}) and transformer tap settings (t_k) [7-10]. In electrical power system, Reactive Power Loss Minimization problem is taken into account as a static, non-linear, single objective optimization

problem. The suggested PSO algorithm solution has been experimented on the standard IEEE 30-Bus test system with both continuous and discrete control variables despite the fact that keeping the system under safe voltage stability limit. The recommended algorithm shows better results

II. PROBLEM FORMULATION

The customary optimization problem is often written in the following form,

Minimise $F(x)$ (the objective function)

subject to:

$h_i(x) = 0, i = 1, 2, ..., n$ (equality constraints)

$g_j(x) = 0, j = 1, 2, ...,m$ (inequality constraints)

The reactive power optimization problem targets to minimize the power losses in the transmission network and improve voltage profile while satisfying the unit and system constraints. The aim is achieved by appropriate setting of reactive power variables like generator voltage magnitudes (V_{gi}), reactive power generation of capacitor banks (Q_{ci}) and transformer tap settings (t_k) [7-8].The equality constraints are power/reactive power equalities, the inequality constraints consist of bus voltage constraints, generator reactive power constraints, reactive power capacity constraints and the transformer tap position constraints, etc.At this juncture the reactive power dispatch problem is treated as a single objective optimization problem by linear combination of two objective functions i.e. P_{Loss}

$$F = min. P_{loss} \ldots \ldots\ldots\ldots\ldots\ldots [1]$$

A. Energy Saving through Minimization of power system losses (P_{loss})

The RPD problem targets at saving of energy by minimizing the real power loss in a power system while satisfying the unit and system constraints. This objective is accomplished by appropriate adjustment of reactive power variables like generator voltage magnitudes (V_{Gi}), reactive power generation of capacitor banks (Q_{Ci}) and transformer tap settings (T_k).

The minimization of system real power losses (MW) is calculated as follows:

$$\text{Min } F = P_{Loss} = \sum_{K=1}^{nl} g_k \left[V_i^2 + V_j^2 - 2V_i V_j \cos(\delta_i - \delta_j)\right]$$

The real power loss given by (P_{Loss}) is a non-linear function of bus voltages and phase angles that are a function of control variables and n_l is the number of transmission lines; g_k is the conductance of the k^{th} line; V_i and $V_j$are the voltage magnitude at the end buses i and j of the k^{th} line, respectively, and δ_i and δ_j are the voltage phase angles at the end buses i and j.

III. CONSTRAINTS

The real power loss (given by equation) is treated as a non-linear function of bus voltages and phase angles that are functions of control variables. The minimization problem is subjected to the following equality and inequality constraints:

Equality constraints

These constraints are typical load flow equations which can be represented as follows

1. Real Power Constraints:

$$P_{Gi} - P_{Di} - V_i \sum_{j=1}^{N_B} V_j \left(G_{ij} Cos(\delta_i - \delta_j) + B_{ij} Sin(\delta_i - \delta_j)\right) = 0 \ldots [2]$$

$$i = 1,2 \ldots\ldots\ldots N_B$$

2. Reactive Power Constraints:

$$Q_{Gi} - Q_{Di} - V_i \sum_{j=1}^{N_B} V_j \left(G_{ij} Sin(\delta_i - \delta_j) - B_{ij} Cos(\delta_i - \delta_j)\right) = 0, \ldots [3]$$

$$i = 1,2 \ldots\ldots\ldots N_{PQ}$$

Where,

V_i= Voltage magnitude at bus I

V_j = Voltage magnitude at bus j

P_i, Q_i = Real and reactive powers injected into network at bus i

G_{ij}, B_{ij} = Mutual conductance and susceptance between bus i and bus j

Q_{gi} = Reactive power generation at bus i

$N_B - 1$ = Total number of buses excluding slack bus

N_{PQ} =Number of PQ buses

δ_{ij} = Voltage angle difference between bus i and bus j

Inequality constraints :

3. Bus Voltage magnitude constraints:

$V_i^{min} \leq V_i \leq V_i^{max}$; $i \varepsilon N_B$… [4]

4. Transformer Tap position constraints:

$t_k^{min} \leq t_k \leq t_k^{max}$; $i \varepsilon N_T$… [5]

5. Generator bus reactive power constraint:

$Q_{gi}^{min} \leq Q_{gi} \leq Q_{gi}^{max}$; $i \varepsilon N_g$..[6]

6. Reactive power source capacity constraints:

$$Q_{ci}^{min} \leq Q_{ci} \leq Q_{ci}^{max} \; ; \; i \varepsilon N_c \ldots [7]$$

7. Transmission line flow constraints:

$|s_1| \leq |s_1^{max}|$….[8]

$|s_1| \leq |s_1^{max}|$…[9]

8. Generation capacity constraint:

$P_{Gi}^{min} \leq P_{Gi} \leq P_{Gi}^{max}$; $i \in N_B$[10]

The total power generation should cover the overall demand $P_D$and the real power loss in transmission lines P_L. This relation is often expressed by Power Balance Constraint:

9. Power balance constraint:

$\sum_{i=1}^{NB} P_{Gi} = P_D + P_L$….[11]

The symbols used are as follows:

t_k= Tap setting of transformer at branch k

Q_{Ci}= Reactive power generated by i^{th} capacitor bank

Q_{gi} = Reactive power generation at bus i

S_l = Apparent power flow through the i^{th} branch

N_B = Total number of buses

g_k= Conductance of buses

N_T= Number of tap-setting transformer branches

N_c= Number of capacitor banks

N_g= Number of generator buses

The control variables for voltage-control problem, which will be modified by the Particle Swarm optimization process, are:

a. Voltages magnitude at voltage-controlled buses (PV-buses) including the slack bus.
b. Transformers tap settings.
c. Adjustable shunt capacitor banks.

IV. PARTICLE SWARM OPTIMIZATION

PSO is an acronym for Particle Swarm Optimization. Particle Swarm Algorithm was introduced by Kennedy and Eberhart in 1995 [14]. PSO is a swarm intelligence method for global optimization.Particle Swarm Optimization is a concept introduced for the optimization of nonlinear functions using particle swarm methodology. Basically Particle Swarm Optimization is a method for optimization of continuous nonlinear functions. The method was discovered through simulation of a simplified social model. Particle Swarm Optimization comprises a very simple concept, and paradigms can be implemented in a few lines of computer code. It requires only primitive mathematical operators, and is computationally inexpensive in terms of both memory requirements and speed. Early testing has found the implementation to be effective with several kinds of problems.

PSO is based on the natural process of group communication to share individual knowledge when a group of birds or insects search food or migrate and so forth in a searching space, although all birds or insects do not know where the best position is. But from the nature of the social behaviour, if any member can find out a desirable path to go, the rest of the members will follow quickly.PSO traces its evolution to the emergent motion of a flock of birds searching for food. PSO uses a number of particles that constitute a swarm. Each particle traverses the search space looking for the global minimum (or maximum). In a PSO system, particles fly around in a multidimensional search space. During flight, each particle adjusts its position according to its own experience, and the experience of neighbouring particles, making use of the best position encountered by itself and its neighbours. The swarm direction of a particle is defined by the set of particles neighbouring to the particle and its history experience.

The basic elements of the PSO techniques are defined as:

1. **Particle X (t):**It is a candidate solution described by a k- dimensional real-valued vector, where k is the number of optimized parameters. At iteration i, the jth particle X (i,j) can be expressed as:

$X_i(t)=[x_{i,1}(t); x_{i,2}(t); \ldots\ldots;x_{i,k}(t)]$.

Where: x's are the optimized parameters and d signifies number of control variables

2. **Population**: It is basically a set of n particles at iteration i.

Pop (i) = [$X_1(i)$, X_2 (i), …….. X_n (i)] T

Where n signifies the number of candidate solutions

3. **Swarm**: Swarm is defined as an apparently unsystematic population of moving particles that tend to bunch together while each particle appears to be moving in a random direction.

4. **Particle velocity V (t):**Particle velocity is the velocity of the moving particles signified by a d-dimensional real valued vector. Particle Velocity is the step size of the swarm. It is the velocity of the moving particles represented by a k-dimensional real-valued vector. At time t, the i_{th} particle $V_i(t)$ can be described as

$V_i(t)=[v_{i,1}(t); v_{i,2}(t); \ldots\ldots;v_{i,k}(t)]$.

5. **Inertia weight ω(t)**: It is a regulation parameter, which is used to regulate the impact of the past (previous) velocity on the present velocity. Hence, it effects the trade-off between the global and local exploration capacities of the particles. For the initial stages of the search method, large inertia weight to reinforce the global exploration is usually recommended while it must be reduced at the last stages for higher local exploration. Therefore, the inertia factor drops linearly from about 0.9 to 0.4 throughout a run. In general, the inertia weight factor is set according to the equation given below:

$$W = \frac{(W_{max} - W_{min})}{iter_{max}} \times iter$$

All the control variables transformer tap positions and switch-able shunt capacitor banks are integer variables and not continuousvariables. Therefore, the value of the inertia weight is considered to be 1 in this study.

6. **Individual best X* (t)**: When particles are moving through the search space , it matches its fitness value at the existing position to the best fitness value it has ever grasped at any iteration up to the current iteration. The best position that is related with the best fitness faced so far is called the individual best X* (i). For every particle in the swarm, X* (i) may be determined and updated throughout the search.

7. **Global best X** (t):** It is the best position among all of the individual best positions achieved so far.

Various steps concerned with the implementation of PSO to the RPO problem are:

Step 1: Firstly scan the Input parameters of the system (bus, line and generator data) and alsoidentify the lower and upper boundaries of every variable. For N generators, optimization is applied out for N-1 generators and generator of maximum capacity is considered at slack bus.

Step 2: Then the particles of the population are randomly initialized i.e. are randomly selected between the respective minimum and maximum values. Also assign the velocity V initially between [-1 and 1].

Step 3: Obtain power flow solution and compute losses by Newton-Raphson method.

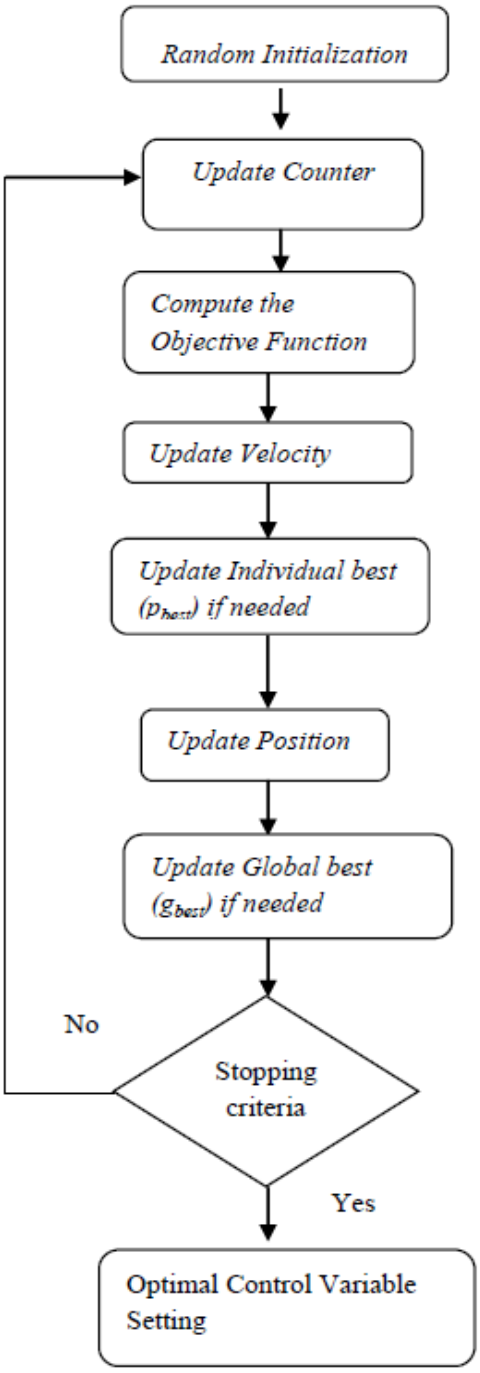

Fig.: **Flowchart for Basic PSO Algorithm**

Step 4: The best fitness is assigned as p_{Best}. At this stage the p_{Best} is also the g_{Best}.
Step 5: Iteration*i*= i+1 is updated.
Step 6: Modify the inertia weight *w* given by $W = \frac{(W_{max} - W_{min})}{iter_{max}} \times iter$

Step 7: Update the velocity *v* of each particle according to the stated equation
$V(k,j,i+1) = W^{*}V(k,j,i) + C1^{*}rand^{*}\left(p_{bestx}(j,k) - X(k,j,i)\right) + C2^{*}rand^{*}\left(g_{bestx}(k) - X(k,j,i)\right)$
Step 8:Position of each particle is also modified as per the mentioned equation. If a particle violates the position limits in any dimension, its position is set at the right limit.
$x(k,j,i\,1)\;\; x(k,j,1\,i)\;\; v(k,j,i)$

Table: optimal parameter setting for PSO

Parameters	
Number of iterations	300
Cognitive constant, c_1	2.0
Social constant, c_2	2.0
Max. and Min. inertia weights W	0.4 and 0.95
Population size	30

Step 9: Evaluation of each particle is done according to its updated position by runningpower flow and calculate the fitness function. If the evaluation value of each particle is better than the previous $\mathbf{p_{Best}}$ then the current value is set to be $\mathbf{p_{Best}}$. If the best $\mathbf{p_{Best}}$ is better than $\mathbf{g_{Best}}$, the value is set to be $\mathbf{g_{Best}}$.

Step 10: If one of the stopping criteria is fulfilled then we go to Step 11. Else, we go to Step 5.
Step11: $\mathbf{g_{Best}}$is the optimal/best value that is newest generated by the particle.

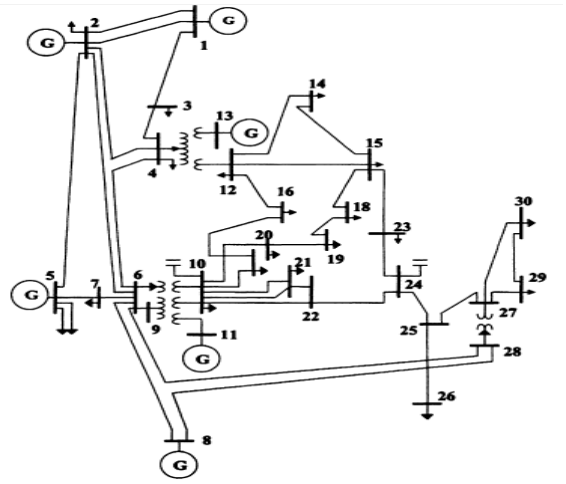

Fig.: IEEE 30 Bus System

V. RESULTS

Energy Saving through Minimization of systempower losses (P_{loss})

The proposed algorithm is run with minimization of real power losses as the objective function. As mentioned above, the real power settings of the generators are taken from [15-16]. The algorithm reaches a minimum loss of 5.3191MW. IEEE30 bus system is shown. The optimal values of the control variables are given in table shown above..

Table1: Test results of proposed approach.

Proposed Method	**Power Loss (MW)**
Particle Swarm Optimization	5.3191

	Min.	Max.	Initial(Base case)	Proposed PSO algorithm
V1	1.0	1.1	1.05	1.0824
V2	1.0	1.1	1.04	1.0470
V5	1.0	1.1	1.01	1.0347
V8	1.0	1.1	1.01	1.0209

V11	1.0	1.1	1.05	1.0376
V13	1.0	1.1	1.05	1.0402
T11	1.0	1.1	1.078	1.0196
T12	1.0	1.1	1.069	1.0783
T15	1.0	1.1	1.032	1.0573
T36	1.0	1.1	1.068	1.0963
Qc10	0.0	5.0	0.0	1.2677
Qc12	0.0	5.0	0.0	1.0610
Qc15	0.0	5.0	0.0	0.8607
Qc17	0.0	5.0	0.0	0
Qc20	0.0	5.0	0.0	2.5792
Qc21	0.0	5.0	0.0	1.7678
Qc23	0.0	5.0	0.0	1.6902
Qc24	0.0	5.0	0.0	0.5076
Qc29	0.0	5.0	0.0	0.6881
Power loss(MW)			5.8708	**5.3191**

Table 2:- Best results of individually run of p_{loss} as main function (IEEE-30 Bus)

Total Energy Saving :
From the table (shown below),
Reduction in losses – (5.8708 – 5.3191) = 0.5517 MW = 551.7 KW
Converting these reduced active power losses in form of energy we find:
Saved Energy in One Hour => 551.7 KWh
Saved Energy in One Day => 551.7 *24 = 13240.8 KWh
Saved Energy in One Week => 551.7 *24*7 = 92685.6 KWh
Saved Energy in One Year – 551.7 *24*365 = 4832892 KWh
So for an IEEE 30 bus system, estimation of energy saving is shown.For a standard IEEE 30 Bus system, 4832892 KWh (Units) is saved in a year by using PSO.

VI. CONCLUSION

A new improved integer coding Particle Swarm Algorithm is presented to solve this problem. The main objective is to minimize the active power loss in the network, while satisfying all the power system operation constraints. The particle swarm algorithm has been coded as well as the power flow fast-decoupled method using MATLAB. The simulation results show that PSO algorithm always leads to a better result.

VII. ACKNOWLEDGEMENT:

The authors are thankful to Director, Apex Institute of Engineering and Technology, Jaipur (Rajasthan) for providing support and facilities to carry out this research work

REFERENCES:

[1] H. W. Dommel and W. F. Tinny, "Optimal power flow solutions," IEEE 1968, pp 1866-1876.
[2] K. Y. Lee, Y. M. Park, and J. L. Ortiz, "A united approach to optimal real and reactive power dispatch," IEEE trans. on PAS, 104, 1985, pp. 1147-1153.
[3] G. R. M. Da Costa, "Optimal reactive dispatch through primal-dual method," IEEE trans. on power systems, Vol. 12, No. 2, May 1997, pp 669-674.
[4] L. D. B. Terra and M. J. Short "Security constrained reactive power dispatch," IEEE Trans. on power systems, Vol. 6, No. 1, February 1991.
[6] K. Iba, "Reactive power optimization by genetic algorithm," IEEE trans. on power systems, Vol. 9 No. 2, 1994, pp 685-692.
[7] Q. H. Wu and J. T. Ma , "Power system optimal reactive power dispatch using evolutionary programming," IEEE trans. on power systems, Vol. 10, No. 3, August 1995, pp 1243-1248.
[8] B. Das and C. Patvardhan, "A new hybrid evolutionary strategy for reactive power dispatch," Electric power system research, Vol. 65, 2003, pp 83-90.
[9] O. Alsac and B. Scott, "Optimal load flow with steady-state security," IEEE Trans. on power systems, Vol. 93, 1974, pp 745-751.
[10] K. Y. Lee, Y. M. Park and J. L. Ortiz, "Optimal real and reactive power dispatch" Electric power system research, Vol. 7, 1984, pp 201-212.
[11] Saadat Hadi, "Power System Analysis", McGraw-Hill, 1999.
[12] Kothari D.P. and Nagrath I.J., Modern Power System Analysis. Tata McGraw-Hill, Third Edition, 2003.

[13] Kennedy J., "The Particle Swarm: Social Adaptation of Knowledge", Proceedings of IEEE International Conference on Evolutionary Computation, Indianapolis, USA, pp.303-308, 1997.
[14] Yuhui Shi, Russell C. Eberhart, "Empirical Study of Particle Swarm Optimization", Evolutionary Computation, CEC 99, Vol. 3, 6-9 July 1999
[15] A.A. Abou El Ela, M.A. Abido, S.R. Spea , "Differential Evolution algorithm for optimal reactive power dispatch ", Electric Power Systems Research 81 (2011) 458–464.
[16] H.D. Chiang, J.C. Wang, O. Cockings, and H.D. Shin, "Optimal capacitor placements in distribution systems: part 2: solution algorithms and numerical results", IEEE Trans. Power Delivery, Vol. 5, No. 2, pp. 634-641, April 1990.

ISSN (e): 2250 – 3005 || Vol, 04 || Issue, 11 || November – 2014 ||
International Journal of Computational Engineering Research (IJCER)

Quality of service Routing Using Stable Nodes in Mobile Ad hoc Networks

[1,]G.Madhukar Rao, [2,]T.santhosh
1Assistant Professor, Dept.of Computer Engineering, Sanjivani College of Engineering
2 Assistant Professor, Dept. of Computer Science Engineering, Dehradun Institute of Technology

ABSTRACT *:*
An efficient and secured routing protocol design is the vital concern for mobile ad hoc networks in view of major problems raising on security issues and loss of the network resources is due to changes within the connections of the network like Node failures, link breakages in the network. Our proposed scheme enhances the secured and reliable transmission of data, which also improves the network constancy, efficient packet delivery ratio and network life time by integrating through the AODV Routing protocol. It unites the authentication, stable routes and signal strength of the nodes to attain the secure and reliable transmission of data through nodes.

KEY WORDS: *Ad hoc network, Routing protocols, AODV, power, signal strength, Quality of Service, authentication.*

I. INTRODUCTION

A Mobile Ad hoc Network (MANET) is compilation of mobile nodes with no existing pre established infrastructure, forming a temporary network. Each mobile node in the network act as a router. Such networks are characterized by: Dynamic topologies, existence of bandwidth constrained and variable capacity links, energy constrained operations and are highly prone to security threats. Due to all these features routing is a major concern in ad hoc networks. MANET is viewed as suitable systems which can support some specific applications as virtual classrooms, military communications, emergency search and rescue operations, data acquisition in hostile environments, communications set up in Exhibitions, conferences and meetings, in battle field among soldiers to coordinate defense or attack, at airport terminals for workers to share files etc. Due to the frequent changes in network topology and the lack of the network resources both in the wireless medium and in the mobile nodes, mobile ad hoc networking becomes a challenging task. Routing in Ad hoc networks experiences more link failures than in other networks. Hence, a routing protocol that supports QoS for ad hoc networks requires considering the reasons for link failure to improve its performance. Link failure stem from node mobility, secured transmission and lack of the network resources. In such a case, it is Important that the network intelligently adapts the session to its new and changed conditions.

Secured and Quality of service means providing a set of secure and service requirements to the flows while routing them through the network. A new scheme has been suggested which combines four basic features to Achieve security in terms of modification, impersonation, and fabrication exploits against ad hoc routing protocols and QoS; these are authentication ,stable routing, concept of battery power and signal strength. The scheme uses Certificate Authorities (CAs), backbone nodes for stable routes and uses power factor and signal strength to determine active nodes to participate in routing. The rest of the paper is organized as follows: Section 2 takes a look at the Routing protocols classificatio Section 3 analyzes new proposed scheme and Section 4 summarizes the study and the status of the work.

II. ROUTING PROTOCOL CLASSIFICATIONS

A routing protocol has to find a route for packet delivery and make the packet delivered to the correct destination. Many protocols [2] have been suggested keeping applications and type of network in view. Routing Protocols in Ad Hoc Networks can be classified into two types:

A. Table Driven or Proactive Protocols : Table driven routing protocols maintain consistent, upto-date routing information from each node to every other node in the network. These protocols require each node to maintain one or more tables to store routing information. These routing protocols respond to changes in network topology by propagating updates information throughout network. This type of routing is called as source routing. The areas in which they differ are the number of necessary routing tables and changes in network structure are broadcast. Some of the table driven or proactive protocols are: GSR, WRP, ZRP, STAR etc.

B. On Demand or Reactive Protocols : A different approach from table-driven routing is source-initiated on-demand routing. This type of routing creates routes only when desired by the source node. When a node requires a route to a destination, it initiates a route discovery process within the network. This process is completed once a route is found or all possible route permutations have been examined. Once a route has been established, it is maintained by a route maintenance procedure until either the destination becomes inaccessible along every path from the source or until the route is no longer desired. Some famous on demand routing protocols are: DSR, RDMAR, AODV etc. Authenticated Routing for Ad hoc Networks (ARAN), [17] detects and protects against malicious actions by third parties and peers in one particular ad hoc environment. ARAN [17] introduces authentication, message integrity, and non-repudiation to an ad hoc environment as a part of a minimal security policy. The study has been concentrated on reactive routing protocols because of proposed scheme is suitable for this protocols.

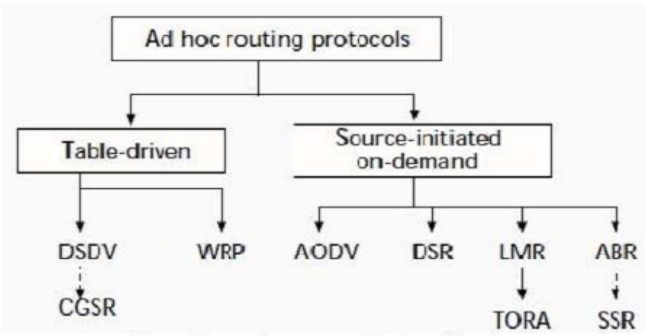

Figure1: routing protocols classification

III. PROPOSED SCHEME: AARRP

The proposed scheme"Authenticated Reliable Routing Protocol for Mobile Ad hoc Networks" takes care of on demand routing along with a new concept of Authenticated backbone nodes with optimal power factor and signal strength. This scheme concerns about the secure, reliable routes and better packet delivery ratio. The emphasis is on concept of authentication, battery power and signal strength or energy requirement for routing process. In this paper four different concepts have been joined together to make an efficient protocol. The backbone nodes help in reconstruction phase i.e., they assist in fast selection of new routes. Selection of backbone nodes is made upon availability of nodes, battery status and signal strength. Each route table has an entry for number of backbone nodes attached to it and their CAs(Certificate authorities), battery status and signal strength. The protocol is divided into three phases. Route Request (RREQ), Route Repair (RREP) and Error Phase (ERR). The proposed scheme is explained with the help of an example shown in Figure 2. The light colored nodes depict the node with less power factor. The Route selection from S (source) to D (destination) is made via 1-2-3-4-5 using shortest path routing

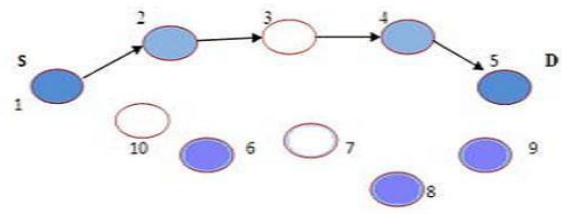

Figure 2: Example of routing

In case any of the participating nodes get damaged or move out of the range, the backbone nodes (6,8 and 9) can be takes care of the process. These nodes are nearer to the routing path nodes and have a sufficient power and signal strength so they can join the process any time. This may lead to slight delay but improves overall efficiency of the protocol by sending more packets without link break than the state when some node is unable to process route due to inadequate battery power and signal strength. The process also helps when some intermediate node moves out of the range and link break occurs. In such cases the backbone nodes take care of the process and the route is established again without much overhead. The nodes which are having battery power and signal strength can be selected for route reconstruction. Backbone Node will be selected at one hop distance from the affected node.

A. Route Construction(REQ) Phase : In AODV routing protocol [5], route request and route reply operations are the most important, and route discovery with AODV is purely on-demand. When a node wishes to send a packet to a destination node, it checks its route table to determine whether it currently has a route to that node. If so, it forwards the packet to the next appropriate hop toward the destination; otherwise, it has to initiate a route discovery process. The source node broadcasts a flooding RREQ packet, which contains the ce rt i f i c at es of t h e no d e; i p a dd r ess broadcast ID to form a unique identifier for the RREQ. The intermediate nodes can avoid processing the same RREQ using this unique identifier. After broadcasting the RREQ, the source node sets a timer to wait for a reply. The node that successfully received the RREQ should The node that successfully received the RREQ should judge whether it is the destination or it has a route to the destination with corresponding sequence number greater than or equal to that contained in the RREQ. In the latter case, the node uncast a route reply (RREP) packet back to the source; otherwise, it rebroadcasts the RREQ. If the intermediate nodes receive the RREQ they have already processed, the RREQ should be discarded directly. When the route reply process is done, a forward route is set up. When a link break in an active route is detected, an ERR message is used to notify that the loss of link has occurred to its one hop neighbor. Here ERR message indicates those destinations which are no longer reachable. Taking advantage of the broadcast nature of wireless communications, a node promiscuously overhears packets that are transmitted by their neighboring nodes. When a node that is not part of the route overhears a REP packet not directed to itself transmit by a neighbor (on the primary route), it records that neighbor as the next hop to the destination in its alternate route table. From these packets, a node obtains alternate path information and makes entries of these backbone nodes (BN) in its route table. If route breaks occurs it just starts route construction phase from that node. The protocol updates list of BNs and their c e r t i f i c a t e s , power status and signal strength periodically in the route table.

B. Route Maintenance : When node detects a link break [1], it performs a one hop data broadcast to its immediate neighbors. The node specifies in the data header that the link is disconnected and thus the packet is candidate for alternate routing. Upon receiving this packet route maintenance phase starts by selecting alternate path and checking power status, signal strength.

C. Local Repair : When a link break in an active route occurs as shown in figure 3, the node upstream of that break may choose to repair the link locally if the destination was no farther and there exists BNs that are active. When a link break occurs the route is disconnected. Backbone nodes are broad casts their certificates, power status and signal strength to the neighbor nodes. The node which are having authenticated certificate, maximum battery power and signal strength can be selected as route[7].

.The received signal strength can be calculated as

$Pr = cert(n) + Pt/4*pi*di^2$+power status

Here Pr is the total received signal strength, Pt is the transmission power of the node and di is the distance of the node and cert(n) is the certificate of the node.

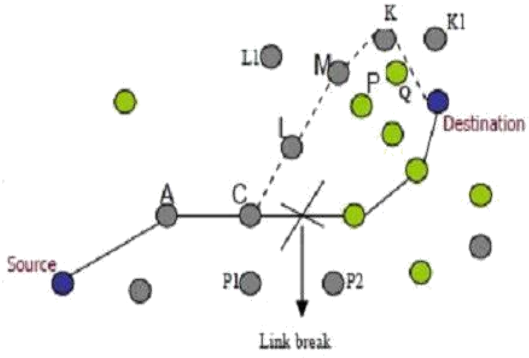

Figure 3: Local repair

When link breaks at node C, route repair starts, node C starts searching for new paths, buffering packets from S-A in its buffer. The nodes L, M, K, K1, L1, P1, P2 are broadcasts their certificates, power status and signal strength to its neighbor nodes. Now backbone nodes are selected and proper selection of nodes is done based on authenticated nodes, power factor and signal strength. Path selected becomes [C - L – M – K – Destination], instead of [C – L– P –Destination], since the node P is not in active state. Even though the route may become longer, the selected route path is far more stable and delivery of packets is reliable. Stability and reliability of route depends upon four major aspects as: Authentication, Life time, Power status and signal strength.

IV. SIMULATION AND RESULTS

Simulation study has been carried out to study the Performance study of existing different protocols Simulation Environment used is NS-2 (network simulator) version NS2.29 to carry out the process. Simulation results have been compared with AODV, DSR and TORA. Simulation study has been performed for packet delivery ratio.

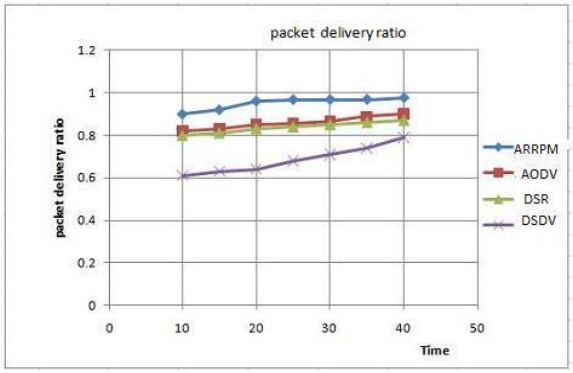

REFERENCES

[1] Vinay Rishiwal, Ashwani Kush, Shekhar Verma "Stable and Energy Efficient Routing for Mobile Adhoc Networks" Fifth International Conference on Information Technology: New Generations 2008, 1028-1033.
[2] E.M. Royer and C.K. Toh, "A review of current routing protocols for ad hoc mobile wireless networks". IEEE Personal Communications, pages 46–55, April 1999.
[3] J.J. Garcia, M. Spohn and D. Bayer, "Source Tree Adaptive Routing protocol", IETF draft, October 1999.
[4] D.B. Johnson, D.A. Maltz, "Dynamic Source Routing in Ad Hoc Networks", Mobile Computing, T. Imielinski and H. Korth, Eds., Kulwer, 1996, pp. 152-81 protocol for mobile ad hoc networks (RDMAR)", CCSR ,UK.
[5] C.E. Perkins, E.M. Royer, "Ad-Hoc On Demand Distance Vector Routing", Proceedings of the 2nd IEEE Workshop on Mobile Computing Systems and Application New Orleans, LA, February 1999, pp. 90-100.
[6] Josh Broch, David A.Maltz and Jorjeta Jetcheva, "A performance Comparison of Multi hop Wireless Adhoc Network Routing Protocols", Mobicomm'98, Texas, Oct 1998.
[7] WU Da-peng , WU Mu-qing, ZHEN Yan, "Reliable routing mechanism based on neighbor stability for MANET" www.buptjournal.cn/xben June 2009, 16(3): 33–39.
[8] C. K. Toh, "Maximum battery life routing to support ubiquitous mobile computing in wireless ad hoc networks", IEEE Comm. Mag., June 2001, pp. 138-147.
[9] Z.J. Hass, M.R. Pearlman, "Zone routing protocol (ZRP)", Internet draft. June 1999, at www.ietf.org

[10] E. Crawley, R. Nair, B. Rajagopalan, and H.Sandick, "A framework for QoS based routing in the internet," RFC 2386, Aug. 1998.
[11] M. Ettus. System Capacity, Latency, and Power Consumption in Multihop-routed SS-CDMA Wireless Networks. In Radio and Wireless Conference (RAWCON '98), pages 55–58, Aug.1998.
[12] X. Lin and I. Stojmenovic. Power-Aware Routing in Ad Hoc Wireless Networks. In SITE, University of Ottawa, TR-98- 11, Dec. 1998.
[13] A. Chockalingam and M. Zorzi, "Energy Consumption Performance of a Class of Access Protocols for Mobile Data Networks," Proc. IEEE VTC, May 1998, pp. 820–24.
[14] A. Michail and A. Ephremides, "Energy Efficient Routing for Connection Oriented Traffic in Ad-hoc Wireless Networks," Proc. IEEE PIMRC, Sept. 2000, pp. 762–66.
[15] G. Zussman and A. Segall. Energy efficient routing in ad hoc disaster recovery networks. Proceedings of IEEE INFOCOM, April, 2003.
[16] C. Schurgers and M. B. Srivastava. Energy efficient routing in wireless sensor networks. Proceedings of IEEE MILCOM, pages 28–31, October 2001.
[17] K. Sanzgiri, B. Dahill, B. N. Levine, C. Shields, E. M. Belding-Royer, "A Secure Routing Protocol for Ad Hoc Networks," 10th IEEE International Conference on Network Protocols (ICNP'02) November 12-15, pages 78-89, 2002.

ISSN (e): 2250 – 3005 || Vol, 04 || Issue, 11 || November – 2014 ||
International Journal of Computational Engineering Research (IJCER)

Authentication Using Graphical Password

Mayur Patel[1], Nimit Modi[2]
[1]Department of CE Sigma Institute of Engineering, Baroda, India
[2] Assistant Professor Department of CE Sigma Institute of Engineering, Baroda, India

ABSTRACT:
This paper introduces image based captcha to protect user data or unauthorized access of information. In that password is created from images and text password. Current system is based on only text password but it has disadvantages small password mostly used and easy to remember. This type of password is easy to guess through different attack i.e. dictionary attack and brute force attack. In this paper we have proposed a new image password scheme. In this Recognition based technique is used with numerical password which provide more security and easy to remember text and graphical password.

KEYWORDS: *Captcha, brute force attack, Authentication, Graphical Password, images, security, dictionary attack.*

I. INTRODUCTION

Security is most important in our daily life. CAPTCHA standing for "Completely Automated Public Turing test to tell Computers and Humans Apart", is an automatic challenge-response test to distinguish between humans and machines [2].Captcha is used for protection against different attack i.e. bot.In image based captcha is click based graphical passwords, where sequence of clicks on an image is used to derive a password. It provides protection against online dictionary attacks on password. In this for login every time click on images. Captcha can be applied on touch screen devices where on typing passwords is not more secure, especially for secure internet applications such as e-banks. For example ICBC (www.icbc.com.cn) used captcha. This bank is largest bank in world for every login user has to solve Captcha challenges. Captcha helps to reduce spam emails [1].In early system only text password is used which is very difficult to remember if enter a long password. If we use smaller password then it can be easily identify and we also use common password for many accounts so for that Image based captcha provide more security during authentication.

Literature Survey : Bin B. Zhu [1] implemented the Captcha as Graphical Passwords-A New Security rimitive Based on Hard AI Problems. This authentication system is based on Animal Grid and Click text which can be used in smartphone as well as desktop computers. Hossein Nejati [2] implemented the DeepCAPTCHA: An Image CAPTCHA Based on Depth Perception. In this system 6 images of different objects and different sizes of images is used and user task is to order these images in terms of their relative size. Hadyn Ellis [3] implemented the Science behind Passfaces. In this system 3x3 grid is used. User also uses the human faces or a numerical keypad value this value is corresponds to the faces on the grid. In that at least 3 to 7 faces user have to select for login process. But in this system required login time can be increased if user selects more passfaces.

P. R. Devale [4] implemented Cued Click Points with Click Draw Based Graphical Password. In this system increasing security using secret drawing in particular image during authentication process. Correct password or incorrect password is displayed after final click.Pankaja Patil [5] implemented Graphical password authentication using persuasive cued click point. In this system after filling the form user can select user define picture or system define picture after that user have to click any pixels in the images as click point to create graphical password. During creation of password one view port that is randomly positioned on the image User also change this view port if user does not want that view port. View port can be changed using Shuffle. During registration phase user has to click 5 point within that view port and at a login time sequence must be in correct order.Nilesh Kawale [6] implemented A Recognization Based Graphical Password System. In this system 3x3 grid is used. During registration phase user has to select 3 images from that grid. After completion of registration process one message send to user mobile which contain a password which is entered during login phase. During login phase user have to enter username which is entered during registration phase, text password, and select 3 images from current grid which is selected during registration phase.Darryl D'Souza [7] implemented Avatar Captcha: Telling Computers and humans apart via face classification. In this system based

on combination of human faces and Avatar faces. In that 2 rows are used each row having 6 images total 12 images in that. Each images having checkbox which is used to select only avatar faces for successful login.
Robert Biddle [8] discussed on Graphical Passwords: Learning from the first Twelve Year. A survey and conducted a brief study on existing graphical password techniques.
Mohamed Sylla [9] implemented Combinatoric Drag Pattern Graphical Password. In this System one graphical keyboard is provided to user for selection of a password. During selection of password user has to choose set of characters from the graphical keyboard. These characters shown in textbox. User must follow the sequence for creation of password. After that system check password if it is not strong then system suggests different character between passwords. And for that user has to draw pattern for that to create a password.

II. EXISTING SYSTEM

Graphical Password was originally defined by Blonder (1996).In graphical passwords techniques are classified into two main categories: recognition-based and recall based graphical techniques. In Recognition based techniques, a user is presented with a set of images and the user passes the authentication by recognizing and identifying the images he selected during the registration stage. In recall based graphical password, a user is asked to reproduce something that he/she created or selected earlier during registration phase [5].Existing System is based on recognition techniques in that A. Click Text and Animal Grid two method introduce. A. Click Text In this method 33 Capital Letters except I, J, O, and Z digits except 0 and 1, and three special characters #,@,and &.The last three characters is used to balance the security. Characters were arranged in 5 rows. Each character was randomly rotate from -30 degree to 30 degree and scaled from 60% to 120%.Neighboring characters could overlap up to 3 pixels [1].

"Figure 1. Click Text image with 33 characters [1]."

B. Animal Grid : In this method 10 animals used: bird, cow, horse, dog, giraffe, pig, rabbit, camel, element and dinosaur. Each animal had three 3d models.3d animal model was randomly selected and posed at a random view in generating a 2d object. Each click animal image was also set to 400 by 400 pixels. A 6x6 grid was used for CAS. Cells were labeled clockwise starting from cell 0.

"Figure 2. Click Animal images (left) and 6x6 grid (right) [1]."

The main disadvantage of above two methods is increasing load on system. Click text letters overlap with each other so it is time consuming sometimes during login process. In Animal grid 3d model is used and size of each animal is smaller. It does not protect from shoulder surfing attack. There is no theoretical model for this System.

III. PROPOSED SYSTEM

Our system is based on Recognition Technique. In this three different group of image is used in that 1.Famous Places 2. Famous People 3.Reputed Company Name. Each group contains 25 images. User has to select at least one image from each group during registration phase. During login time user has to click on that images which is selected during registration phase. This system provide protection against shoulder surfing attack, dictionary attack, brute force attack using text password as well as graphical password.

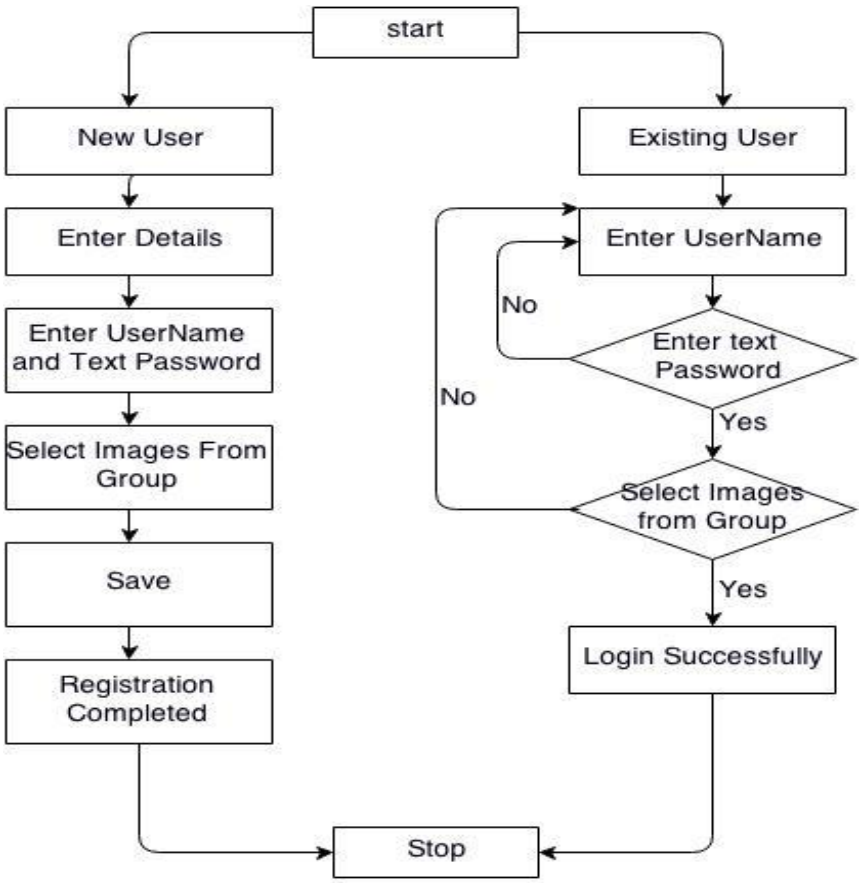

"Figure 3. Architecture Diagram of System."

IV. CONCLUSION AND FUTURE WORK

Our graphical password system provides more security to data and protection against different attack. Our graphical password system is based on text password and graphical password. For successful login user has to select correct image which is chosen by user during a registration and this system provide text password which provide more security to data. Future work is based on Pattern.

V. AKNOWLEDGEMENT

The authors wish to thank the Management, Principal, Head of the Department (Computer Engineering) and Guide of Sigma Institute of Engineering for the support and help in completing this work.

REFERENCES

[1] Bin B.Zhu, Jeff Yan, Guanbo Bao, Maowei Yang, and Ning Xu. Captcha as Graphical Passwords-A New Security Primitive Based on Hard AI Problems. IEEE TRANSACTIONS ON INFORMATION FORENSIS AND SECURITY, VOL.9, NO 6, June 2014.

[2] Hossein Nejati, Ngai-man Cheung, Ricardo Sosa and Dawn C.I.Koh. DeepCaptcha: An Image CAPTCHA Based on Depth Perception. ACM digital Library, March 2014.

[3] Hadyn Ellis. The Science behind Passfaces. www.realuser.com,Feb 2012.

[4] P.R.Devale Shrikala, M. Deshmukh and Anil B.Pawar. Persuasive Cued Click Points with Click Draw Based Graphical Password Scheme. International Journal of Soft Computing and Engineering, Volume-3, Issue-2 May 2013.
[5] Iranna A M and Pankaja Patil. Graphical Password Authentication using Persuasive Cued Click Point, International Journal of Advanced Research in Electrical,Elecrtorics and Instrumentation Engineering, Vol.2, Issue 7, July 2013.
[6] Nilesh Kawale and Shubhangi Patil. A Recognization Based Graphical Password System. International Journal of Current Engineering and Technology, Vol.4, No.2, Apr 10, 2014
[7] Darryl D'Souza Phani, C.Polina, Roman V and Yampolskiy.Avatar Captcha: Telling Computers and humans apart via face classification.IEEE, 2012.
[8] Robert Biddle, Sonia Chiasson and P.C.van Oorschot. Graphical Passwords: Learning from the First Twelve Year. School of Computer Science, Carleton University, Jan 4, 2012.
[9] Mohamed Sylla, Gul Muhammad, Kaleem Habib and Jamaludin lbrahim.Combinatoric Drag-Pattern Graphical Password. Journal of Emerging Trends in Computing Information Sciences, Vol.4,No.12,Dec 2013.

ISSN (e): 2250 – 3005 || Vol, 04 || Issue, 11 || November – 2014 ||
International Journal of Computational Engineering Research (IJCER)

Quick Routing for Communication in MANET using Zone Routing Protocol

Prof. Shrishail C. Gurav
Department of Electronics & Telecommunication Engineering, SVERI's College of Engineering, Pandharpur/Solapur University, Solapur, India.

ABSTRACT:
Mobile Adhoc Networks is non-infrastructure, self configuring and decentralized set of mobile nodes. So the routing protocols for mobile adhoc networks have to face the challenge of frequently changing topology low transmission power and asymmetric links. This work deals with one of the most popular routing protocols in MANETs i.e. Zone Routing Protocol (ZRP). In this work, we address the issue of self configuring framework for the ZRP to provide the best performance for a particular network at any time. As the name indicates the MANET's are specially defined for the mobility of the nodes in the networks. The nodes may move at a different speed, which may enter or move out of the network, which leads the delay, jitter, and link failure conditions during the transmission of packets. In the large networks, the more number of nodes will accept these parameters at a same time or random time. Such that scalability problem in the network may arise. Without a fixed infrastructure, mobile adhoc networks have to rely on the portable, limited power sources. Therefore the energy-efficiency becomes one of the most important problems in MANETs. Other challenging aspects on MANETs are node cooperation, interoperation with the internet, aggregation, multicast as well as changing the network topologies. Technologies such as smart antennas, software's will also bring new problems along with impetus to adhoc to MANETs. We discuss the factors influencing on improvement in performance of Zone routing protocol, performed in number of related works. This work is based on literature research. The proposed protocol is based on the principle of self reconfiguring, multicast, query detection based, low bit error rate mode of operation. This work aims to optimize the Quality of Service in transmission for the zone routing protocol. Through test-bed simulation, we demonstrate that our proposed work will allow the ZRP to operate a better reconfiguration framework during link failure conditions.

Keywords: *Ad-hoc, MANET, Routing, Throughput, ZRP,* IERP, IARP

I. INTRODUCTION

In this new era of communication, the advent of mobile computing has revolutionized our information society. Now a day's a new, powerful, efficient and compact communicating devices like personnel digital assistants (PDAs), pagers, laptops and cellular phones, having extraordinary processing power paved the way for advance mobile connectivity. We are moving from the Personal Computer age to the Ubiquitous Computing age in which a user utilizes, at the same time, several electronic platforms through which he can access all the required information whenever and wherever needed. The nature of ubiquitous devices makes wireless networks the easiest solution for their interconnection and, as a consequence, the wireless area has been experiencing exponential growth in the past decade [1].

Currently, most of the connections among the wireless devices are achieved via fixed infrastructure-based service provider, or private networks. For example, connections between two cell phones are setup by BSC and MSC in cellular networks; laptops are connected to Internet via wireless access points. While infrastructure-based networks provide a great way for mobile devices to get network services, it takes time and potentially high cost to set up the necessary infrastructure. There are, furthermore, situations where user required networking connections are not available in a given geographic area, and providing the needed connectivity and network services in these situations becomes a real challenge.

For all these reasons, combined with significance advances in technology and standardization, new alternative ways to deliver mobile connectivity have been emerging. These are focused around having the mobile devices connect to each other in the transmission range through automatic configuration, setting up an ad hoc mobile network that is both flexible and powerful. A mobile ad hoc network (MANET) sometimes called a **wireless ad hoc network** or a **mobile mesh network** is a wireless network, comprised of mobile computing devices (nodes) that use wireless transmission for communication, without the aid of any established infrastructure or centralized administration such as a base station or an access point [1, 2, 3, 4]. Unlike traditional mobile wireless networks, mobile ad hoc networks do not rely on any central coordinator but communicate in a self organized way. Mobile nodes that are within each other's radio range communicate directly via wireless links, while those far apart rely on other nodes to relay messages as routers. In ad hoc network each node acts both as a host (which is capable of sending and receiving) and a router which forwards the data intended for some other node. Ad hoc wireless networks can be deployed quickly anywhere and anytime as they eliminate the complexity of infrastructure setup. Applications of ad hoc network range from military operations and emergency disaster relief, to commercial uses such as community networking and interaction between attendees at a meeting or students during a lecture. Most of these applications demand a secure and reliable communication.

Mobile wireless networks are generally more vulnerable to information and physical security threats than fixed wired networks. Vulnerability of channels and nodes, absence of infrastructure and dynamically changing topology, make ad hoc networks security a difficult task [1]. Broadcast wireless channels allow message eavesdropping and injection (vulnerability of channels). Nodes do not reside in physically protected places, and hence can easily fall under the attackers' control (node vulnerability). The absence of infrastructure makes the classical security solutions based on certification authorities and on-line servers inapplicable. In addition to this, the security of routing protocols in the MANET dynamic environment is an additional challenge.

Most of the previous research on ad hoc networking has been done focusing only upon the efficiency of the network. There are quite a number of routing protocols proposed [5, 6, 7] that are excellent in terms of efficiency. However, they were generally designed for a non-adversarial network setting, assuming a trusted environment; hence no security mechanism has been considered. But in a more realistic setting such as a battle field or a police rescue operation, in which, an adversary may attempt to disrupt the communication; a secure ad hoc routing protocol is highly desirable. The unique characteristics of ad hoc networks present a host of research areas related to security, such as, key management models, secure routing protocols, instruction detection systems and trust based models.

II. RELATED WORK

In this paper, we are dealing with related works somehow that are proposed for improvement in performance ZRP protocol in asymmetrical networks. Some of them are discussed here which related to our proposed work. The multicast routing and route reconfiguration for Zone Routing Protocol is proposed on [25]. It assume that all the routes in any routing table are active, usable and only need updating when a node joined the network and sent update message or an error message is received regarding to a specific non reachable node or a broken link, then partial updates are needed for some entries which have the non reachable node as a destination or intermediate. Therefore, MDVZRP reduces the proactive scope to a zone centered on each node. MDVZRP uses a topological map of the zone centered on a node to guarantee loop freedom, alternative paths in the case of route failure and disjoint paths. Within the zone, routes are immediately available, but for destinations outside the zone, MDVZRP uses a route discovery mechanism to add routes to the table. In the case of link failure, MDVZRP uses a link-id field to identify routes affected by the failure.

To reduce the network load by limiting the number of control packets when the protocol searches for a new route is proposed in SBZRP [26]. When the node stops for a short period of time, that means the moving degree is high, the SBZRP has higher link usability than ZRP. When node moving degree is high, the route search failure becomes high. For the SBZRP, if the route search fails, a new route search starts from the failed node. Thus, the new route search time is shorter than ZRP and the number of data sent to the DN becomes high.

The performance of the existing ZRP protocol is proposed on [27] this proposed work describes the performance of the ZRP protocol comparing with AODV and DSR protocols with considering two different scenarios. The main characteristics are carried out and a thorough evaluation it is clear that the ZRP against DSR and AODV has low performance and ZRP was not up to the task and it performed poorly throughout all the simulation sequences. In particular it demonstrated a really low packet delivery ratio when compared to DSR and AODV. DSR on the other hand performed admirably and it would be the clear winner if not for its bad behavior in high traffic cases. AODV performed well in most of the network sizes (better than ZRP).

To address the issue of configuring the ZRP to provide the best performance for a particular network, at any time. Adaptation of the ZRP to changing network conditions requires both an understanding of the ZRP and reacts to changes in network behavior and a mechanism to allow individual nodes to identify these changes, given only limited knowledge of the network behavior.

III. PROPOSED WORK:

The proposed ZRP uses for intra-zone routing the IARP the same as ZRP, but uses a new IERP for inter-zone routing. To explain IARP let consider Fig.1 . The node A generates the IARP packet (S is Source Node (SN)

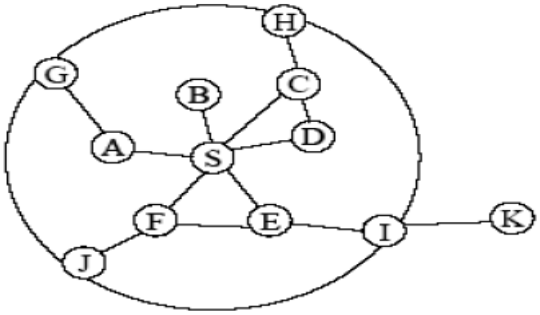

Figure1. Routing zone of node S with zone radius ρ =2

and the HC is 2) and sends it to all neighbor nodes (nodes A, B, C, D, E, F). The node after receiving IARP packet updates its own routing table using IARP packet information. The nodes are moving so the route information may be inappropriate after a period of time.

Since ZRP assumes that local neighbor discovery is implemented on the link-layer and is provided by the NDP, the first protocol to be part of ZRP is the *Intrazone Routing Protocol*, or IARP. This protocol is used by a node to communicate with the interior nodes of its zone and as such is limited by the zones radius ρ (the number of hops from the node to its peripheral nodes). Since the local neighborhood of a node may rapidly changing, and since changes in the local topology are likely to have a bigger impact on a nodes routing behavior than a change on the other end of the network.

As the global reactive routing component of the ZRP, the Interzone Routing Protocol, or IERP, takes advantage of the known local topology of a node's zone and, using a reactive approach enables communication with nodes in other zones. The reactive route discovery process consists of two phases: the route request phase and the route reply phase. The route request phase is initiated when a node requires a route to a destination, but does not have the route stored in its route table. This query source issues a route request packet and sends this packet to each of its neighbors. When a node with an active route to the query destination receives the request, it may respond with a reply. Otherwise, it forwards the request packet to its neighbors. Subsequent copies of the route request are considered to be redundant and are discarded.

When a queried node can provide a route to the destination, a reply containing information about the discovered route is sent back to the query source. In order to relay the reply, the request needs to accumulate route information as it progresses through the network. Before forwarding a query packet, a node appends its address and relevant node/link metrics to the packet. When a query packet reaches the destination, the sequence of recorded nodes represents a route from the source to the destination. This route may be reversed and used to send the reply back to the query source. Transmission resources can be saved during the route request phase by distributing previous hop information among the intermediate nodes, instead of appending node addresses to increasingly longer packets. A similar approach can be used during the reply phase.

The query source may receive an entire source route to the query destination, or each route node can record the next-hop address to the destination in its routing table. A route request broadcast traverses all network links, allowing any reachable destination to be discovered. However, the undirected nature of broadcasting results in redundant coverage. Nodes are sent copies of the same route request by each neighbor. An optimal probing mechanism would direct the query outward, away from the query source and away from regions that have already been covered by the query.

When a node has no valid route to forward a data packet, it launches a route discovery, probing the network via broadcast RREQ packets. When a node receives a RREQ packet, it appends its IP address along with metrics for the link on which the packet was received. It then checks its Routing Tables for a valid route to the query destination. If a valid route to the query destination is known, then the route is appended to the RREQ's accumulated route. The complete route is copied to a RREP packet. The RREP is forwarded back to the query source, by IERP, along the reversed accumulated route. The IERP Packet format has shown in figure 2.

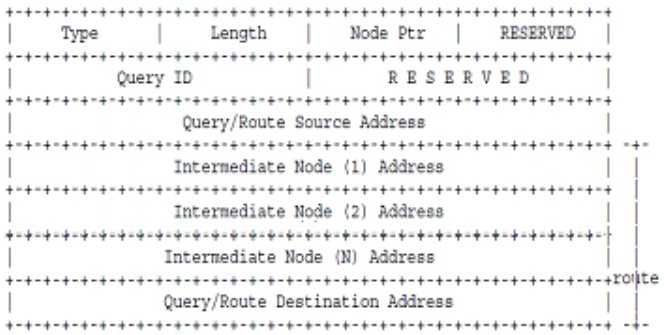

Figure 2. The IERP packet structure.

3.1 Field Description:

* Type (char) (8 bits)
  Identifies the type of IERP packet. The current version of IERP contains two packet types:
  1. ROUTE_REQUEST (RREQ): Request for a route to the Query Destination. The RREQ records the path that it has traveled from the Query Source.
  2. ROUTE_REPLY (RREP): Response to a ROUTE_REQUEST packet, issued by the node that discovers a route to the Query Destination, and sent back to the Query Source.
* Length (char) (8 bits)
  Length of the packet, in multiples of 32 bit words.
* Node Pointer (char) (8 bits)
  Index into the route (see below) corresponding to the node that has just received, or is next to receive, this packet.
* Query ID (unsigned int) (16 bits)
  Sequence number which, along with the Query Source Address (see below) uniquely identifies any RREQ in the network.
* Query/Route Source Address (node_id) (32 bits)
  IP address of the node that initiates the RREQ. In subsequent stages, this corresponds to the IP address of the discovered route's source node.
* Query/Route Destination Address (node_id) (32 bits)
  IP address to be located during the RREQ phase. In subsequent stages, this field contains the IP address of the discovered route's destination node.
* Route (node_id) (N * 32 bits)
  Variable length field that contains the recorded IP addresses of nodes along the path traveled by this RREQ packet from the Query Source. After a route to the Query Destination has been discovered, this set of IP addresses provides a specification of the route between the Route Source and Route Destination.

The IERP routing table is shown in Fig 3.

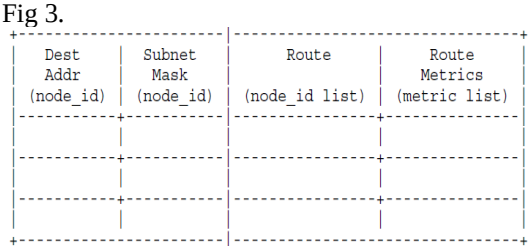

Figure3. IERP Routing Table

a. Proposed algorithm for the reconfigure the broken link

The following algorithm were proposed for the IERP protocol in ZRP which selects another optimum route from the routing table such that dropping factor of the data packets is to be minimized. The proposed algorithm for the ZRP protocol is shown Fig 4.

Condition that the next hop (neighbor node) is not reachable in the sense it is moved out of current node's coverage area.

Condition 1: If (next hop node == UNREACHABLE)
{
Step 1: delete failed nodes routing entry in the routing table.
}
Step 2: Search another optimum route in IERP's routing table.
Step 3: get another route from the table.
Condition 2: If (IERP routing Table!= NULL)
{
Step 4: add route address to the data packet.
Step 5: enter IERP to Route the Packet on alternative route.
}
Else
{
Step 6: update from the IARP
Step 7: send RREQ packets to discover the new route to the destination.
Step 8: update new route in routing table which holds the routing path to destination.
}

Figure 4. The proposed algorithm for Zone Routing Protocol

The Route Discovery procedure is shown in Figure 5. The source node S sends a packet to the destination D. To find a route within the network, S first checks whether D is within its routing zone. Since D does not lie within S's routing zone, S broadcasts a route request to all of its peripheral nodes: that is, to nodes C, G, and H. Upon receiving the route request, nodes C,H and G determine that D is not in their routing zones and they therefore broadcast the request to their peripheral nodes. One of H's peripheral nodes, B, recognizes D as being in its routing zone and responds to the route request, indicating the forwarding path: S-H-B-D. as shown in Fig 6,

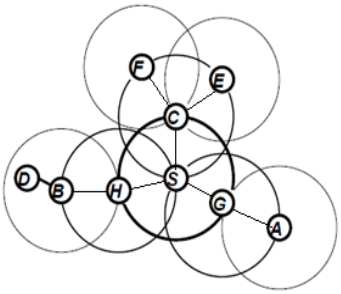

Figure 5. The IERP operation in proposed protocol.

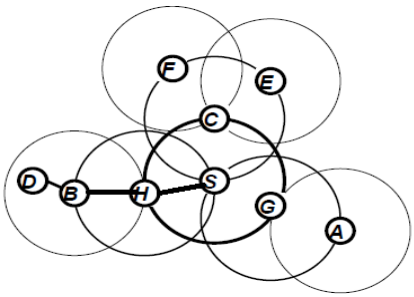

Figure 6. The shortest path in proposed IERP protocol.

In MANET's the main problems with routing protocols is link failure conditions due to mobility of the nodes. Consider Fig 7, which the link between B and H are broken and similarly the node F has moved near to the node of shortest route so the proposed protocol uses alternative way as shown in the figure which adds new route address to the data packet and continues the data transmission. Hence the cost of route discovery can be significantly reduced by using alternative path by using routing table. The path repair procedure substitutes a broken link by a mini-path between the ends of the broken link. A path update is then generated and sent to the end points of the path. Path repair procedures tend to reduce the path optimality (e.g., increase the length for shortest path routing). Thus, after some number of repairs, the path end points will initiate a new Route Discovery procedure to replace the path with a new optimal one.

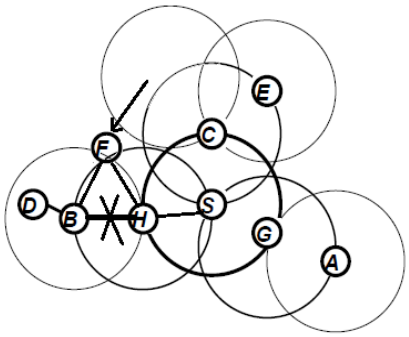

Figure 7. A case of broken link occurs during transmission.

When a destination node moves outside a zone, but the period of time from the last search is short, it can be considered that node is not too far from the route recorded in the IERP. Therefore, a node in the IERP can search to find a new route to node J. In Fig. 8, when a RP arrives in node G, but it has not found a route to node J, a new search is started from node G. Thus, the number of the border nodes and IERP packets can be decreased resulting in the increase of the throughput and the decrease of packet mean delay.

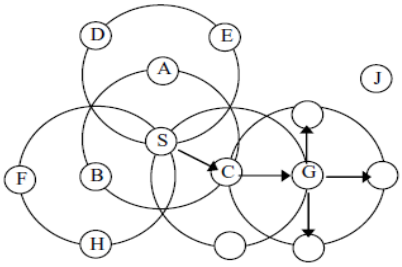

Figure 8. A case when DN moves outside the zone.

A node is moving for a period of time then stops for a moment of time. This pattern is repeated in a random way. When the node stops for a short period of time, that means the moving degree is high, the proposed ZRP protocol has higher link usability than existing ZRP. When node moving degree is high, the route search failure becomes high. For the proposed ZRP, if the route search fails, a new route search starts from the failed node. Thus, the new route search time is shorter than ZRP and the number of data sent to the DN becomes high.

IV. SIMULATION RESULTS AND ANALYSIS

4.1. Throughput without mobility

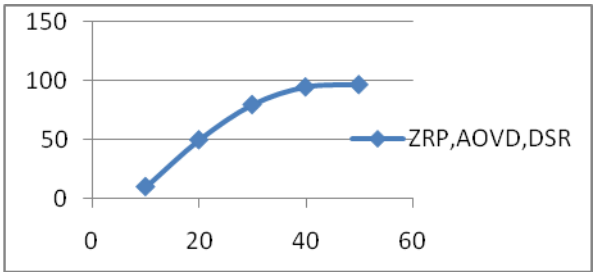

Figure 9. Throughput Vs Node Density

In Fig 9, the simulation results for proposed ZRP and AOVD, DSR under no mobility patterns and traffic scenarios show that both the protocols gives same efficient result.

4.2. Throughput with mobility

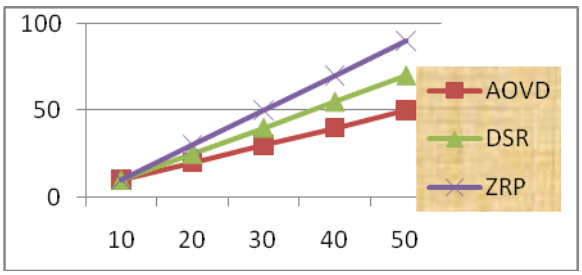

Figure 10: Throughput Vs Node Density

The Fig 10, the simulation results for proposed ZRP and AOVD, DSR under different mobility patterns and traffic scenarios show that the proposed protocol is as efficient than AOVD and DSR in discovering and maintaining routes, at the cost of using larger routing packets which result in a higher overall routing load, and at the cost of higher latency in reroute discovery because of the cryptographic computation that must occur.

4.3. End-toEnd Delay without mobility

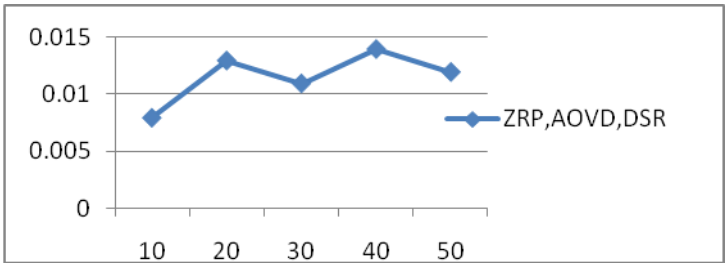

Figure11. End-toEnd Delay vs node Density

From the Fig 11, it represents the plotting ratio of End-to-End Delay measurements for both protocols which shows the End-to-End delay of flows. Looking at the figure, it can be recognised that the End-to-End Delay with no mobility and traffic gives same efficient Delay.

4.4. End-toEnd Delay with mobility

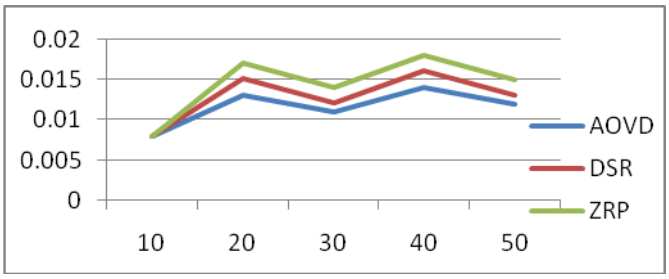

Figure12.End-toEnd Delay vs node Density

From the Fig 12, it represents the plotting ratio of End-to-End Delay measurements for both protocols which shows the End-to-End delay of flows. Looking at the figure, it can be recognised that the End-to-End Delay of traffic flows in existing ZRP in incresed as the number of the nodes density increases in the network, but in the proposed algorithm, the end-to-end delay has less osscilations and also average delay in each class is less than existing AOVD and DSR algorithms. So the throughput of the packets or bytes is more while comparing to existing AOVD and DSR.

4.5. Total Packets received without mobility

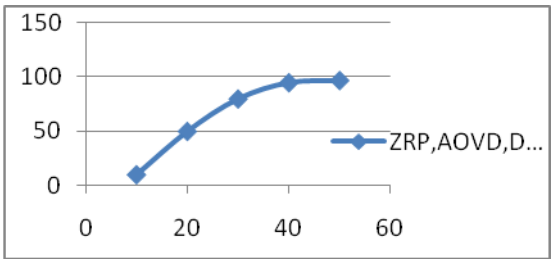

Figure 13. Total packets received Vs node density

In this Fig 13, it represents the plotting ratio of packet receiving capacity of all the three protocols.

4.6. Total Packets received with mobility

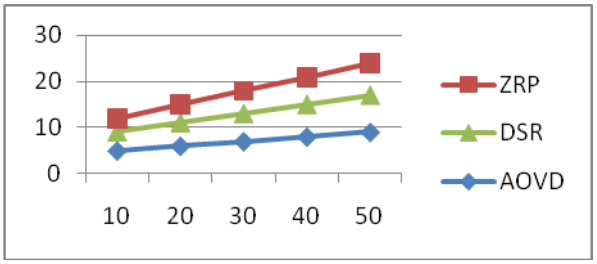

Figure 14. Total packets received Vs node density

The Fig 14, describes the data packet recived ratio on discovered route with the assymetrical links in the network. From the figure it concluded that the proposed alogorithm fives better result when comparing to existing protocols on deliering the data packets while plotted againest time being parameters. From the Fig, it is clear that route reconfiguration increases the ratio of throughput. Hence the the receiced bytes were also increased while comparing the existing protocols, which performing the less in the delivering ratio. Hence the increasing value of the data packets to the destination through the assymetrical links is also increased.

V. CONCLUSION

The Zone Routing Protocol (ZRP) provides a flexible solution to the challenge of discovering and maintaining routes in the Reconfigurable Wireless Network communication environment. ZRP combines two radically different methods of routing into one protocol. Inter zone route discovery is based on a reactive route request/route reply scheme. By contrast, intra zone routing uses a proactive protocol to maintain up-to-date routing information to all nodes within its routing zone.

We have presented the design and analysis of a new algorithm in Zone Routing Protocol to reconfiguring the route for mobile ad hoc networks. The proposed protocol is hybrid in nature and developed on the concept of zone routing protocol (ZRP). It provides a solution for link failure conditions asymmetrical environments. In designing proposed work, we carefully fit the algorithms to each part of the protocol functionality to create an efficient protocol that is robust against link failure conditions in the network. The proposed protocol gives a better solution towards achieving the high throughput goals like packet ratio, minimizing of End-to-end delay, minimum jitter and low latency in transmission of data packets.

We have simulated the proposed work for the ZRP protocol under different network scenarios and different traffic with different node densities, it's quite clear that proposed algorithm for the reconfiguration of route for link failure problems in the asymmetrical networks, will provide a better result for the Zone Routing Protocol while comparing to the existing protocols. The proposed ZRP can compete with other two protocols with somewhat difference may visible but better performance than existing protocols.

There are many areas in network movement planning that must still be researched to determine the true impact of a network plan. The direct areas of research stemming from this study include creating a more robust protocol to investigate high-speed movement and protocol optimization. The addition of mobility to a wireless structure network, in the form of mobile routers, can also be investigated for throughput improvements. Other aspects of protocol performance, such as network control overhead, end-to-end delay and dropped packets could be researched.

Many areas in planning can be explored, such as exploring alternative implementations of planning, attempting to design and implement a self-sustaining plan, and exploring locally omniscient plan compared to the centralized plan used in the test simulations. The effects of planning with respect to various protocol algorithms could be explored, to determine what the most efficient protocol-planning combination would be.

VI. ACKNOWLEDGE

Most importantly, I would like to thank our beloved principal and HOD, SVERI's COE, Phandarpur, for supporting me to do this work.

References

[1] Imrich Chlamtac, Marco Conti, Jenifer J.-N. Liu, "Mobile Ad Hoc Networking:Imperatives and Challanges", Elsevier Network Magazine, vol. 13, pages 13-64, 2003.
[2] C. Siva Ram Murthy and B. S Manoj, "Ad Hoc Wireless Networks, Architecture and Protocols", Prentice Hall PTR, 2004.
[3] Stefano Basagni, Macro Conti, Silvia Giordano and Ivan Stojmenovic, "Mobile Ad Hoc Networks" , IEEE press, A john Wily & Sons, INC. publication, 2003
[4] George Aggelou, "Mobile Ad Hoc Networks", 2nd edition, Mc GRAW Hill 1. professional engineering, 2004
[5] E.M. Belding-Royer and C. K. Toh, "A review of current routing protocols for adhoc mobile wireless networks", IEEE Personal Communications Magazine, pages 46–55, April 1999.
[6] Haas Z. J., Pearlman M. R., and Samar P., "The Zone Routing Protocol (ZRP)", IETF Internet Draft, draft-ietf-manet-zone-zrp-04.txt, July 2002.
[7] M.Joa-Ng and I. T. Lu, "A Peer-to-Peer Zone-Based Two-Level Link State Routing for Mobile Ad Hoc Networks," IEEE journal on Selected areas in Communications, vol. 17, no. 8, pp. 1415- 1425, August 1999.
[8] Jan Schaumann, "Analysis of Zone Routing Protocol", Course CS765, Stevens Institute of Technology Hoboken, New Jersey, USA, 8th December 2002.
[9] Behrouz A. Forouzan, "Data communication and Networking," 2nd edition, Tata McHill publication, 2001.
[10] C. E. Perkins and P. Bhagwat, "Highly Dynamic Destination-Sequenced Distance-Vector Routing (DSDV) for Mobile Computers," Comp. Commun. Rev., Oct. 1994, pp. 234–44.
[11] C.-C. Chiang, "Routing in Clustered Multihop, Mobile Wireless Networks with Fading Channel," Proc. IEEE SICON '97, Apr. 1997, pp. 197–211.
[12] S. Murthy and J. J. Garcia-Luna-Aceves, "An Efficient Routing Protocol for Wireless Networks," ACM Mobile Networks and App. J., Special Issue on Routing in Mobile Communication Networks, Oct. 1996, pp. 183–97.
[13] P. Jacquet, P. Muhlethaler, A. Qayyum, "Optimized Link State Routing Protocol", Internet Draft, draft-ietf-manetolsr- 00.txt, November 1998.
[14] D.B. Johnson, D.A. Maltz, "Dynamic source routing in adhoc wireless networks", in: T. Imielinski, H. Korth (Eds.), Mobile Computing, Kluwer Academic Publishers, Dordrecht, 1996, pp. 153–181.
[15] C. E. Perkins and E. M. Royer, "Ad hoc on-demand distance vector routing", In IEEE Workshop on Mobile Computing Systems and Applications, pages 90–100, Feb. 1999.
[16] V. D. Park and M. S. Corson, "A Highly Adaptive Distributed Routing Algorithm for Mobile Wireless Networks," Proc. INFOCOM '97, Apr. 1997.
[17] C-K. Toh, "A Novel Distributed Routing Protocol to Support Ad-Hoc Mobile Computing", Proc. 1996 IEEE 15th Annual Int'l. Phoenix Conf. Comp. and Commun., Mar. 1996, pp. 480–86.
[18] A. Laouiti, A.Qayyum, and L.Viennot, "Multipoint Relaying; An Efficient Technique for Flooding in Mobile Wireless Networks," in Proceeedings of the 35th Annual Hawaii International Conference on System Science (HICSS' 2002), Waikoloa, HI, January 2002.
[19] J. Broch, David A. Maltz, David B. Johnson, Y-Ch Hu and J Jetcheva, ―A performance Comparison of Multi-hop Wireless Ad Hoc Network for mobile ad hoc networks‖, in Proc. 4th annual IEEE/ACM international conference on Mobile Computing and Networking, Dallas, Texas, U.S. pp. 85-97, Oct. 1998.
[20] P. Jacquet, P. Muhlethaler, T. Clausen, A. Laouiti, A. Qayyum and L. Viennot, " Optimized Link State Routing Protocol for Ad-Hoc Networks", Proceedings of 5th IEEE Multi Topic conference (INMIC 2001), 2001.
[21] Jochen Schiller. Mobile Communications. Addison-Wesley, 2000.
[22] Haas, Zygmunt J., Pearlman, Marc R., Samar, P.: "Intrazone Routing Protocol (IARP)", IETF Internet Draft, draft-ietf-manet-iarp-01.txt, June 2001
[23] Haas, Zygmunt J., Pearlman, Marc R., Samar, P.: "Interzone Routing Protocol (IERP)", IETF Internet Draft, draft-ietf-manet-ierp-01.txt, June 2001.
[24] Haas, Zygmunt J., Pearlman, Marc R., Samar, P.: "The Bordercast Resolution Protocol (BRP) for Ad Hoc Networks", IETF Internet Draft, draft-ietf-manet-brp- 01.txt, June 2001.
[25] Idris Skloul Ibrahim, A. Etorban and Dr Peter J.B King: Multipath Distance Vector Zone Routing Protocol (MDVZRP),9th PG Net, Liverpool John Moores University,Uk 23-24 June 2008.
[26] Leonard baroli, Yoshitaka Honma, akio Koyama, arjan duress, junepei aria." A Selective Bordercasting Zone routing Protocol for Ad-Hoc Networks", proceedings of 15th international worshop on database and expert systems applications (DEXa'04), 1529-4188/04-2004.
[27] Prof: M. N. Sree Rangaraju, kiran runkana, jitendranath mungara, "ZRP versus AODV and DSR: A Comprehensive study on ZRP performance", International journal on computer applications, No-12, Article-7, 2010.
[28] Pearlman, M.R. and Haas, Z.J., "Determining the Optimal Configuration for the Zone Routing Protocol," IEEE JSAC, August, 1999.

ISSN (e): 2250 – 3005 || Vol, 04 || Issue, 11 || November – 2014 ||
International Journal of Computational Engineering Research (IJCER)

Enhancement of power quality by DVR using "ANN Technique" under unbalanced and non-linear loads

[1]K.Anand Dev Singh, [2]K.Vasantha Sena
[1] PG STUDENT, Department of EEE, DIET College of Engineering, Anakapalle, Visakhapatnam- 531 002
[2]Assistant Professor, Department of EEE, DIET College of Engineering, Anakapalle, Visakhapatnam- 531 002

ABSTRACT

The paper discusses the voltage control of a critical load bus using dynamic voltage restorer (DVR) in a distribution system. The critical load requires a balanced sinusoidal waveform across its terminals preferably at system nominal frequency of 50Hz .It is assumed that the frequency of the supply voltage can be varied and it is different from the system nominal frequency. The DVR is operated such that it holds the voltage across critical load bus terminals constant at system nominal frequency irrespective of the frequency of the source voltage. In case of a frequency mismatch, the total real power requirement of the critical load bus has to be supplied by the DVR. Proposed method used to compensate for frequency variation, the DC link of the DVR is supplied through an uncontrolled rectifier that provides a path for the real power required by the critical load to flow .A simple frequency estimation technique is discussed which are Discrete Fourier transform (DFT), ANN controller. The present work study the compensation principle and different control strategies of DVR used here are based on DFT, and ANN Controller .Through detailed analysis and simulation studies using MATLAB. It is shown that the voltage is completely controlled across the critical load.

KEYWORDS : Critical load; DVR; Distribution system; Nominal frequency; Power quality; Voltage control; VSI DFT, kalman Filter and ANN Controller.

I. INTRODUCTION

The power quality (PQ) characteristics fall into two major categories: steady-state PQ variations and disturbances. The steady-state PQ characteristics of the supply voltage include frequency variations, voltage variations, voltage fluctuations, unbalance the three-phase voltages, and flicker in harmonic distortion. There are many devices, such as power electronic equipment and arc furnaces, etc., those generate harmonics and noise in modern power systems. Power frequency variations are defined as deviation of the power system fundamental frequency from its specified nominal values (e.g., 50Hz or 60Hz). The duration of a frequency deviation can range between several cycles to several hours. These variations are usually caused by rapid changes in the load connected to the system. The maximum tolerable variation in supply frequency is often limited within +ve or –ve 0.5Hz. Voltage notching can be sometimes mistaken for frequency deviation. Accurate frequency estimation is often problematic and may yield incorrect results. A number of numerical methods are available for frequency estimation from the digitized samples of the supply voltage. These methods assumed that the power system voltage waveform is purely sinusoidal and therefore the time between two zero crossing is an indication of system frequency. Digital signal processing techniques are used for frequency measurement of power system signals. These techniques provide accurate estimation near-nominal and off-nominal frequencies. The application of enhanced phase locked loop (EPLL) system for the online estimation of stationary and instantaneous symmetrical components.

The well known custom power devices such as distribution STATCOM (DSTATCOM), dynamic voltage restorer (DVR) and unified power quality conditioner (UPQC) are available for protection of a critical load from disturbances occurring in the distribution system. In this paper we will discuss voltage control of a critical load bus using DVR. The critical load requires balanced sinusoidal waveforms across its terminals preferably at system nominal frequency of 50Hz. It is assumed that the frequency of the supply voltage can vary and it is different from the system nominal frequency. A DVR is a power electronic controller and it is realized using voltage source inverter (VSIs). It injects three independent single phase voltages in the distribution feeder such that load voltage is perfectly regulated at system nominal frequency.

In general, the DVR is operated in such a fashion that it does not supply or absorb any real power during study state operation [12].In case of a frequency mismatch; the total real power requirement of the load has to be supplied by the DVR. To provide this amount of real power, the dc link of the DVR is supplied through an uncontrolled rectifier connected to the distribution feeder. First of all, the analysis of the DVR operation supported through a dc battery has been discussed. A simple frequency estimation technique is discussed which uses a moving average process along with a zero-crossing detector. The reference voltages injected by the DVR are tracked in the closed loop output feedback switching control. A simple frequency estimation technique is discussed which are Discrete Fourier transform (DFT), Kalman Filter and ANN controller. The present work study the compensation principle and different control strategies of DVR used here are based on DFT, kalman Filter & ANN Controller .Through detailed analysis and simulation studies using MATLAB.

II. DVR STRUCTURE AND CONTROL

The single-line diagram of a DVR compensated distribution system is shown in figure 1. The source voltage and PCC (or terminal) voltages are denoted by v_s and v_t respectively. Note that the variables in the small case letter indicate instantaneous values. The three-phase source, v_s is connected to the DVR terminals by a feeder with an impedance of R_s+jX_s. The instantaneous powers flowing in the different parts of the distribution system are indicated. These are PCC power (P_{s1}), DVR injected power (P_{sd}) and load power (P_{12}).Using KVL at PCC we get

$$v_t + v_k = v \text{----------} (1)$$

The DVR is operated in voltage regulation mode. The DVR injects a voltage, v_k in the distribution system such that it regulates the critical load bus voltage, v_1 to a reference v_1^* having a pre-specified magnitude and angle at system nominal frequency. The reference voltage of the DVR v_k^* is then given by

$$v_k^* = v_1^* - v_t \text{----------} (2)$$

The DVR structure is shown in fig.2. It contains three H-bridge inverter. The dc bus of all the three inverters is supplied through a common dc energy storage capacitor C_{dc} [12].

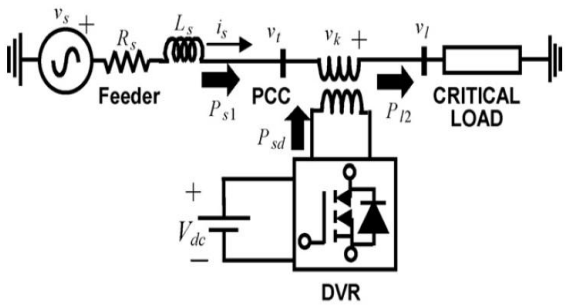

Fig.1: Single-line diagram of a DVR connected distribution system

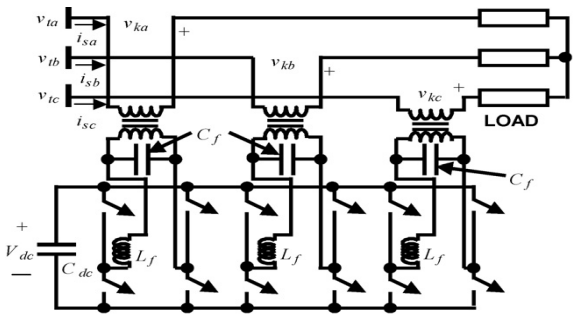

Fig.2: DVR H-bridge with LC filter

combination. Each VSI is connected to the distribution feeder through a transformer. The transformer not only reduces the voltage rating of the inverter but also provide isolation between the inverter and the ac system. In this, a switch frequency LC filter (L_f _C_f) is placed in the transformer primary (inverter side). The secondary of each transformer is directly connected to the distribution feeder. This will constrain the switch frequency harmonics too mainly in the primary side of the transformer. The three H-bridge inverter are controlled independently. The technique of output feedback control is incorporated to determine the switching actions of the inverters. The controller is designed in discrete-time using pole shifting law in the polynomial domain that radically shifts the open-loop system poles towards the origin. The controller is used to track the reference injected voltages (v_k*) given by (2).

III. NORMAL OPERATION OF DVR

The DVR operation using above structure and control has been discussed here. A detailed simulation has been carried out using MATLAB software to verify the efficacy of the DVR system. Let us assume that the source frequency is constant at the distribution system nominal frequency, i.e., at 50Hz. The DVR is connected between the PCC and the critical load. The distribution system and the DVR parameters used for the simulation studies are given in table 1. The dc link of the inverter is supplied through a dc battery. The DVR is operated such that the load voltage is maintained with 9KV peak at system nominal frequency of 50Hz. Note that this value is same as the peak of the source voltage.The study state system voltages are shown in fig.3.it can be seen from fig.3 (a), that the load bus voltages are perfectly balanced at 50Hz. The PCC bus voltages are also balanced as the source voltages are balanced. It can be seen from fig.3 (b), that the magnitude of the injected voltages by the DVR is very small. This is because the DVR is compensating only for the voltage drop across the feeder.

IV. ANALYSIS OF DVR OPERATION UNDER FREQUENCY VARIATION

Let us now investigate through MATLAB simulation, what happens when the source frequency is not the same as the system nominal frequency. Note that, this is a simulation study to demonstrate the consequences of frequency mismatch the DVR is operated such that it maintains the load voltage at the nominal frequency, of the system, i.e., 50Hz. It is assumed that the source voltage v_s has a frequency of 48Hz.

TABLE I. System Parameters

System quantities	Values
Source voltage	11KV(L-L),phase angle 0^o
System normal frequency	50HZ
Feeder Impedance	0.605+j4.838 ohms
Balanced load impedance	72.6+j54.44 ohms
Desired load voltage	9.0KV peak at nominal frequency, phase angle0^o
Single-phase transformers	1MVA,1.5KV/11KV with leakage inductance of 10%
dc-link voltage	1.5kV
Filter parameters(primary side)	L = 61.62µF Ct = 2348.8 µF
Pole shift factor(λ)	0.70

The system current and voltage waveforms are shown in the fig.4.for clarity, only the a-phase waveforms are shown here. It can be seen from fig.4 that the load voltages distortions free and has a fundamental frequency component of 50Hz. Since the load is passive and linear, the load current will also have a frequency of 50Hz.

The DVR is a series device, the source current is identical with line current and has only 50Hz component. The system equivalent circuit at the two frequencies is shown in fig.5. From fig5, the injected voltage is given without ANN Controller by

$$v_k = v_{k1} + v_{k2} \text{---------- (3)}$$

The component v_{k2} is exactly negative of the 48Hz source voltage, v_s such that the line current has no 48Hz component. The component v_{k1} approximately equals the 50Hz reference voltage v_1*. It can be seen from fig.4, that a-phase injected voltage by the DVR has modulation due to the frequency components. The PCC bus voltage has a 48Hz component equal to v_s and a small 50Hz component corresponding to feeder drop. Again as per(1),the DVR injected voltage must cancel the 48Hz load voltage. This is obvious from the modulating waveform shown in the fig.4.

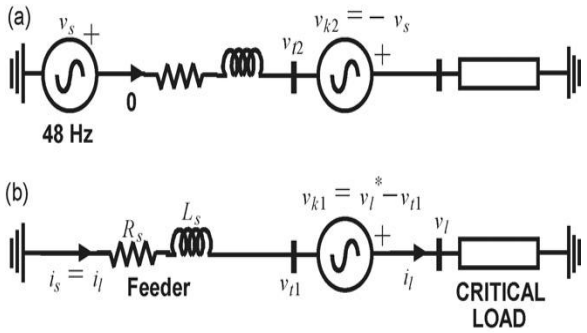

Fig.3: Equivalent circuits at (a) 48Hz and (b) 50Hz

The frequency spectrum of waveforms in fig.4.is shown in fig.6. Note that the spectrum of voltages in fig.6 is normalized with respect to the 50Hz component present in the DVR injected voltage. It can be seen that the line current and the load voltage are at 50Hz component .from (1), the 48Hz component of DVR voltage has the same magnitude as the 48Hz of the PCC voltage, except that they are in phase opposition, which is not shown here. Also, it can be seen from fig.6, that the magnitude of 50Hz load voltage is the different between 50 Hz DVR injected voltage and the corresponding PCC voltage. Let us assume that the PCC voltage contains a component at the fundamental frequency of ω_1 and a component at another frequency ω_2.these three phase voltages (v_{ta},v_{tb},v_{tc}) are

Equations

$V_{ta} = Vt_1 \sin(\omega_1 t) + Vt_2 \sin(\omega_2 t)$, $V_{tb} = Vt_1 \sin(\omega_1 t - 120) + Vt_2 \sin(\omega_2 t - 120)$,

$V_{tc} = Vt_1 \sin(\omega_1 t + 120^\circ) + V_t \sin(\omega_2 t + 120^\circ)$,_____(4)

The line currents (Isa, Isb , Isc) are at fundamental frequency and are given by

$I_{sa} = Is_1 \sin(\omega_1 t - \varphi)$, $Isb = Is_1 \sin(\omega_1 t - 120^\circ - \varphi)$, $I_{sc} = Is_1 \sin(\omega_1 t + 120 - \varphi)$_____(5)

From Fig. 1, the instantaneous power (Ps1) entering at the PCC bus is given by

$P_{s1} = p_a + p_b + p_c = v_{ta} i_{sa} + v_{tb} i_{sb} + v_{tc} i_{sc}$ _____(6)

Where

$P_a = Vt_1 Is \sin(\omega_1 t) \sin(\omega_1 t - \varphi) + Vt_2 Is_1 \sin(\omega_2 t) \sin(\omega_1 t - \varphi)$ (7a)

$P_b = Vt_1 Is \sin(\omega_1 t - 120) \sin(\omega_1 t - 120 - \varphi)] + Vt_2 Is_1 \sin(\omega_2 t - 120) \sin(\omega_1 t - 120 - \varphi)$ (7b)

$P_c = Vt_1 Is \sin(\omega_1 t + 120) \sin(\omega_1 t + 120 - \varphi) + Vt_2 Is_1 \sin(\omega_2 t + 120) \sin(\omega_1 t + 120 - \varphi)$ (7c)

Expanding (7), we get

$P_a = V_{t1} I_{S1}/2[\cos\varphi - \cos(2\omega_{1t} - \varphi)] + V_{t2} I_{S1}/2[\cos(\omega_1 - \omega_2)t + \varphi] - \cos\{(\omega_1 - \omega_2)t - \varphi\}]$

$P_b = V_{t1} I_{S1}/2[\cos\varphi - \cos(2\omega_{1t} - 240^0 - \varphi)] + V_{t2} I_{S1}/2[\cos(\omega_1 - \omega_2)t + \varphi] - \cos\{(\omega_1 - \omega_2)t - 240^0 - \varphi\}]$

$P_c = V_{t1} I_{S1}/2[\cos\varphi - \cos(2\omega_{1t} + 240^0 - \varphi)] + V_{t2} I_{S1}/2[\cos(\omega_1 - \omega_2)t + \varphi] - \cos\{(\omega_1 - \omega_2)t + 240^0 - \varphi\}]$

Substituting p_a, p_b, and p_c in, the (6), the instantaneous power p_{s1} is calculated as

$P_{s1} = 3/2 I_{S1}[V_{t1} \cos\varphi + V_{t2} \cos\{(\omega_1 - \omega_2)t + \varphi\}]$ (8)

Therefore the power entering at the PCC bus (P_{s1}) should have a Dc component equal to $1.5 * V_{t1} I_{s1} \cos\varphi$ and a component at a frequency of $(\omega_1 - \omega_2)$ radian. For the waveforms shown in figure 4,P_{s1} will have a 2 Hz and a dc component. in a similar way power injected by the DVR (P_{sd}) will also have these two components

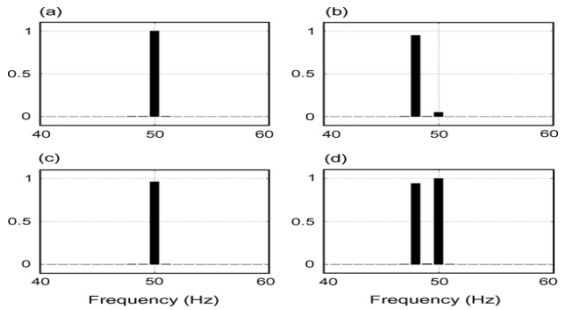

Fig.4: The frequency spectrum of current and voltage waveforms:

(a) line current; (b) PCC voltage; (c) load voltage; (d) DVR voltage .

However, the load power (P_{12}) will only have a dc component at both the load voltages and load currents are at 50 Hz and the load is balanced. The instantaneous powers are shown in figure5.it can be seen that the load power is constant at about 1.1 MW.

The frequency spectrum of the instantaneous power is shown in fig.5.it can be seen from fig.8 that the power entering at the PCC, Ps_1 has a 2 Hz component and a small dc component. The small dc component Is the feeder loss. As the power Ps_1 is oscillating at 2 Hz, it is not contributing anything for the power required by the load. Hence, the entire load power is supplied through the DVR. The power consumed by the load has only a dc component.

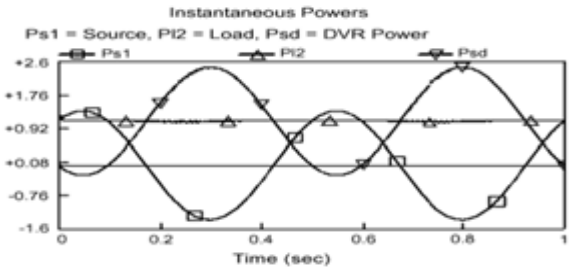

Fig.5: Various instantaneous powers.

The DVR not only supply the load but also supplies the feeder loss, i.e., all 50 Hz components. In addition, DVR also supplies the oscillating 2 Hz component in phase opposition to the 48 Hz component of the source. Therefore, instantaneous maximum value of the DVR injected voltage seems to be very large. The above discussion clearly demonstrates that the entire real load power has to be supplied by a dc capacitor. The dc capacitor will discharge rapidly if it has to supply this real power irrespective of its size. Hence some alternative arrangement has to be made. It is possible to support the dc link through a diode rectifier connected at the PCC bus. We shall now investigate the rectifier-supported DVR operation under frequency mismatch.

V. RECTIFIER-SUPPORTED DVR

The single line diagram of the distribution system for this connection is shown in Fig. 7 where the power flow Parts of the system are indicated. The dc bus of the VSIs realizing the DVR is supported from the distribution feeder itself through a three-phase uncontrolled full bridge diode rectifier. The rectifier is supplied by a Y-Y connected to the PCC. Therefore, The DVR can supply real power from the feeder through the dc bus. A shunt capacitor filter, C_d is also connected at the PCC to provide a low impedance path for the harmonic currents generated by the rectifier to flow. Let us assume that the frequency of the source voltage be 48 Hz. The rectifier transformer and capacitor values are given in Table 2 while the rest of the system parameters are the same as given in Table 1.

System quantities	Values
System nominal frequency	50HZ
Source frequency	48HZ
Rectifier transformers	1MVA, 11KVA/2KV(Y-Y), With Leakage inductance 10%.
Capacitor filter (C_d)	30 µF
Dc capacitor (C_{dc})	4000 µF
Reference load voltage (v_1^*)	11KV(L-L) or 9KV Peak at normal frequency ,phase angle0

TABLE II. Rectifier Parameters

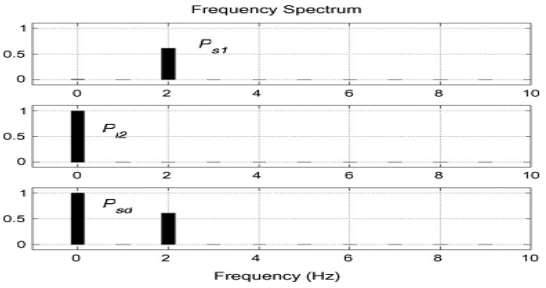

Fig.6: Frequency spectrum of powers

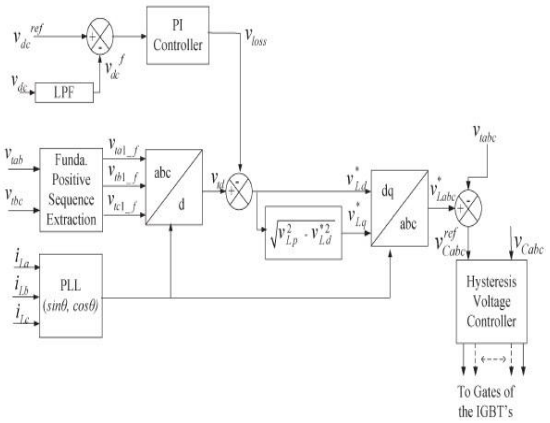

Fig.7: Main block diagram of proposed DVR

The PCC voltage, the load and the injected voltage are shown in Fig. 8. It can be seen that the critical load voltage is perfectly regulated to its pre-specified magnitude, i.e., 9 kV. In this connection also a large amount of voltage is injected by the DVR is having a magnitude of about 20 kV at 0.25s. Note from Fig. 9, that the load current is not equal to the source current due to the shunt path through the rectifier. The source current, the load current and the dc capacitor voltage waveforms are shown in Fig. 11. Using analysis similar to that in Section 4, we can say that the PCC bus voltage has a large 48Hz component and a very small 50Hz component. The voltage across the dc capacitor supplying the inverters is maintained at about 2.75 kV.The frequency spectrum of the currents and voltages are shown in Fig. 10. Voltages are shown in Fig. 10. Note that the spectrum of the voltages is normalized. With respect to v_t. It can be seen that due to the presence of rectifier, the PCC bus voltage has harmonic components n×48 and side bands at frequencies n×48±2Hz where n =1,2,3,.... Hence, the current flowing between the source and the PCC, i.e., is also has these components. As the load voltage is at 50Hz, the load current is also at 50Hz.The instantaneous powers flowing in the system and their corresponding frequency spectrum (normalized with respect to Ps1) are shown in Figs. 8 and 9, respectively. The load power (Pl2) is constant at about 1.1MW. However, the power flowing in the line, i.e., Ps2 is oscillating at 2Hz and its average over 1 s is nearly zero. The power injected by the DVR (Psd) is oscillating at 2Hz and is riding over a dc value. The dc value being the average critical load power required. The power supplied from the source (Ps1) is having a large dc component and other frequencies of very small magnitudes. The difference in the powers Ps1 and Pl2 is due to the losses occurring in the inverter circuit.

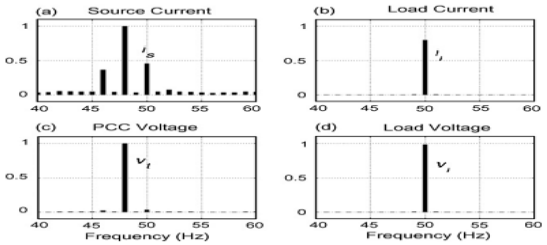

Fig.8: Frequency spectrum of voltages & currents

The above discussion clearly shows that it is very important for the power utilities to somehow measure or estimate the supply frequency and accordingly operate the DVR such that it injects the voltage in the distribution system in sympathy with the changes in the source voltage frequency. One possible solution is to phase lock the DVR from the supply. Alternatively, through communication channels, information regarding the frequency at the source end can be transferred to the DVR end. However if the communication fails or if the voltage comes out of the phase lock, the dc bus starts supporting the load. This is undesirable.

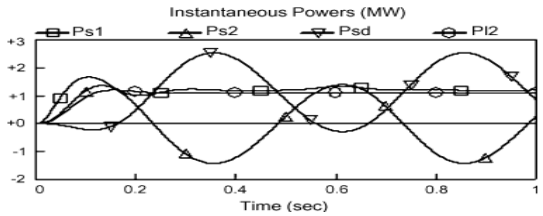

Fig.9: The instantaneous powers

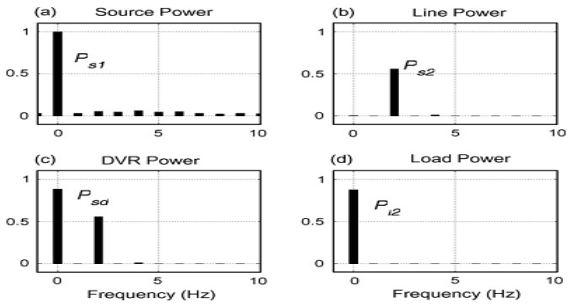

Fig.10: Frequency spectrum of powers

VI. A NEW FREQUENCY ESTIMATION TECHNIQUE

In order to avoid such a large amount of injected voltages into the distribution system, the numerical methods are available for the online frequency estimation from the samples of the supply voltage. Most of these methods are very effective when the system voltage or current contains one single frequency. For example the extended kalman filter based method has a settling time of only a few samples and can track variations in the system frequency quickly. However the formulation cannot be easily extended for signals containing two frequencies. Given below a new algorithm based on instantaneous symmetrical components for frequency estimation. Consider the phase PCC voltage, V_{ta} given in (4).wherever the frequency ω_1 is assumed to know and we have to estimate the unknown frequency ω_2 based on the measurement of the PCC voltages.

$V_{ta}= Vt_1 \sin(\omega_1 t) + Vt_2 \sin(\omega_2 t)$ (9)

Let us denote the time periods of two frequencies $\omega_1$and ω_2 as $T_1$and T2 respectively such that

$T_1=2\pi/\omega_1$, $T_2=2\pi/\omega_2$ taking an average of V_{ta} over the $V_{ta.avg} = 1/T1 =$

$t_1 \int t_1+T \{V_{t1} \sin(\omega_1 t) + V_{t2} \sin(\omega_2 t)\} dt$ (10)

$V_{ta.avg} = 1/T \; t_1 \int t_1+T \; Vt2 \sin(\omega 2t)\, dt = \gamma \sin(\omega_2 t1 + \pi\omega_2/\omega_1)$ (11)

$\gamma=v_{t2}\omega_1/ \Pi \omega_2 \; \sin(\Pi\omega_2/\omega_1)$

now if the average $V_{ta\cdot avg}$ is computed using a moving average process with a time window of T_1 as time t_1 changes, we shall get a sinusoidal waveform that varies with frequency ω_2.two successive zero crossing of this waveform can be used to determine the frequency based on which the frequency v_k^* of (2) is computed.

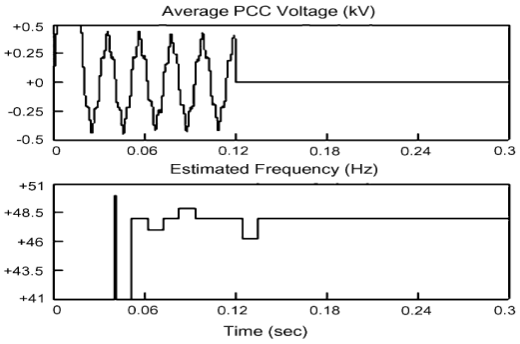

Fig.11: Average PCC voltage, $V_{ta.avg}$ the estimated frequency ($\omega_2/2\pi$).

Consider the same system as discussed in session 4.in which the DVR injects the voltage in the distribution system such that the voltage across the critical load is at a frequency ($\omega_1/2\pi$) of 50 Hz, while the source frequency ($\omega_2/2\pi$) is 48 Hz. The results with the frequency estimation technique mentioned above are shown in fig11 .it can be seen from the fig 11 that a large overshoot (2.5kv) peak arises in the average voltage signal as soon as the frequency mismatch occurs. Note that this is a signal obtained by integration of PCC voltage, V_{ta} over one period. This will cause the zero-crossings of the average voltage to shift for a few successive cycles. Once the variations in the zero-crossings stops, the source frequency estimated to be 48Hz at 0.1s.at this instant, the DVR starts injecting voltages at the estimated frequency. this estimated frequency is then used in the average process of (10) in which both the frequencies are now 48Hz and hence the time window T_1 is 1/48s.this will result in average being zero with a delay of one 48 Hz cycle .However, some small variations in the zero-crossings of the average voltage will persist for a few more cycles. The variations in the frequency during this time must be disregarded. if the frequency is allowed to vary in sympathy with the changes in the estimated frequency during this period, the terminal voltage will never be able to settle and the average will not become zero.

So far, we have considered that the source voltages, V_s (Fig. 1) are balanced and are free from harmonics. Let us assume that V_s contains 20% fifth harmonic component. Then the a-phase PCC voltage can be written as

$V_{ta} = Vt_1 \sin(\omega_1 t) + Vt_2\{\sin(\omega_2 t) + 1/5\sin(5\omega 2t)\}$ (12)

The average of V_{ta} of (12) over the period $T1$ will be

$V_{ta.avg} = 1/T_1 \int_{t1}^{t1+T1} Vt_2\{\sin(\omega_2 t) + 1/5\sin(5\omega_2 t)\}dt = \gamma\sin(\omega_2 t_1 + \pi\omega_2/\omega_1) + \gamma 5\sin 5(\omega_2 t_1 + \pi\omega_2/\omega_1)$ (13)

Where the constant term γ and $\gamma 5$ are given by

$\gamma = Vt_2\omega_1/\pi\omega_2 \sin(\Pi\omega_2/\omega_1)$, $\gamma 5 = Vt_2\omega_1\sin(5\Pi\omega_2/\omega_1)$

The procedure for estimating the frequency described above can now be applied to $V_{ta.avg}$ as per (13). The estimated frequency.

Along with average PCC voltage is shown in Fig. 11.It can be seen that that the harmonic in the source does not affect the Estimation technique, because the zero crossings are unaffected by the addition of an integer harmonics in (12). In general, addition of integer harmonics whose magnitudes Reduce as harmonic number increases; do not cause a shift in zero crossing. Therefore, the presence of such integer harmonics does not affect the estimation of frequency.

VII. TRAINING AN ARTIFICIAL NEURAL NETWORK

Once a network has been structured for a particular application, that network is ready to be trained. To start this process the initial weights are chosen randomly. Then, the training, or learning, begins. There are two approaches to training – 'SUPERVISED' and 'UNSUPERVISED'. Supervised training involves a mechanism of providing the network with the desired output either by manually "grading" the network's performance or by providing the desired outputs with the inputs. Unsupervised training is where the network has to make sense of the inputs without outside help. The vast bulk of networks utilize supervised training. Unsupervised training is used to perform some initial characterization on inputs.Training can also be classified on basis of how the training pairs are presented to the network. They are 'INCREMENTAL TRAINING' and 'BATCH TRAINING'. In incremental training the weights and biases of the network are updated each time an input is presented to the network. In batch training the weights and biases are only updated after all of the inputs have been presented.

Supervised Training:

In supervised training, both the inputs and the outputs are provided. The network then processes the inputs and compares its resulting outputs against the desired outputs. Errors are then propagated back through the system, causing the system to adjust the weights are continually tweaked. The set of data which enables the training is called the "training set". During the training of a network the same set of data is processed many times as the connection weights are ever refined. However, some networks never learn. This could be because the input data does not contain the specific information from which the desired output is derived. Networks also don't converge if there is not enough data to enable complete learning. Many layered networks with multiple nodes are capable of memorizing data. To monitor the network to determine if the system is simply memorizing its data in some non significant way, supervised training needs to hold back a set of data to be used to test the system after it has undergone its training. Typical diagrams for supervised training of a network is given in figure 12.1

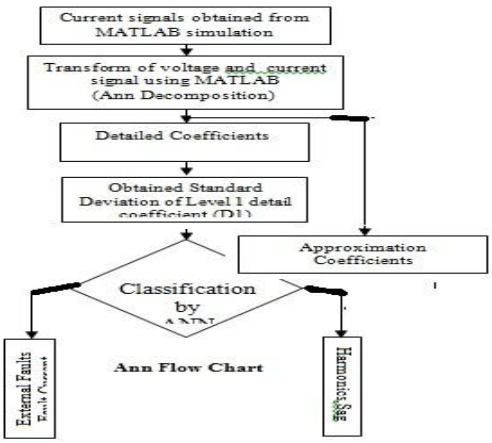

Fig.12.1: ANN Program Flow Chart

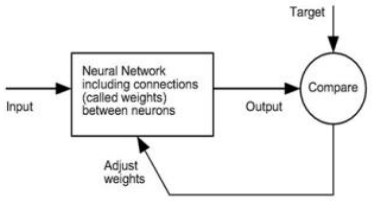

Fig 12.2 Supervised Training

If a network is simply can't solve the problem, the designer then has to review the input and outputs, the number of layers, the number of elements per layer, the connections between the layers, the summation, transfer, and training functions, and even the initial weights themselves. Those changes required to create a successful network constitute a process wherein the "art" of neural networking occurs. Another part of the designer's creativity governs the rules of training. There are many laws (algorithms) used to implement the adaptive feedback required to adjust the weights during training. The most common technique is backward-error propagation, more commonly known as back-propagation. Yet, training is not just a technique. It involves a "feel", and conscious analysis, to insure that the network is not 'over trained'. Initially, an artificial neural network configures itself with the general statistical trends of the data. Later, it continues to "learn" about other aspects of the data which may be spurious from a general viewpoint. When finally the system has been correctly trained, and no further learning is needed, the weights can, if desired, be "frozen". In this paper, a simple linear model has been applied because it offers good reliability, minimum detection time and low computational complexity. This last factor is especially critical in the final implementation in the DVR control algorithm.

VIII. SIMULATION RESULTS

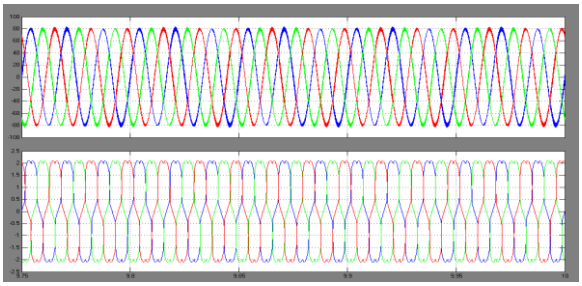

(a)

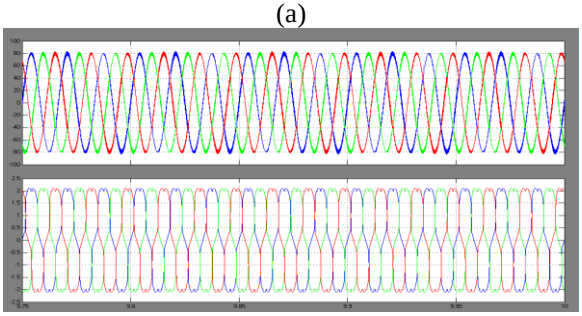

(b)

Fig.13: System performance without DVR: (a) Source voltage (kv), source current(A), (b) Load voltage (kv), load current(A) under unbalanced & non-linear loads.

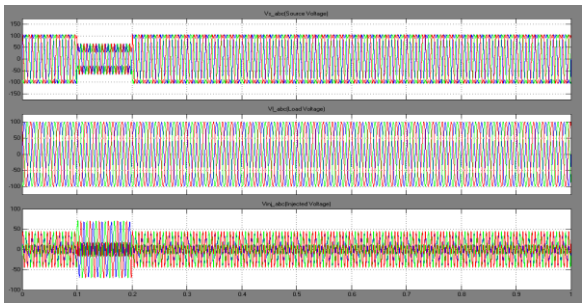

(a)

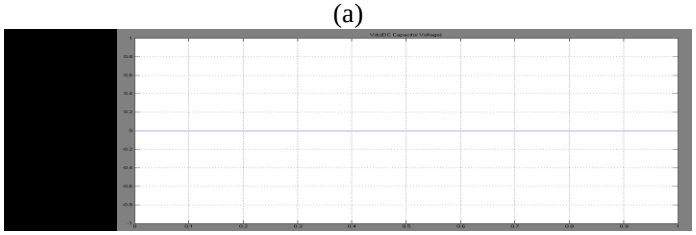

(b)

Fig.14: System performance under sag condition with DVR: (a) Source voltage (kv), Load voltage (kv), Injected Voltage (kv) for unbalanced & non-linear loads, (b) Capacitor voltage (v_{dc}), kv.

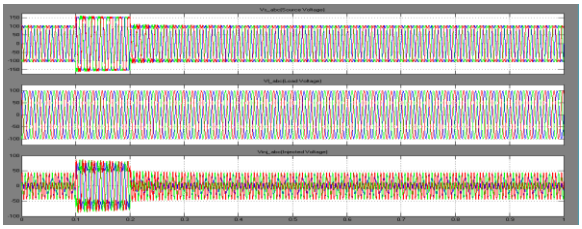

(a)

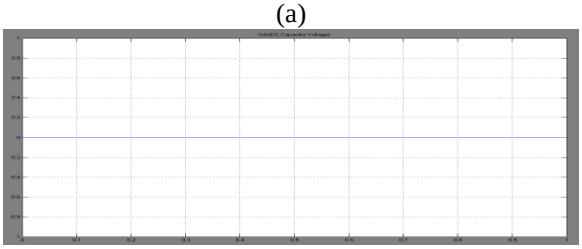

(b)

Fig.15: System performance under swell condition with DVR: (a) Source voltage (kv), Load voltage (kv), Injected Voltage (kv) for unbalanced & non-linear loads, (b) Capacitor voltage (v_{dc}), kv.

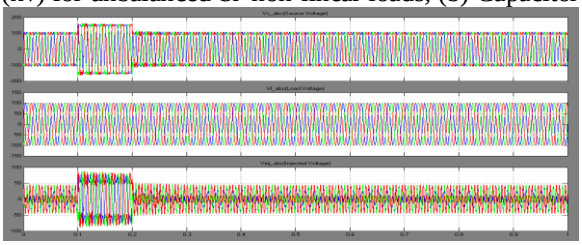

(a)

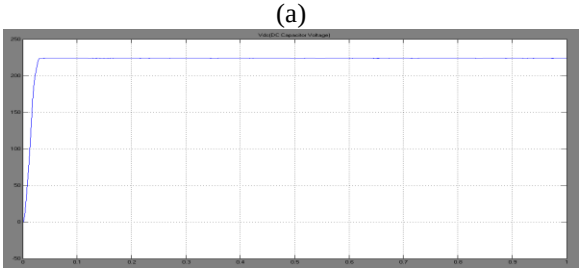

(b)

Fig.16: System performance under swell condition with DVR & ANN Controller: (a) Source voltage (kv), Load voltage (kv), Injected Voltage (kv) for unbalanced & non-linear loads, (b) Capacitor voltage (v_{dc}), kv.

IX. CONCLUSIONS

The critical load bus voltage regulation using a DVR is discussed in this paper. It has been assumed that the source voltage Frequency is not same as the distribution system nominal frequency. It has been shown that in order to maintain the load voltage at system frequency of 50 Hz, a rectifier-supported DVR is able to provide the required amount of real power in the distribution system. The rectifier takes this real power from the distribution feeder itself and maintains the voltage across the dc capacitor supplying the DVR and control with Ann Technique. However, the rectifier power contains a large ac component at the difference

frequency. As investigated in Section, the injected voltage and magnitude of powers are unacceptably high if the frequency variation is large.

A simple frequency estimation technique is discussed which uses a moving average process along with zero-crossing detector. It has been shown that once the frequency of the injected voltage latches on to that of the source voltage, the DVR injection reduces drastically.

REFERENCES

[1] A. K. Pradhan, A. Routray, and A. Basak, "Power System Frequency Estimation Using Least Mean Square Technique," *IEEE Trans. Power Delivery*, Vol. 20, No. 3, pp. 1812-1816, July 2005.

[2] R. Aghazadeh, H. Lesani, M. Sanaye-Pasand and B. Ganji, "New technique for frequency and amplitude estimation of power system signals,"*IEE Proc.-Gener. Transm. Distrib*., Vol. 152, No. 3, pp. 435-440, May 2005.

[3] K. Kennedy,G. Lightbody and R. Yacamini, "Power System harmonic analysis using the Kalman Filter," in *Proc. IEEE Power Eng. Soc. General Meeting*, Toronto, Vol. 2, pp. 752-757 , July 2003.

[4] A. G. Phadke, J. S. Thorp and M. G. Adamiak, "A new measurement technique for tracking voltage phasors, local system frequency, and rate of change of frequency," *IEEE Trans. Power App. Syst.*, Vol. PAS-102, No. 5, pp. 1025–1038, May 1983.

[5] M. M. Begovic, Petar M. Djuric, S. Dunlap and A. G. Phadke, "Frequency tracking in power networks in the presence of harmonics", *IEEE Trans. Power Delivery*, Vol. 8, No. 2, pp. 480-486, April 1993.

[6] J. Z. Yang and C. W. Liu, "A precise calculation of power system frequency and phasor", *IEEE Trans. Power Delivery*, Vol. 15, No. 2, pp. 494-499, April 2000.

[7] V. V. Terzija, M. B. Djuric, and B. D. Kovacevic, "Voltage phasor and local system frequency estimation using newton type algorithm," *IEEETrans. Power Del.*, Vol. 9, No. 3, pp. 1368–1374, July 1994.

[8] T. S. Sidhu and M. S. Sachdev, "An iterative technique for fast and accurate measurement of power system frequency," *IEEE Trans. Power Delivery*, Vol. 13, No. 1, pp. 109-115, January 1998.

[9] T. S. Sidhu, "Accurate measurement of power system frequency usinga digital signal processing technique," *IEEE Trans. Insrum. Meas.*, Vol.48, No. 1, pp. 75-81, February 1999.

[10] A. Ghosh, A. K. Jindal and A. Joshi, "Inverter control using output feedback for power compensating devices," *IEEE TENCON 2003 Conf. on Convergent Technologies for Asia-Pacific Region*, Vol. 1, pp. 48-52, 14-17 Oct. 2003.

[11] A. K. Jindal, A. Ghosh, and A. Joshi, "Voltage Regulation using Dynamic Voltage Restorer for large frequency Variations," in *Proc. IEEE Power Eng. Soc. Gen. Meeting*, San Francisco, CA, pp 1780-1786,June 2005.

[12] A. Ghosh and G. Ledwich, "Structures and control of a dynamic voltage regulator (DVR)," in *Proc. IEEE Power Eng. Soc. Winter Meeting*,Columbus, OH, 2001.

[13] A. Ghosh and G. Ledwich, *Power Quality Enhancement Using Custom Power Devices*, Norwell, MA: Kluwer, 2002.

I K. Anand Dev Singh was born in Visakhapatnam, India . I received the B.Tech degree in Electronics & Electrical Engineering from Chaitanya Engineering College, Jawaharlal Nehru Technological University Kakinada, India in 2009 and I am currently pursuing the M.Tech degree in Power & Industrial Drives at Dadi Institute of Engineering & Technology, JNTU Kakinada, India. My interests include power quality, electrical machines and power electronics applications in distribution systems.